AD-A253 800

⊓TION PAGE

... average 1 hour per response, including the time for reviewing instructions, searching existing data sources, ...g the collection of information. Send comments regarding this burden estimate or any other aspect of this ...to Washington headquarters Services, Directorate for Information Operations and Reports, 1215 Jefferson ... Management and Budget, Paperwork Reduction Project (0704-0188), Washington, DC 20503.

1. AGENCY USE ONLY (Leave blank)	2. REPORT DATE	3. REPORT TYPE AND DATES COVERED
	July 1992	Final Tech. Rpt. 6/01/90–5/31/92

4. TITLE AND SUBTITLE	5. FUNDING NUMBERS
Advanced Modeling and Optimization of Piezoelectric Composites	N00014-90-J-1924

6. AUTHOR(S)

John A. Hossack and Bert A. Auld

7. PERFORMING ORGANIZATION NAME(S) AND ADDRESS(ES)	8. PERFORMING ORGANIZATION REPORT NUMBER
The Board of Trustees of the Leland Stanford Jr. University c/o Sponsored Projects Office, Stanford University 125 Panama Street, Jordon Quad/Birch Stanford, CA 94305-4125	

9. SPONSORING/MONITORING AGENCY NAME(S) AND ADDRESS(ES)	10. SPONSORING/MONITORING AGENCY REPORT NUMBER
Department of the Navy Office of the Chief of Naval Research 800 N. Quincy St., Arlington VA 22217-5000 Wallace A. Smith, Code 1131	

**DTIC
ELECTE
JUL 23 1992
S D**

11. SUPPLEMENTARY NOTES

12a. DISTRIBUTION/AVAILABILITY STATEMENT	12b. DISTRIBUTION CODE
Unlimited	A

> This document has been approved for public release and sale; its distribution is unlimited.

13. ABSTRACT (Maximum 200 words)

The aim of this project was to obtain a more complete understanding of the physical phenomena occurring in piezoelectric transducers, with the aim of obtaining optimal designs and improved manufacturability. Of key importance in design are conversion efficiency, bandwidth, and control of spurious modes. The transducer structures considered are 1:3, 0:3, 2:2, and 1:3:1. Contributions to the advancement of 1:3 modeling and fabrication are: (i) finite element modeling of composite lattices with complex unit cells, (ii) transmission line and reciprocity modeling of distributed period composites, (iii) fabrication of test transducers for verification of the modeling principles. New modeling theory for 0:3 composites aims at replacing the empirical "cubes" model with a model consisting of nearly close-packed spherical particles. This approach estimates more closely the performance of 0:3 composites and points the way for further studies. The 2:2 structures considered are, in fact, multilayered electroded transducers with a single piezoelectric material. But multiple piezoelectrics and alternating piezo and nonpiezo layers may also be considered. A procedure has been developed, and confirmed experimentally, for tailoring the transducer time-domain response by applying multiple excitations. Finally, 1:3:1 transducers with a periodic addition of empty voids have been developed. This version produces a more uniform thickness mode displacement and improved coupling, predicted from finite element modeling and confirmed experimentally.

14. SUBJECT TERMS	15. NUMBER OF PAGES
Transducer, Composite, Finite Element, Piezoelectric, Multilayer, Spurious Modes, 1:3, 0:3, 2:2, 1:3:1, Time-domain Response, Thickness Mode, Optimal Designs, Improved Manufacturability.	118
	16. PRICE CODE

17. SECURITY CLASSIFICATION OF REPORT	18. SECURITY CLASSIFICATION OF THIS PAGE	19. SECURITY CLASSIFICATION OF ABSTRACT	20. LIMITATION OF ABSTRACT
Unclassified	unclassified	unclassified	unlimited

NSN 7540-01-280-5500

Standard Form 298 (Rev. 2-89)

FINAL TECHNICAL REPORT

ADVANCED MODELING AND OPTIMIZATION
OF PIEZOELECTRIC COMPOSITES

John A. Hossack and Bert A. Auld

For the period June 1, 1990 to May 31, 1992

DTIC QUALITY INSPECTED 2

July 1992

92-19373

92 7 21 048

TABLE OF CONTENTS

1. INTRODUCTION

The objective of this project was to obtain a more complete understanding of the physical phenomena occurring in piezoelectric composite transducers. Techniques for controlling parasitic resonance mode activity in 1:3 composite transducers have been developed. The mechanisms governing the behavior of 0:3 transducers have been considered in detail. The concept of using transducers with separately excited, but mechanically coupled, layers has been proposed. Finally, an enhanced 1:3 composite transducer, with a compressible third phase, has been developed.

2. 1:3 COMPOSITE TRANSDUCERS

This type of composite, comprising piezoceramic pillars embedded in a polymer matrix, has applications in both active and passive modes of operation. The present work has concentrated on identifying the influence of pillar geometry and configuration on device performance.

2.1. Floquet Analysis

In this approach the material parameters (density and stiffness) are written as arbitrary periodic functions of the spatial coordinates. In a 1-3 composite the material properties are periodic in a plane (xy) and uniform along the perpendicular axis.

The advantage of this approach is that it permits a full treatment of an infinite 1-3 composite. Simple approximations for small volume fraction ($< 10\%$) and high volume fraction ($> 90\%$) of ceramic give excellent physical insight into the behavior of waves and vibrations in these materials, and facilitate the development of design concepts based on physical principles. Within the above limitations this approach permits a full development of wave dispersion curves and lateral standing wave resonances at all of the material stopbands. The approach is not practical for intermediate volume fractions, where the finite element method (2-dimensional periodicity) and the wave transmission matrix method (1-dimensional periodicity) must be used to flesh out the details. Floquet theory can, in principle, be applied to the analysis of a composite plate, but this is not practical because of the complexity of the equations. Finite element analysis must be used to make a connection between Floquet-based concepts and the behavior of 1-3 composite plates, especially those having intermediate volume fractions of ceramic in their composition.

(a) Basic Wave Equation

Previous analysis and experiment show that lateral resonances in 1-3 composites are basically shear waves polarized parallel to the length direction of the ceramic elements.

A simple periodic wave equation can be developed for model calculations based on this approximation.

Define a coordinate system with x and y axes in the basal plane and the z axis parallel to the ceramic elements. The displacement field of the z-polarized vibration is

$$u_z(x, y)$$

Since the z displacement is a function of both x and y, the strain componenets are

$$S_{zx} = \frac{1}{2}\, S_5 = \frac{1}{2}\frac{\partial u_z}{\partial x}$$

$$S_{zy} = \frac{1}{2}\, S_6 = \frac{1}{2}\frac{\partial u_z}{\partial y}$$

If the two composite phases are isotropic the stresses are

$$T_{zx} = T_5 = c_{44}\frac{\partial u_z}{\partial x}$$

$$T_{zy} = T_6 = c_{44}\frac{\partial u_y}{\partial y}$$

The dynamic equation

$$\frac{\partial T_{ij}}{\partial r_j} = -\rho\omega^2 u_i$$

then yields

$$\frac{\partial}{\partial x}T_{zx} + \frac{\partial}{\partial y}T_{zy} = -\rho\omega^2 u_z$$

or

$$\left(\frac{\partial}{\partial x}c_{44}\frac{\partial}{\partial x} + \frac{\partial}{\partial y}c_{44}\frac{\partial}{\partial y}\right)u_z = -\rho^2 y_z \tag{1}$$

Consider a composite with different periods along the horizontal (x) and vertical (y) axes, as shown in part (a) of Fig. 1, from the proposal.
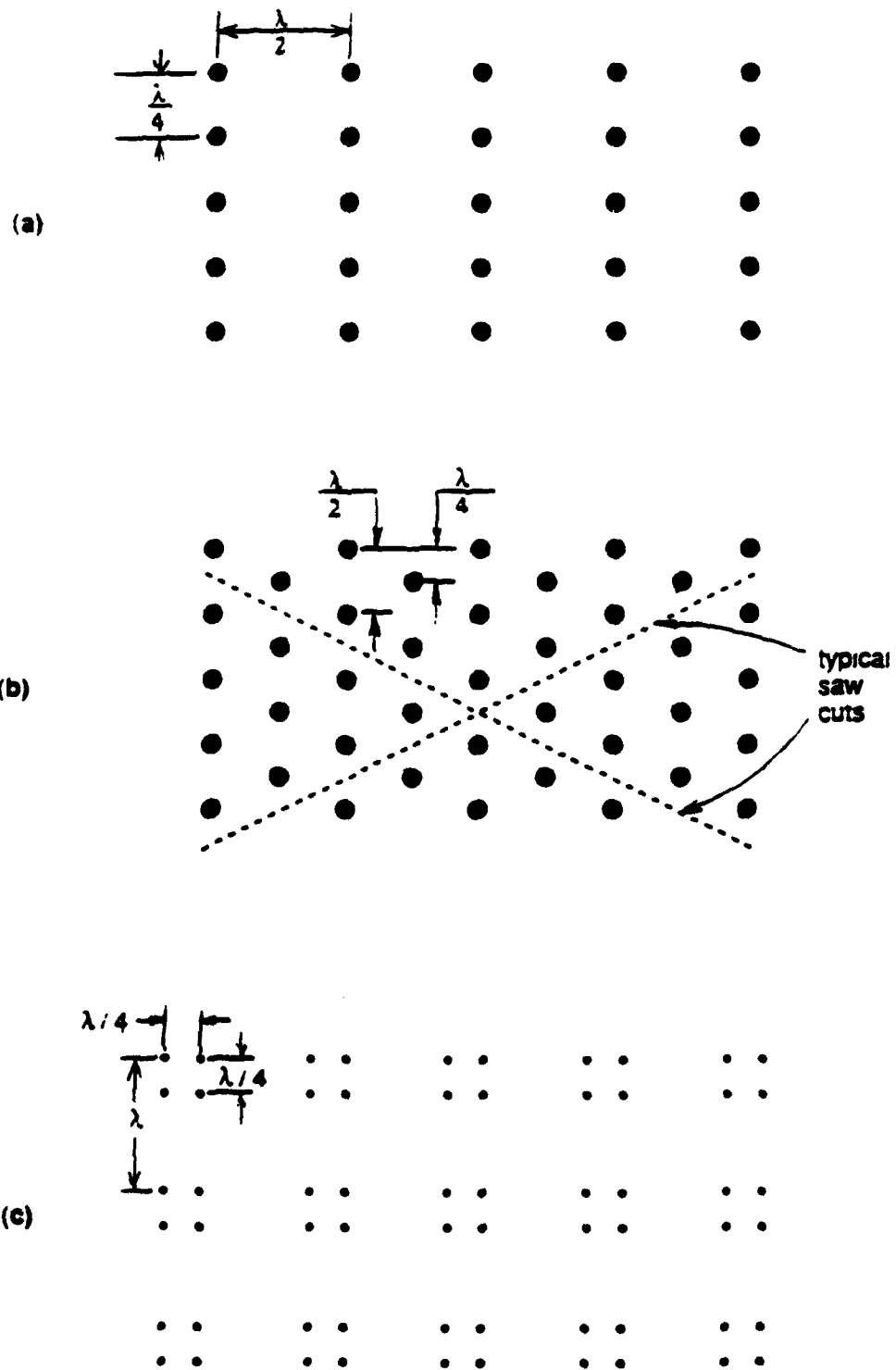
5

Figure 1
Alternative 1-3 composite lattices

6

In this case c_{44} and ρ are doubly periodic functions of x and y, with period d_x along x and d_y along y. Write

$$c_{44}(x,y) = \bar{c}_{44} + \delta \, c_{44}(x,y)$$

$$\rho(x,y) = \bar{\rho} + \delta\rho(x,y)$$

(2)

where the barred quantities are the (constant) spatial average values and $\delta c_{44}(x,y)$, $\delta\rho(x,y)$ are doubly periodic functions, as noted above.

Substitution of Eq. (2) into Eq. (1) gives

$$\left(\bar{c}_{44}\nabla^2_{xy} + \bar{\rho}\omega^2\right) u_z = -\delta W(x,y)u_z$$

(3a)

where

$$\delta W(x,y) = c_{44}(x,y)\nabla^2_{xy} + \delta c_{44}(x,y)\nabla^2_{xy}$$
$$+ \frac{\partial}{\partial x}\delta c_{44}(x,y)\frac{\partial}{\partial x} + \frac{\partial}{\partial y}\delta c_{44}(x,y)\frac{\partial}{\partial y} + \delta\rho(x,y)\omega^2$$

(3b)

(b) General Floquet Solution

The general solution to Eqs. (3a) and (3b) has the form

$$u_z(x,y) = \sum_{m,n} a_{mn}\exp(-i\underline{\beta}_{mn}\cdot\underline{r})$$

(4a)

where

$$\underline{r} = \hat{\underline{x}}x + \hat{\underline{y}}y$$

$$\underline{\beta}_{mn} = \left(\beta_{0x} + \frac{2\pi m}{d_x}\right)\hat{\underline{x}} + \left(\beta_{0y} + \frac{2\pi n}{d_y}\right)\hat{\underline{y}}$$

(4b)

with $m,n = 0,\pm1,\pm2,\pm3$, etc. and β_{0x},β_{0y} arbitrary. Substitution into Eq. (3a) yields

$$\sum_{m,n}\left(\bar{\rho}\omega^2 - \bar{c}_{44}\beta^2_{mn}\right) u_z = -\delta W(x,y)u_z$$

(5)

The problem is to calculate the unknown space harmonic amplitudes a_{mn} in Eq. (4a). In Eq. (5) u_z on the LHS is written as in Eq. (4a), and on the RHS it is written with m, n changed to p, q. Note that

$$\int_0^{d_x} dx \int_0^{d_y} dy \left(e^{i\underline{\beta}_{rs}\cdot\underline{r}}\right)^* \left(e^{i\underline{\beta}_{mn}\cdot\underline{r}}\right) = \begin{cases} 0 & r \neq m, s \neq n \\ d_x d_y & r = m, s = n \end{cases} \tag{6}$$

because of the definition of $\underline{\beta}_{mn}, \underline{\beta}_{rs}$ in Eq. (4b). Multiplying both sides of Eq. (5) with

$$\left(e^{-i\underline{\beta}_{rs}\cdot\underline{r}}\right)^*$$

and integrating over a unit cell in Fig. 1(a) yields a single term on the LHS and gives

$$\left(\bar{\rho}\omega^2 - \bar{c}_{44}\beta_{rs}^2\right) a_{rs} = -\sum_{pq} K_{rs,pq} a_{pq} \tag{7}$$

with

$$K_{rs,pq} = \int_0^{d_y} dx \int_0^{d_y} dy \, \delta W(x,y) \exp i \left(\underline{\beta}_{rs} - \underline{\beta}_{pq}\right) \cdot \overline{r}$$

where rs runs over all positive and negative integers, including zero. Equation (7) is an infinite set of linear equations defining the space harmonic amplitudes in Eq. (4).

(c) **Coupled Mode Approximation**

From Eq. (4b) β_{rs}^2 on the LHS of Eq. (7) is

$$\beta_{rs}^2 = \left(\beta_{0x} + \frac{\partial \pi r}{d_x}\right)^2 + \left(\beta_{0y} + \frac{2\pi s}{d_y}\right) \tag{8}$$

The equation set (7) has an infinite set of LHS's, each with different indices. In Eq. (4a) the leading term has $m = n = 0$, and the corresponding LHS in Eq. (7) is

$$\left(\bar{\rho}\omega^2 - \bar{c}_{44}\beta_{00}^2\right) a_{00}, \quad \text{with} \quad \beta_{00}^2 = \left(\beta_{0x}^2 + \beta_{0y}^2\right)$$

8

For a spatially uniform medium the RHS's of Eqs. (5) and (7) are zero, so that a_{00} is the only nonzero amplitude. For a periodic medium, all space harmonics exist, but some are larger than others. It can be shown that when two of the LHS's of Eq. (7) are simultaneously close to zero, the corresponding space harmonic amplitudes are large. This corresponds to the center of a stopband. If the RHS's of Eq. (7) are small, all of the other space harmonic amplitudes are small and can be neglected.

In the above situation Eq. (4a) is approximated by truncating to the two "near resonance" space harmonics—i.e., harmonics for which the LHS's are close to zero. This is called the coupled wave approximation. In this case Eq. (7) reduces to two or more linear equations in the same number of unknowns. For example,

$$\left(\bar{\rho}\omega^2 - \bar{c}_{44}\beta_{hi}^2\right) a_{hi} = K_{hi,jk} a_{jk}$$
$$\left(\bar{\rho}\omega^2 - \bar{c}_{44}\beta_{jk}^2\right) a_{jk} = K_{jk,hi} a_{hi} \tag{9}$$

The characteristic determinant of this set gives the dispersion relation near the hi, jk stopband. That is

$$\left(\bar{\rho}\omega^2 - \bar{c}_{44}\beta_{hi}^2\right)\left(\bar{\rho}\omega^2 - \bar{c}_{44}\beta_{jk}^2\right) = K_{hi,jk} K_{jk,hi} \tag{10}$$

Solution of Eq. (10) for ω versus β_0 in Eq. (4b) defines the dispersion curve of a stopband centered on the frequency where the two factors of the LHS of Eq. (10) are simultaneously zero. This is a characteristic feature of Floquet theory. Stopbands occur at frequencies when two or more of the factors on the LHS of Eq. (7) are simultaneously zero.

In composite theory the most important stopbands relate to space harmonics that propagate along either the x-axis or the y-axis—that is, with either m or n equal to zero in Eq. (4b). For small volume fraction composites, where the coupled mode approximation is valid, it can be seen that when two of the factors on the LHS of Eq. (7) are simultaneously zero there occurs a Bragg scattering (or a standing wave resonance) along either the x or the y axis. The resonances occur between adjacent rows of ceramic elements aligned

9

perpendicular to the propagation direction. In Fig. 1(a) it is clear from the dimensions that x-directed and y-directed resonances do not occur at the same frequency. However, it can be shown by evaluating the coupling constants in the RHS of Eq. (7) that these standing waves are not coupled. The resonances are therefore uncoupled one-dimensional standing waves. This result has been found to be consistent with a finite element analysis. In Fig. 1(c) x- and y-directed standing wave resonances now exist at a single frequency. But now, by contrast, they are coupled, so that the resonances are two-dimensional standing waves.

2.2. Finite Element Analysis

It has proven possible to obtain a match between analytic (Floquet etc.) and finite element results. A 10% composite was analyzed using finite element analysis and the frequencies of the thickness, and first two lateral modes were determined to be 605 kHz, 793 kHz, and 1109 kHz, respectively. The measured frequencies of these modes were 621 kHz, 802 kHz and 1033 kHz. Hence, good agreement is evident. Furthermore, the finite element displacement plots, shown in Fig. 2, indicate that the first and second lateral modes correspond to resonant activity principally parallel and diagonal to the planes of pillars. These modes are better illustrated in Fig. 3 which presents cross-sections through the thickness direction of a 2% composite. The first mode is shown along a section parallel to a plane of pillars. The second mode is shown for a diagonal cross-section. In accordance with the modes predicted using Floquet theory, the first mode consists of one parallel propagating wavelength and the second mode consists of two diagonally propagating wavelengths. However, when larger volume fractions or wider pillar aspect ratios are considered, the complexity of the resonant behavior necessitates the exclusive use of numerical techniques.
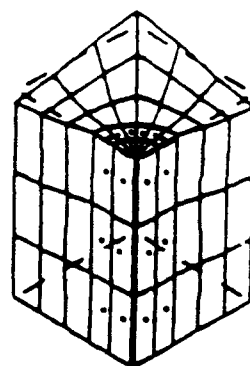
Some novel pillar spacing geometries have been considered. Figure 1(a) illustrates the lowest frequency bandedge resonance for one particular configuration. It possesses half wavelength spacing in the horizontal direction and quarter wavelength spacing along the vertical direction. Therefore, alternate vertical columns vibrate antiphase and hence the net piezoelectric coupling is zero. A similar effect occurs at the next higher resonance, with λ spacing along the horizontal axis and $\lambda/2$ spacing along the vertical axis. This structure was analyzed using finite element analysis and results obtained from a similar
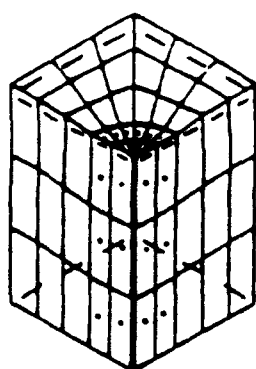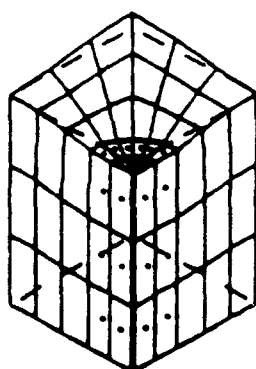
Thickness mode   **1st Lateral mode**   **2nd Lateral mode**
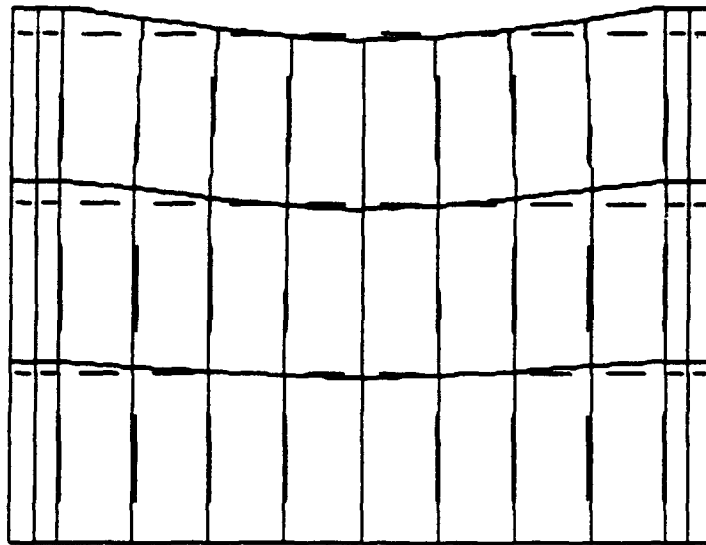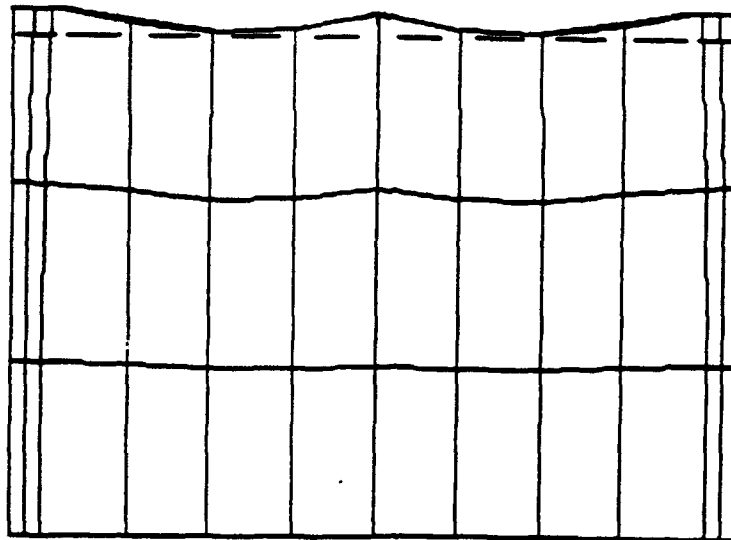
⊡ Ceramic   ▯ Polymer

Figure 2
Modal displacement plots of a 10% composite

First Mode—Parallel, Wavelength Resonance

Second Mode—Diagonal, Double Wavelength Resonance

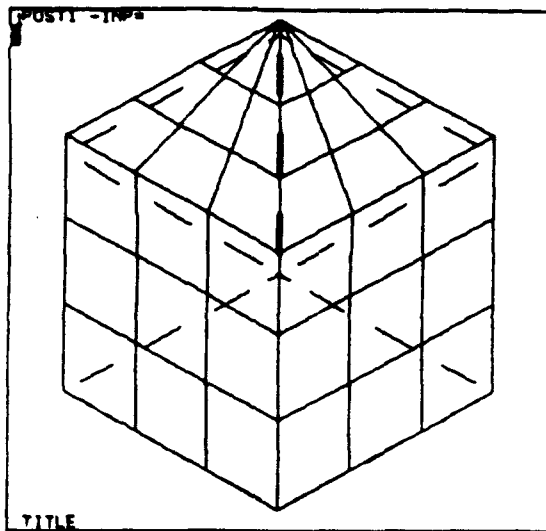Figure 3
Cross-section of a 2% Composite

regular square section geometry were compared.

Figure 4 illustrates the fundamental thickness mode, an extremely weakly-coupled antisymmetric mode and the first and second lateral modes corresponding to the regular square section composite. The electromechanical coupling coefficients associated with each of these modes are 0.178, 0.0, 0.300 and 0.212, respectively. However, when the rectangular configuration was analyzed, the "weakly" coupled mode was no longer weak and had split into two separate resonances corresponding to length and width dimensions, respectively. The higher frequency mode remained. All these mode are illustrated in Fig. 5. The coupling coefficients associated with these modes are 0.121, 0.287, 0.216 and 0.210, respectively. Consequently, the rectangular geometry has produced additional, and initially unexpected, modes. These modes are sufficiently strongly coupled electromechanically that they rule against the use of this design in practical applications.

2.3. Wave Transmission Matrix Technique for Distributed Dimension Composites

Although finite element analysis provides the most versatile means of analysis of composite structures, it is very computationally intensive. Furthermore, it is unsuited to the analysis of more than a few ceramic/polymer cells. If transverse wave propagation is of primary concern and the approximation made in using a one-dimensional stack of ceramic/polymer plates is acceptable, very much more efficient analysis techniques are available. The method employed here was developed and described by Wang [1]. Consider the layered structure illustrated in Fig. 6. Using a knowledge of layer dimensions and acoustic characteristics, it is possible to derive a matrix describing a_n, b_n in terms of a_n, b_{n-1}. This results in the following expression after considerable algebraic manipulation, which is detailed elsewhere [2].

$$\begin{pmatrix} a_{n-1} \\ b_{n-1} \end{pmatrix} = \begin{pmatrix} A & B \\ C & D \end{pmatrix} \begin{pmatrix} a_n \\ b_n \end{pmatrix} \tag{11}$$

Thickness
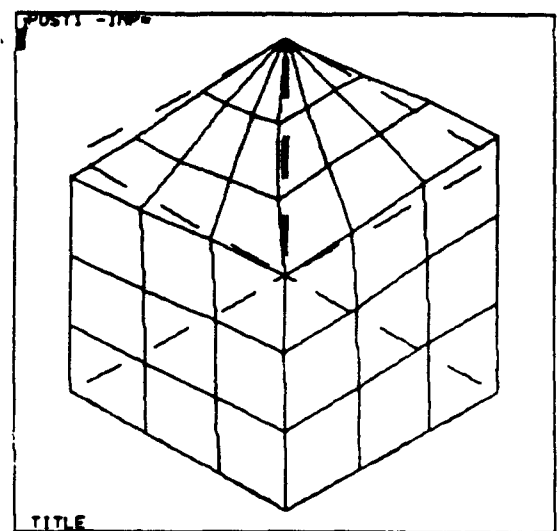
Weak Mode
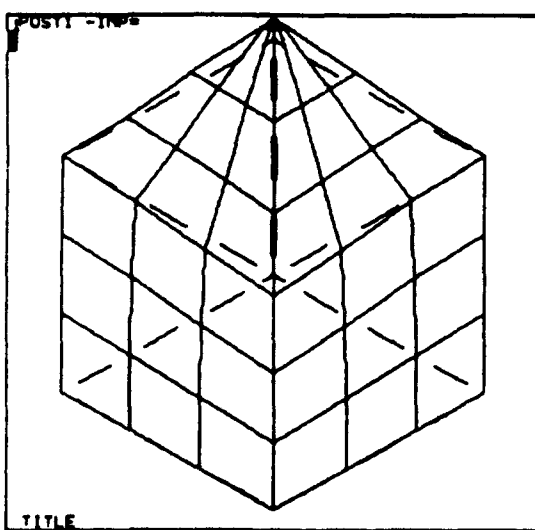
First Lateral
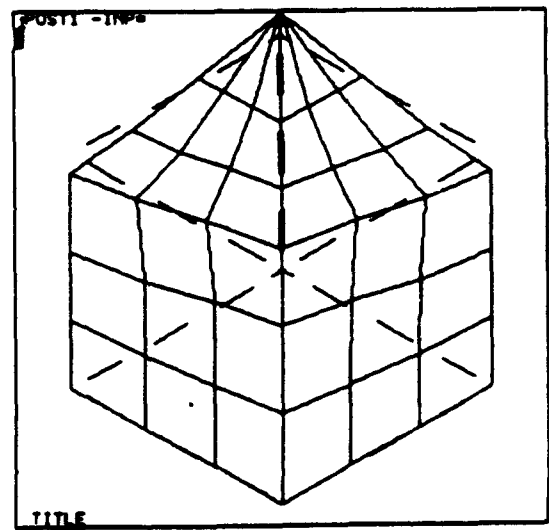
Second Lateral

Figure 4
Modal Displacement Plots of a Square Section 0.5% Composite

14
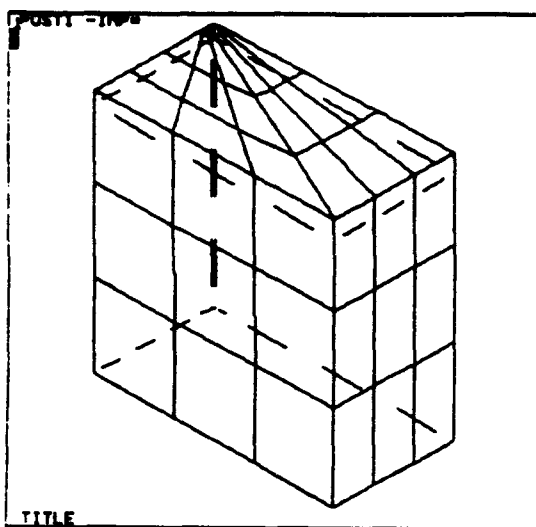
Thickness
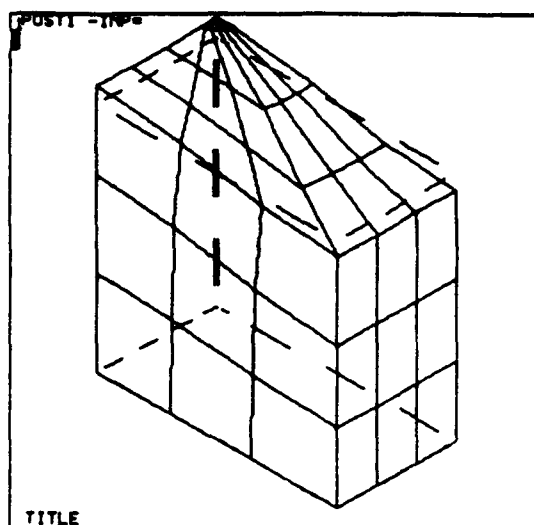
Length direction lateral mode
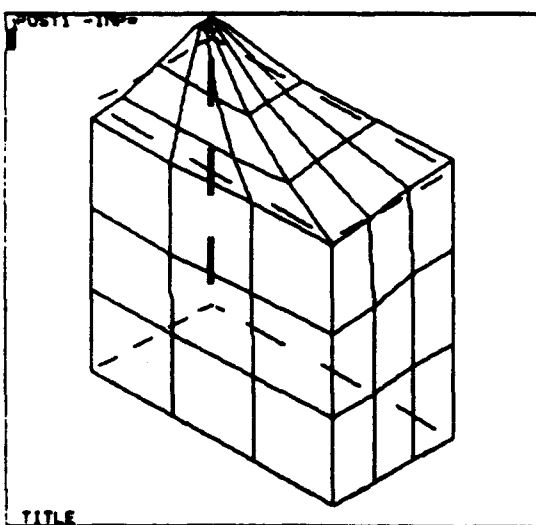
Width direction lateral mode
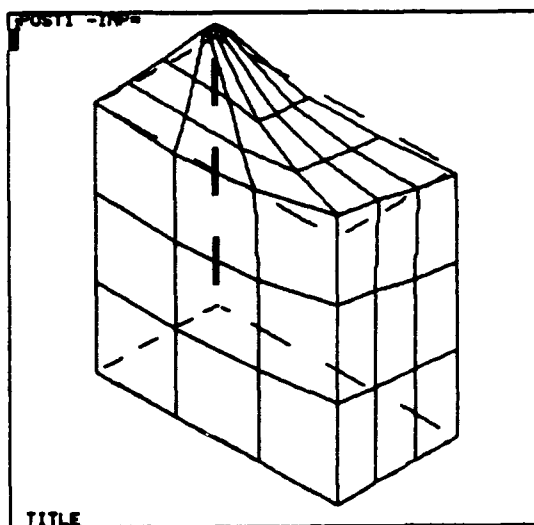
Secondary lateral mode

Figure 5
Modal Displacement Plots of a Rectangular Section 0.5% Composite
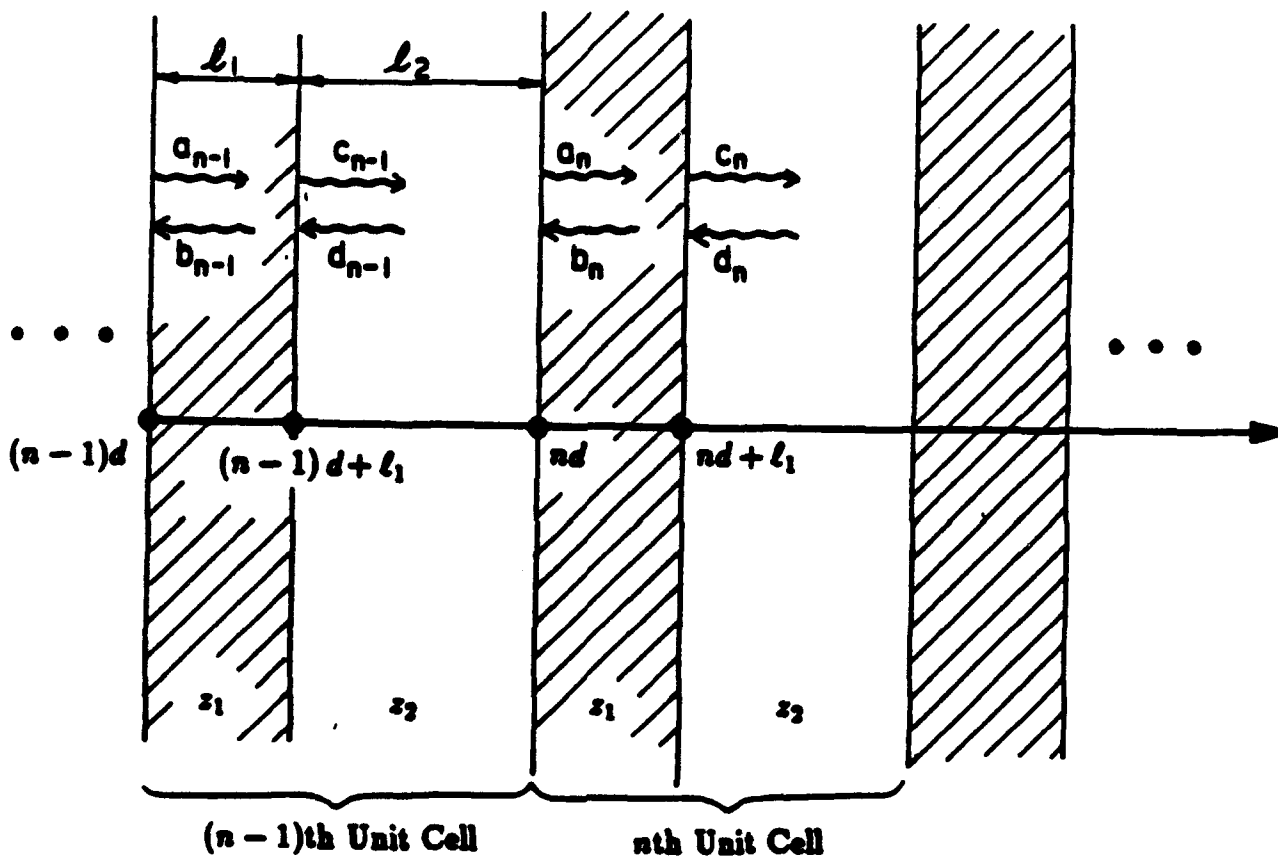
Figure 6
One-dimensional Layered Medium

16

where

$$A = \frac{1}{t_1 t_2} e^{i(k_1 \ell_1 + k_2 \ell_2)} - \frac{\gamma_2^2}{t_1 t_2} e^{i(k_1 \ell_1 - k_2 \ell_2)}$$

$$B = - \left[\frac{\gamma_1}{t_1 t_2} e^{i(k_1 \ell_1 + k_2 \ell_2)} + \frac{\gamma_2}{t_1} \left(t_1 - \frac{\gamma_1 \gamma_2}{t_2} \right) e^{i(k_1 \ell_1 - k_2 \ell_2)} \right]$$

(12)

$$C = \frac{\gamma_1}{t_1 t_2} e^{-i(k_1 \ell_1 - k_2 \ell_2)} + \frac{\gamma_2}{t_2} \left(t_2 - \frac{\gamma_1 \gamma_2}{t_1} \right) e^{-i(k_1 \ell_1 + k_2 \ell_2)}$$

$$D = - \left[\frac{\gamma_1^2}{t_1 t_2} e^{-i(k_1 \ell_1 - k_2 \ell_2)} - \left(t_2 - \frac{\gamma_1 \gamma_2}{t_1} \right) \left(t_1 - \frac{\gamma_1 \gamma_2}{t_2} \right) e^{-i(k_1 \ell_1 + k_2 \ell_2)} \right]$$

Using this information, it is possible to derive the Bloch wave dispersion characteristics using the following expression.

$$K = \frac{1}{d} \cos^{-1} \left[\frac{1}{2}(A + D) \right]$$

(13)

Additionally, the transmission coefficient of a wave transmitted through a stack containing numerous layers may be derived. Assuming that there is no reflection from the last layer (propagation medium), $b_n = 0$. Hence the following expression is obtained.

$$\begin{pmatrix} a_0 \\ b_0 \end{pmatrix} - \begin{pmatrix} A & B \\ C & D \end{pmatrix}^n \begin{pmatrix} a_n \\ 0 \end{pmatrix}$$

(14)

Therefore

$$\frac{a_n}{a_0} = \frac{1}{A'}$$

where A' corresponds to the element in the A position in the nth power matrix, evaluated from Eq. (12) for the specified Bloch wave solution. This technique permits the lateral transverse wave propagation characteristic to be evaluated for a diverse range of ceramic/polymer configurations.

17

The most promising method identified for the suppression of undesirable lateral periodic resonances involves the use of diverse dimensions (distributed periods) between ceramic pillars. In this report recent theoretical and experimental work is reviewed. Some of this work has recently been published [3].

(a) Results Obtained Using Modeling Techniques

It has been established that the degree of attenuation experienced by laterally propagating waves in a 1:3 composite structure is a function of the variance in the distribution used to determine pillar spacings [1]. The attenuation is also a function of volume fraction and it should be noted that variance may be applied to a) the pillar cross-sectional dimensions, b) the inter-pillar spacing, or c) both a) and b) simultaneously. Alternatively, diversity of material characteristics may be introduced—e.g. as alternating slices filled with hard and soft polymers.

Figure 7 illustrates the dependence of wave attenuation on frequency through a 400 layer 10% one dimensional composite comprising layers of PZT-5H and HYSOL RE 2039 epoxy. The regular device consists of 0.2 mm ceramic strips with 1.8 mm polymers strips between them. It is immediately apparent that increasing variance (applied simultaneously to both ceramic and polymer dimensions) results in increasing wave attenuation. Using the same basic geometry, a comparison is made between the effect of applying a 25% variance only to the ceramic and then only to the polymer. Notice that, if the composite is manufactured using the "slice and fill" technique, then it is normally simpler to apply variance to the pillar dimensions since the saw kerf is restricted to the blade width—assuming single saw passes with one blade size. Figure 8 indicates that for this geometry a far greater attenuation effect is obtained by applying variance to the polymer. Since the polymer dimension is greater, and the speed of sound slower in the polymer, with respect to the ceramic, a given percentage change in the dimension of the polymer will result in a greater phase shift.

If the opposite end of the volume fraction range is now considered, different results are obtained. Figure 9 illustrates the relative effects of 25% variances applied separately to the ceramic and polymer phases. In this case applying variance to the ceramic dimension has a greater effect since the wave is within the ceramic phase for a greater proportion of the time. An alternative simple procedure for disrupting the stopband/passband
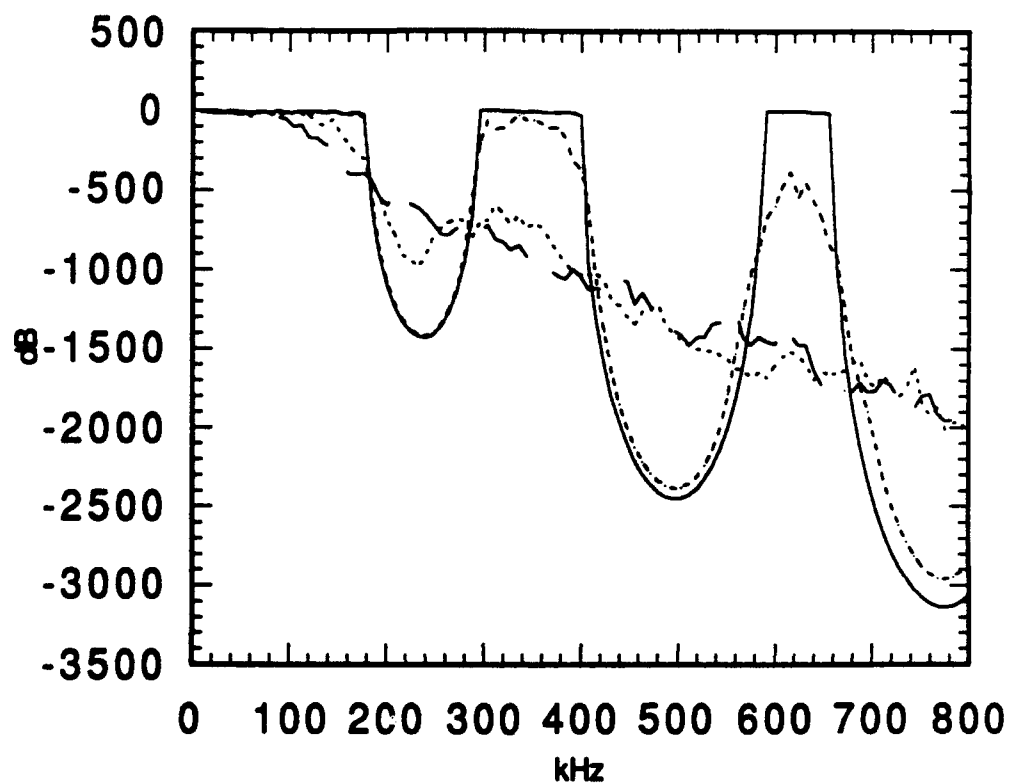
Figure 7

Lateral transmission through a 400 layer structure of alternating PZT-5A ceramic and Hysol RE 2039 epoxy.
Single period (0.2 mm ceramic, 1.8 mm polymer) ————————
5% Variance in dimensions of both phases ———————————·
25% Variance in dimensions of both phases ···············
50% Variance in dimensions of both phases — —— —
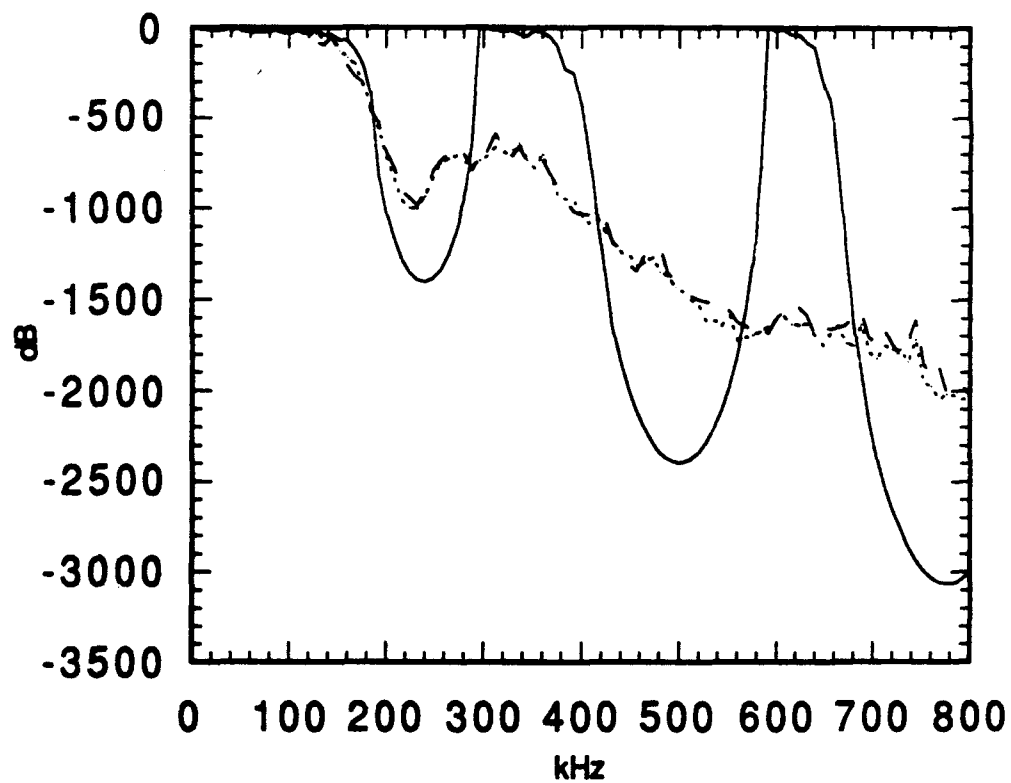
Figure 8

Lateral transmission through a 400 layer, 10%, structure. Variance applied to different phases

25% Variance applied to ceramic dimensions ————————

25% Variance applied to polymer dimensions ·················

25% Variance applied to dimensions of both — — — — — —
   ceramic and polymer
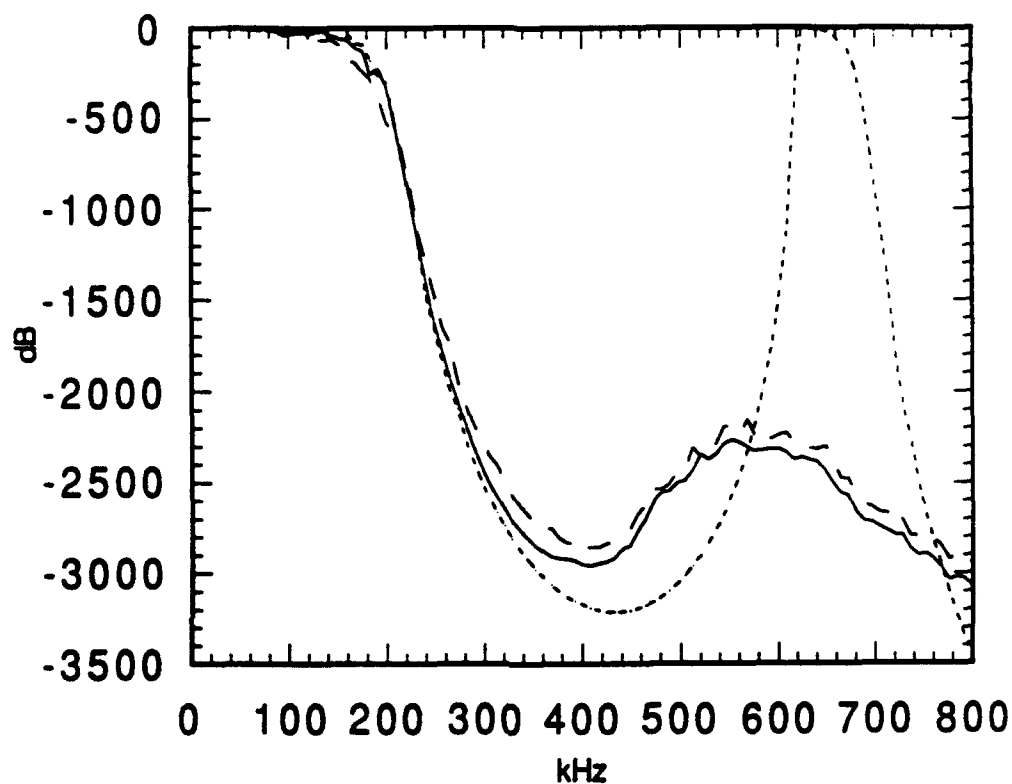
Figure 9

Lateral transmission through a 400 layer, 90%, structure. Nominal dimensions: 1.8 mm
PZT-5A ceramic and 0.2 mm Hysol RE2039 epoxy.

25% Variance applied to ceramic dimensions   ————————

25% Variance applied to polymer dimensions   ·················

25% Variance applied to dimensions of both   — — — — —
    ceramic and polymer

21

characteristics of a regular composite structure is to introduce dual periods rather strictly random periods. This would be simpler to fabricate than using a complete distribution of dimensions. Figure 10 compares the attenuation characteristics of a regular 10% structure, composed of 0.2 mm ceramic strips, and a structure with 0.1 and 0.3 mm thick ceramic strips. The pass- band still exists when the dual period geometry is employed but has been fairly effectively broken. Since a real device possesses significant losses, which are not included in the present model, one would expect that the distortion of the passband of a practical device to be more extreme.

It is possible to achieve a similar effect by filling alternate sawn slots with polymers with quite different elastic properties. In practice, every second slot would be formed and the structure filled with one polymer. In a second operation, the second sequence of slots would be formed, and these filled with the other polymer. Hence, no extra sawing is required but an extra polymer cure interval is added to the manufacturing process. Figure 11 illustrates the disruption of the pass band achieved in 10% composite with 0.2 mm ceramic slots, where alternating polymer strips with wave velocities different by a factor of two are utilized.

On the basis on the limited theoretical work presented here, it is evident that the amount of attenuation encountered is a function of volume fraction, variance characteristics and material characteristics. For a given variance fraction, a greater attenuation effect is achieved if it is applied to the phase in which the wave spends most time (i.e. phase for which dimension/velocity is greatest).

(b) Results Observed in Practical Transducers

At present, theoretical analysis of distributed period composites is limited to one dimensional examples. However, experimental tests of the effect of employing distributed periods in two dimensions has been performed. Some one dimensional samples were manufactured but a more visible effect was observed in the two dimensional samples. Furthermore, one dimensional composites are not encountered in practice to any noticeable extent. Figure 12 illustrates a 50% ceramic volume fraction composite. Both devices have mean ceramic pillar cross-sectional dimensions of 0.7 mm, but the distributed dimension device has a 25% variance applied to the ceramic dimension, across the structure in both X and Y directions. Figure 13 illustrates the measured impedance magnitude spectra of these

22
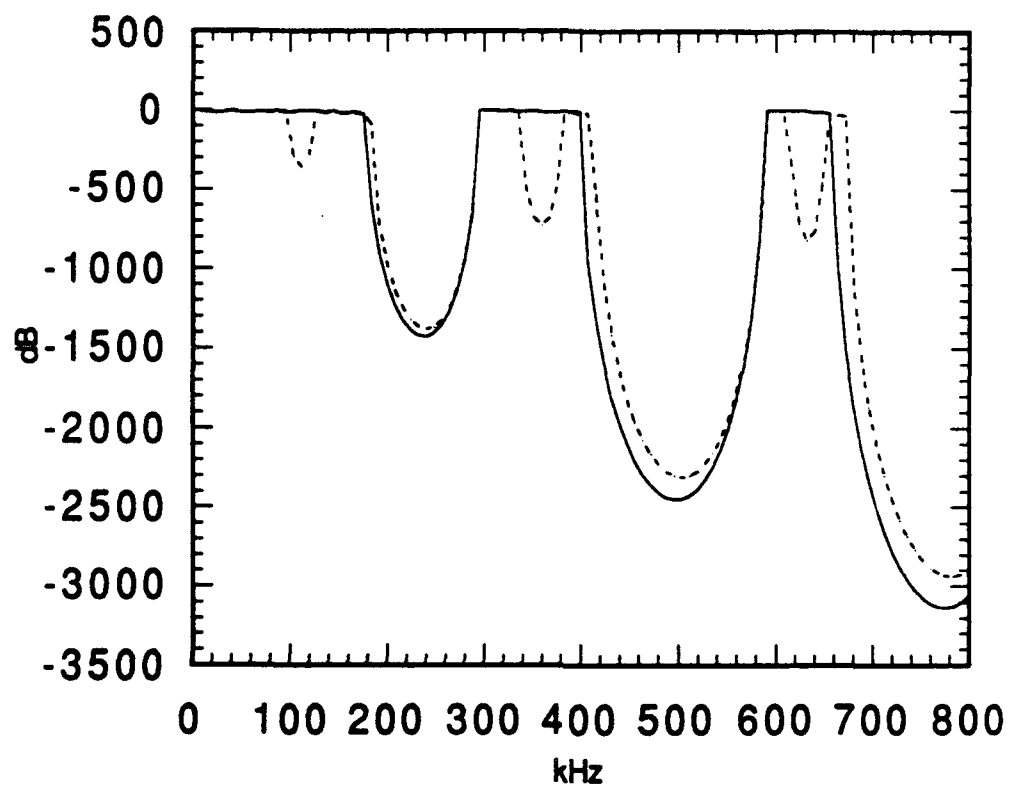
Figure 10
Lateral transmission through a 400 layer structure
Single period (0.2 ceramic, 1.8 polymer) ————————
Double period (0.1/0.3 mm ceramic, 1.8 mm polymer)--------------
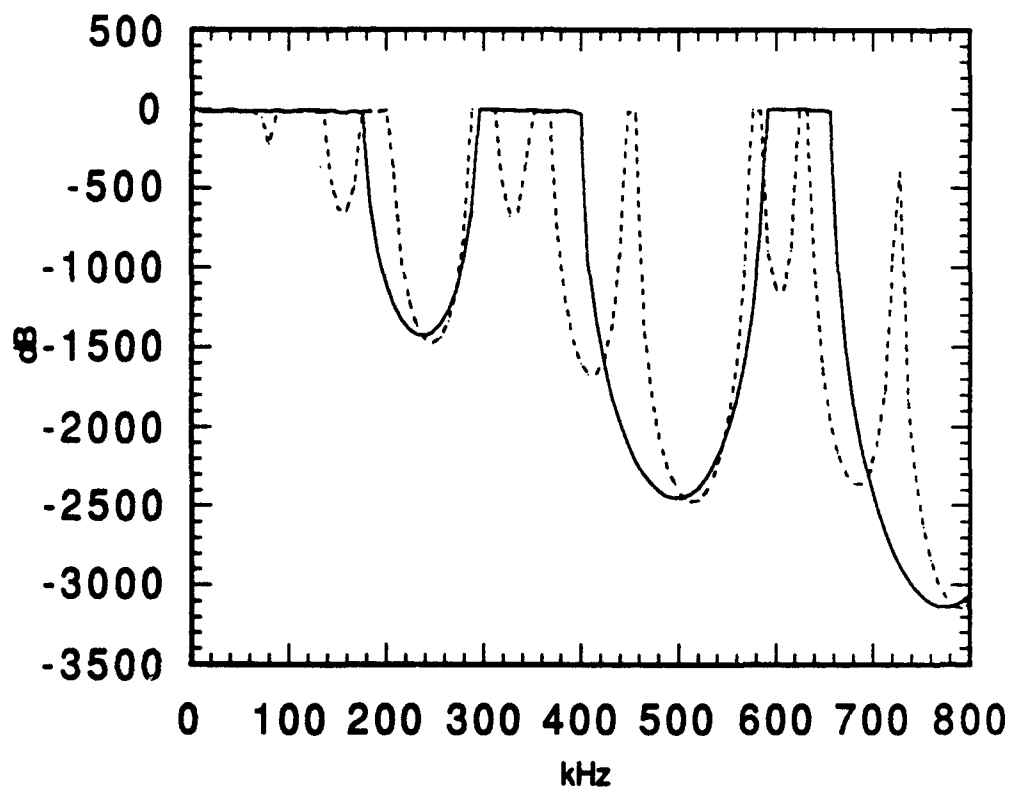
Figure 11
Lateral transmission through a 400 layer structure
Regular structure (0.2 mm ceramic, 1.8 mm RE2039 polymer) ——————————
Multi-polymer (0.2 mm ceramic, 1.8 mm alternating RE2039 polymer ---------------
and a polymer with wave velocity half that of RE2039)

24
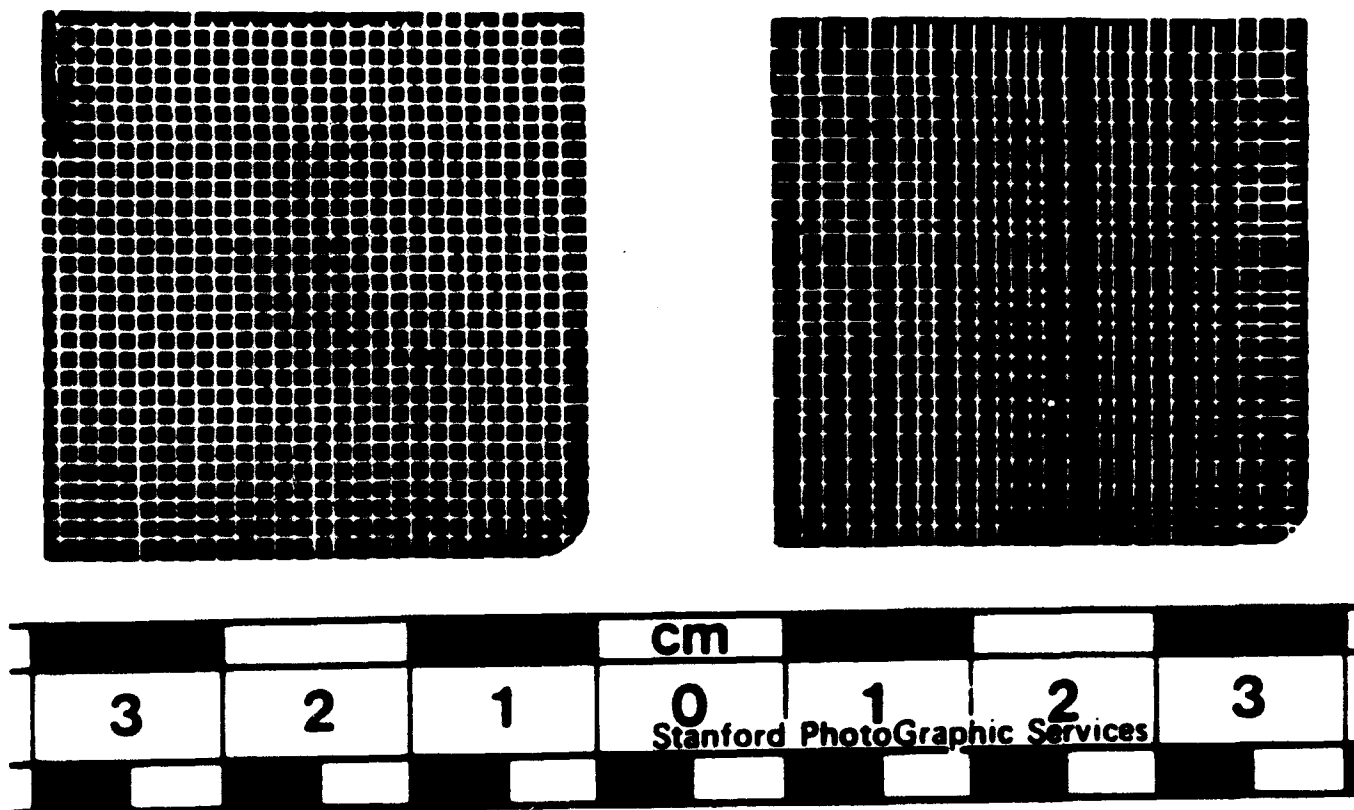
Figure 12
Single Period and Distributed Period (25% Ceramic Dimension Variance) 50% Composite
Transducer.
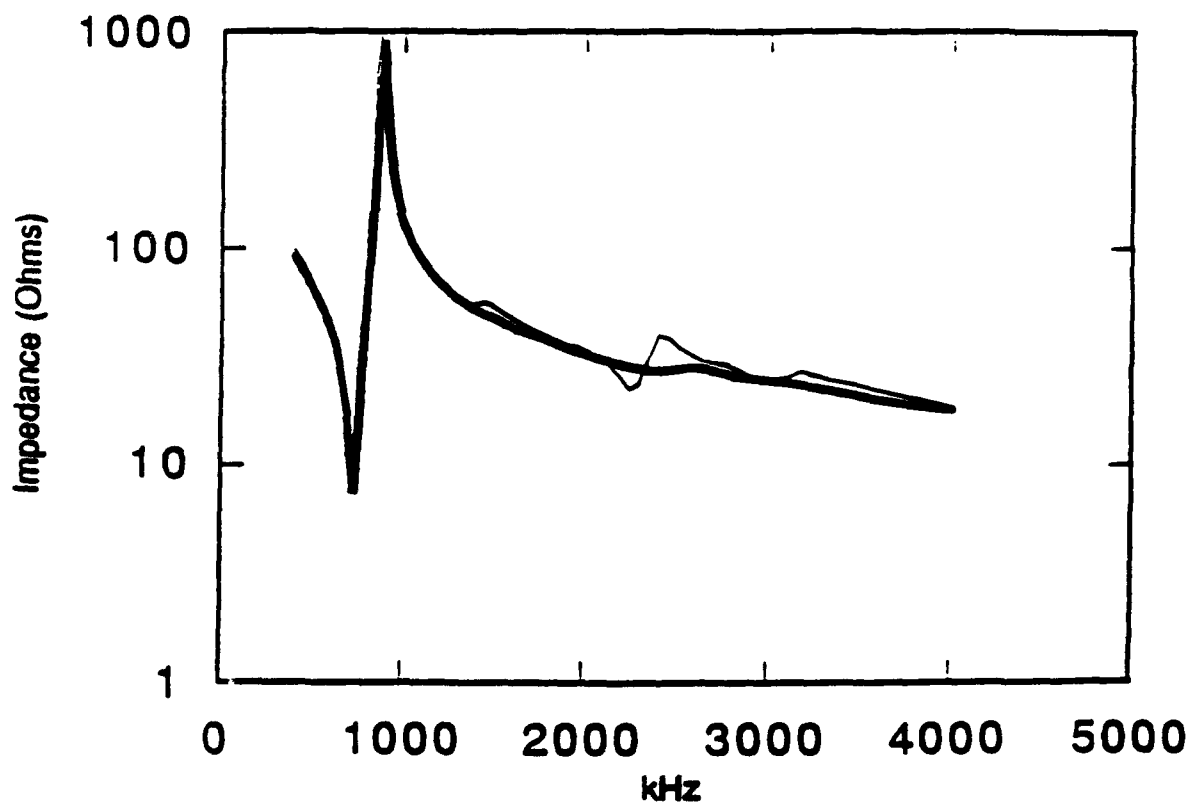
Figure 13
Measured impedance magnitude of 50% composite transducer

Single period _____
25% ceramic variance ▬▬▬▬▬▬

transducers. A reduction in spurious resonant activity is clearly evident. A second pair of transducers, with a 10% volume fraction, were also tested. In this case the transducer with a 25% variance in the polymer dimension also demonstrates reduced spurious resonant activity. This is illustrated in Fig. 14.

Figure 15 illustrates results obtained for 25% ceramic volume fraction composites with single and double-periodic structures. The single period structure has ceramic lateral dimensions of 1.0 mm, and the double period structure dimensions of 0.4 and 1.2 mm alternately. Significant suppression of a strong spurious mode in the vicinity of the thickness mode is evident.

It has been theoretically and experimentally demonstrated that distributed period and double period dicing of 1:3 composites is effective in suppressing spurious (bandedge) resonances. This eliminates the need for very fine dicing in order to shift the modes to higher frequencies. However, overall transducer performance must still be optimized by judicious choice of ceramic volume fraction and mean pillar width-to-height ratio.

3. 0:3 COMPOSITE TRANSDUCERS

0:3 Composite transducers, comprising microscopic piezoceramic particles dispersed in a polymer matrix, have proven particularly difficult to model in a quantifiable manner. As discussed in the interim report [1], most researchers have employed the "cubes" model, or a "modified cubes" model [4]. These are clearly inadequate since the geometries on which they are based are totally unrelated to those encountered in practice. Consequently this model has been largely disregarded in the current work.

A review of experimental observations regarding the dependence of 0:3 transducer performance on manufacturing details has been made. It has become plainly evident that the best results are obtained using a tight packing of globular grains of ceramic. This geometry implies that a ceramic volume fraction of 60 - 65% be used. Devices with volume fractions below this range do not work satisfactorily because of the presence of insulating layers of polymer between the particles. It is physically impossible to construct a 0:3 composite, with a random packing of particles, which has a volume fraction greater than approximately 65%. Hence, it is only relevant to consider this narrow practical volume range. However, during the transition from a suspension of particles in the polymer, to a structure
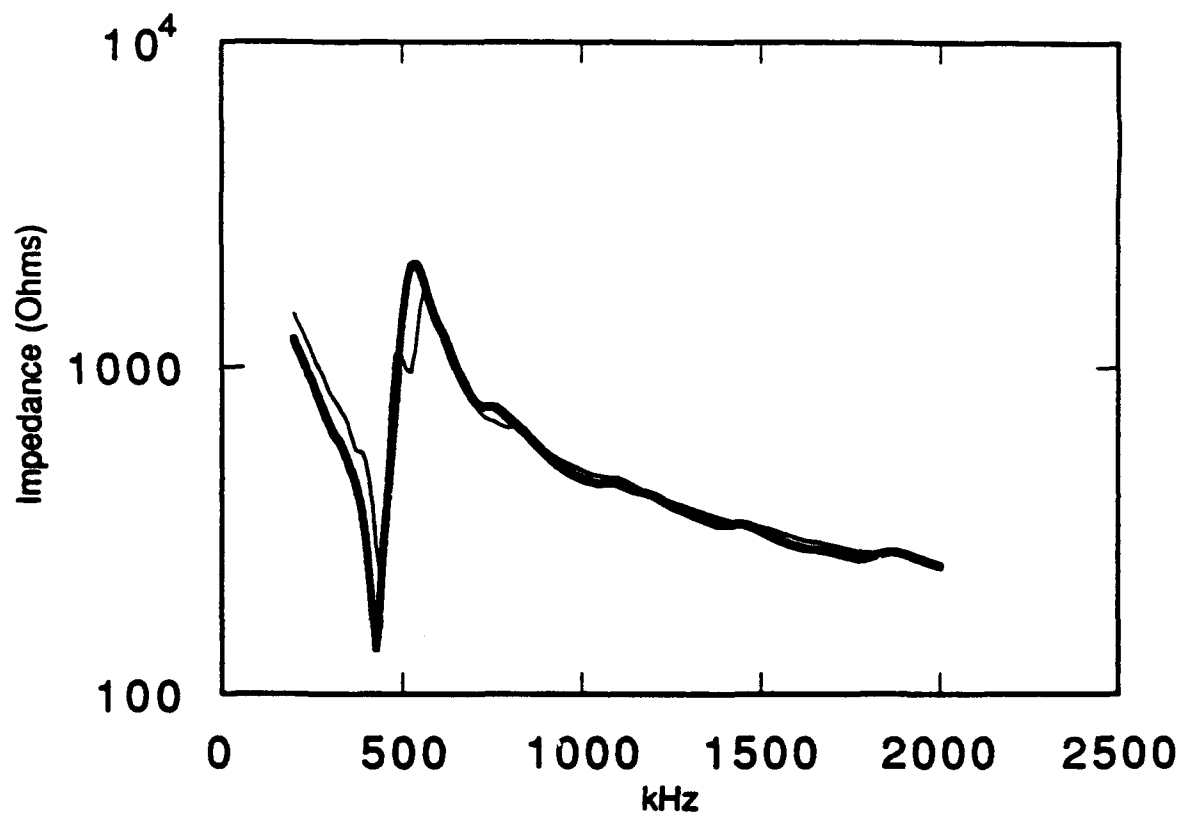
Figure 14

Measured impedance magnitude of 10% composite transducer

Single period ──────────

25% polymer variance ▅▅▅▅▅▅▅▅
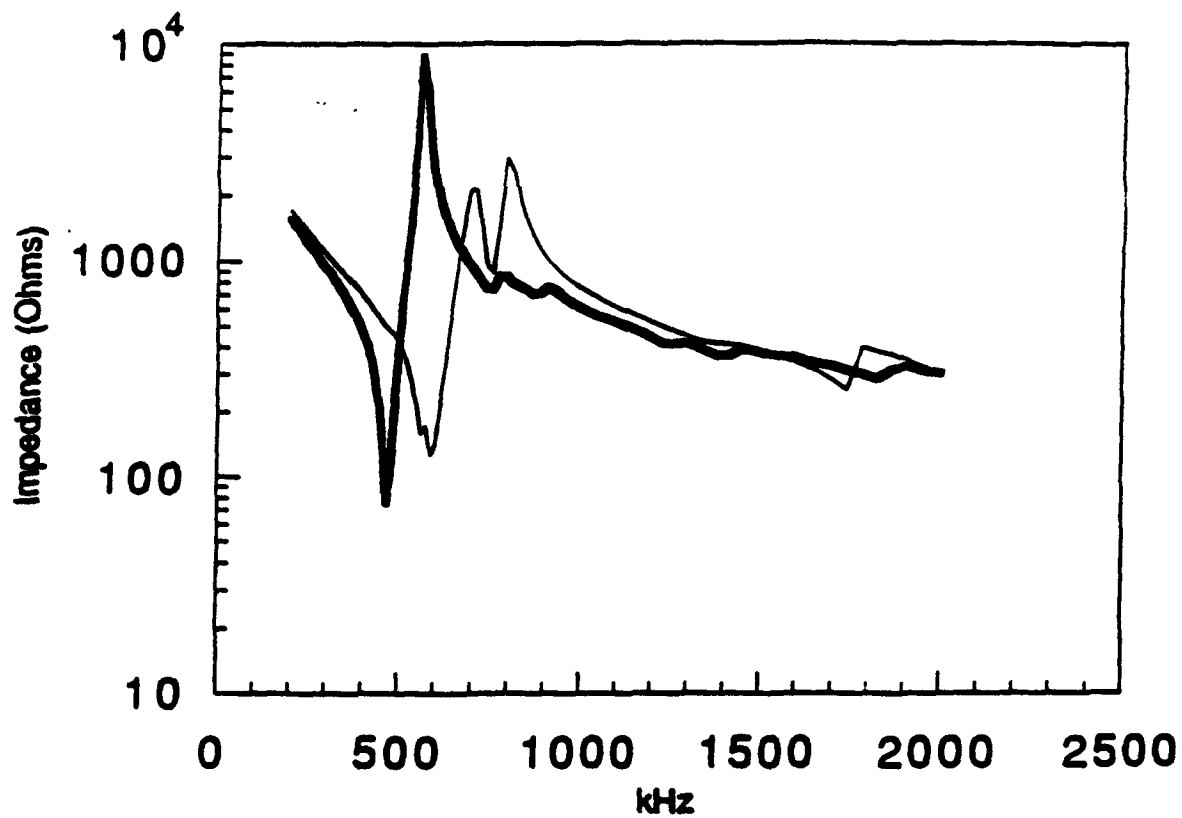
Figure 15
Measured impedance magnitude of 25% composite transducer

Single period ————————
Double period ████████████

29

comprising an interlocking matrix of touching particles, the net properties switch from being dominated by the polymer's properties to being a complex function involving principally the properties of the ceramic particles.

3.1 New Theory for the Effective Medium Properties of 0:3 Composites

The effective medium properties of a packing of spheres is a function of the number of points of contact and the conductance of each contact. The area of particle contact is a function of applied pressure and the elastic properties of the particles. Equations relating these factors have been combined to yield one equation expressing effective medium properties (thermal conductivity, electrical conductivity, permitivity etc.) as a function of all of these factors.

Nomenclature:

a	Radius of particle
r	Radius of circular area of contact between adjacent particles
p	Number of points of contact per particle
k	Electrical conductivity, or thermal conductivity, or dielectric permittivity
k^*	Effective conductivity of the packing
k_m	Conductivity of the matrix
k_p	Conductivity of the particles
H'	Nondimensional conductance of each interface
H	Dimensional conductance of each interface (units 'S' in the case of electrical conduction)
V	Potential across interface
E	Young's modulus of elasticity of each particle
F	Force pressing adjacent particles through the axis which joins their centers
P_h	Hydrostatic (omnidirectional) pressure upon packing
ϕ	Particle volume as a fraction of total packing volume
σ	Poisson's ratio of the particles

In the case of a piezoelectric ceramic powder/ polymer composite, the ceramic has a far higher dielectric permittivity, electrical conductivity and bulk elastic modulus than the polymer phase. Therefore, when any of the simple models for the net effective properties

30

of composite materials are used [5,6,7], a wide gap exists between the upper and lower theoretical bounds. Experimental evidence suggests that the actual properties do not fit with any of the limiting bounding cases. Previous modeling of this type of transducer had typically involved using a "cubes" or "modified cubes" model [4]. This involves a simple elastic analysis of a ceramic cube, or cuboid, surrounded by a thin film of polymer. The aspect ratio of the cuboid was modified until a match between theory and experiment was achieved. The requirement for an improved strategy is readily apparent. The approach presented here is far more realistic. It is based on a quantitative analysis of the particle-particle interactions in a randomly oriented packing of isotropic spherical particles of uniform size. Although practical piezoelectric composites are not composed of particles possessing such a regular geometry, the analysis is of value since it highlights important factors concerning particle properties, the number of points of contact and the containing pressure. Furthermore, a comprehensive analysis of various transducer designs indicates that a close packing of approximately spherical particles, with a narrow size distribution, is a highly desirable design objective [8,9,10]. Although the methodology outlined below is capable of quantitative analysis when all the constituent parameters are known, it is probably of more immediate value as a means of understanding the qualitative relationship between the effective medium properties and the various factors which influence these properties.

It is known that the physical properties of electrical conductivity, thermal conductivity and dielectric permittivity are analogous [11]. Additionally, the bulk elastic modulus is loosely related. It is not related exactly, since in the elastic case an applied "potential" (stress) result in a 'flux' (strain) in perpendicular directions. This phenomenon does not appear in the conductivity and permittivity of the assumed isotropic media. Piezoelectric effective medium theory must, of course, assume anisotropic particles.

Batchelor and O'Brien [12] have considered the problem of conduction in a packed granular structure in detail. Their technique was developed for isotropic spherical particles of uniform size. Additionally, it was necessary to assume that the dielectric permittivity or conductivity of the particles was far greater than that of the matrix in which they are embedded. In the present case the permittivity of the polymer is approximately fifty times greater than that of the polymer and the conductivity is one thousand times greater.

Batchelor obtained an expression for thermal conductivity as a function of particle volume fraction, the number of points of contact per particle and the "conductivity" (non-

31

dimensional) per contact. This was obtained by summing the effects of all the contacts in a specific volume. Exact solutions were presented for geometrically ordered packings. However, for statistically random isotropic geometric structure with contact points uniformly distributed, the following expression was obtained.

$$\frac{k^*}{k_m} = \frac{1}{2} \phi \, H'$$
(15)

Batchelor asserted that if the flux through the contact area between touching particles was very large compared with that through the adjacent matrix, then the distribution of potential inside the particle is similar to that found in the velocity potential in irrotational flow of incompressible fluid through a circular hole in a plate. The total flux in this case is known [13].

$$H = 2 \, k_p \, V \, r$$
(16)

This value may be substituted for H' in Eq. (15). The "non-dimensional" flux term used in Eq. (15) may be converted into a real "dimensional" quantity using the following transformation presented by Batchelor [12].

$$H = p \, k_p \, V \, a \, H'$$
(17)

At this stage, if Eqs. (15) to (17) are combined, then the only unknown parameters are the radius of the contact surface and the number of point of contact per particle. The radius of the contact circle is a function of the force pressing adjacent particles together and their elastic properties. The radius of the contact circle may be evaluated using Hertz contact theory [14].

$$r = F^{1/3} \left(\frac{3 \, (1-\sigma^2) \, a}{E} \right)^{1/3}$$
(18)

Fortunately, the compressing force between adjacent particles may be expressed in terms of the hydrostatic (omnidirectional) pressure experienced by the packing. This is obtained by dividing the total force experienced by each particle due to hydrostatic pressure by the number of contact points and modifying the result to take account of finite particle volume fraction [15].

32

$$F = P_h \frac{4 \pi a^2}{p} \phi \qquad (19)$$

Consequently, Eqs. 15 to 19 may be combined to yield the following expression for the effective medium property.

$$k^* = k_p \left(\frac{\phi p}{\pi} \right)^{2/3} \left(\frac{3 P_h (1-\sigma^2)}{E} \right)^{1/3} \qquad (20)$$

From the analogy noted in [11], this general expression may be used to calculate the effective electrical conductivity, thermal conductivity or dielectric permittivity of a random packing as a function of particle volume fraction, the number of points of contact per particle, the applied hydrostatic pressure, elastic properties of the particles and the relevant "conductivity" of the particle phase. However, major restrictions still apply to feasible values for ϕ and p.

In ordered packings, the particle volume fraction may vary from 0.524 for a simple cubic array to 0.740 for a face centered cubic array. Also, the number of points of contact per particle varies from 6 for the simple cubic case to 12 for the face centered cubic case. Although the range of possible volume fractions, and number of points of contact appears wide, the range obtained for packings allowed to form randomly is surprisingly small. W. O. Smith et al [16] obtained a mean volume fraction of 0.64. He used a packing of lead shot which was soaked in acid. When the acid had evaporated, small rings of lead acetate on the surfaces of the spheres revealed the locations of points of contact. Upon breaking up the packing and counting these rings, the authors observed that the mean number of contacts per sphere was 9. W. O. Smith also proposed that the number of contacts was a linear function of volume fraction between the theoretical limits—i.e., 6 contacts per sphere at a volume fraction of 0.52, to 12 points of contact at a volume fraction of 0.74. G. D. Scott [17] observed that the volume fraction of a packing of uniform spheres varied from 0.60 to 0.64 depending on the extent of agitation. Bernal and Mason [18] observed a mean volume fraction of 0.62 using a technique similar to that of W. O. Smith et al [16], but using black paint instead of acid. The mean number of points of contact per sphere was found to be approximately six. The discrepancy between this result and that of W. O. Smith is perhaps due to slightly differing definitions of what "touching" means (i.e. physical contact or just close proximity). Since the present theory assumes that physical point contact exists before the application of hydrostatic pressure, the lower figure for the

33

number of contacts will be chosen here. It may be observed that while particle size was a factor in most of the preceding equations, it is not in Eq. (20).

It is reasonable to assume that the actual particle volume fraction is closely related to applied hydrostatic pressure. Marion et al [19] have performed an experimental investigation of the relationship between particle volume fraction and applied hydrostatic pressure in a packing of silver coated glass beads. This investigation produced the curve illustrated in Fig. 16. It is clear that for volume fractions in the range 0.63 to 0.65, hydrostatic pressure and particle volume fraction are linearly related. The transition from loose suspension to tightly bound packing is remarkably clear. The volume fraction at which this transition occurs, 0.63, matches that established by previous workers [16,17]. This relationship, like Eq. (20), is only valid for a very small range of volume fractions just above the critical packing density where the system forms a packing rather than a suspension. Assuming this relationship between particle volume fraction and applied pressure, the volume fraction, ϕ, in Eq. (20) may be replaced by, cP_h, where c is a constant of proportionality. Hence, the following proportionality expression is obtained.

$$k^* = c'P_h \qquad (21)$$

where c' is a constant of proportionality.

The effective conductivity is a linear function of applied hydrostatic pressure. Marion also measured the electrical conductivity of a packing of silver coated glass beads as a function of particle volume fraction and applied hydrostatic pressure. The result, illustrated in Fig. 17, indicates that conductivity is, to a close approximation, a linear function of applied pressure. It should be noted that this result was obtained using insulating beads with conducting coatings. Unfortunately, it was impossible to measure the conductivity of solid conducting beads since their conductivities are extremely high. Nevertheless, the conductivity measured here is dominated by the particle-particle contact mechanism and hence the result obtained still serves to validate the theory. Another convincing example of the validity of the above expression was the observation by Edison [20] that the electrical conductivity of a packing of carbon spheres is a function of applied pressure. This characteristic is used in carbon particle telephone microphones.

The accuracy of the model has been tested in a limited sense by considering published results for $PbTiO_3$ particle composites [8]. In this case, the ceramic volume
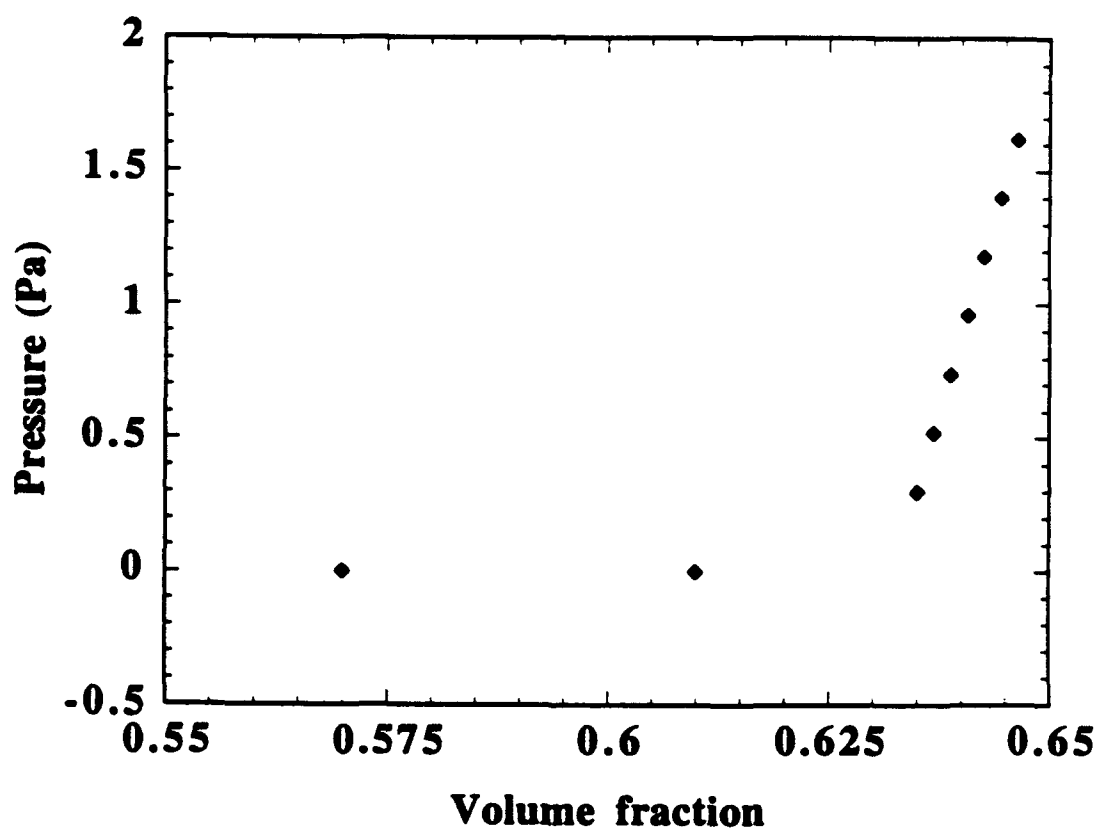
34

Figure 16
Dependence of hydrostatic pressure on particle volume fraction. Particles
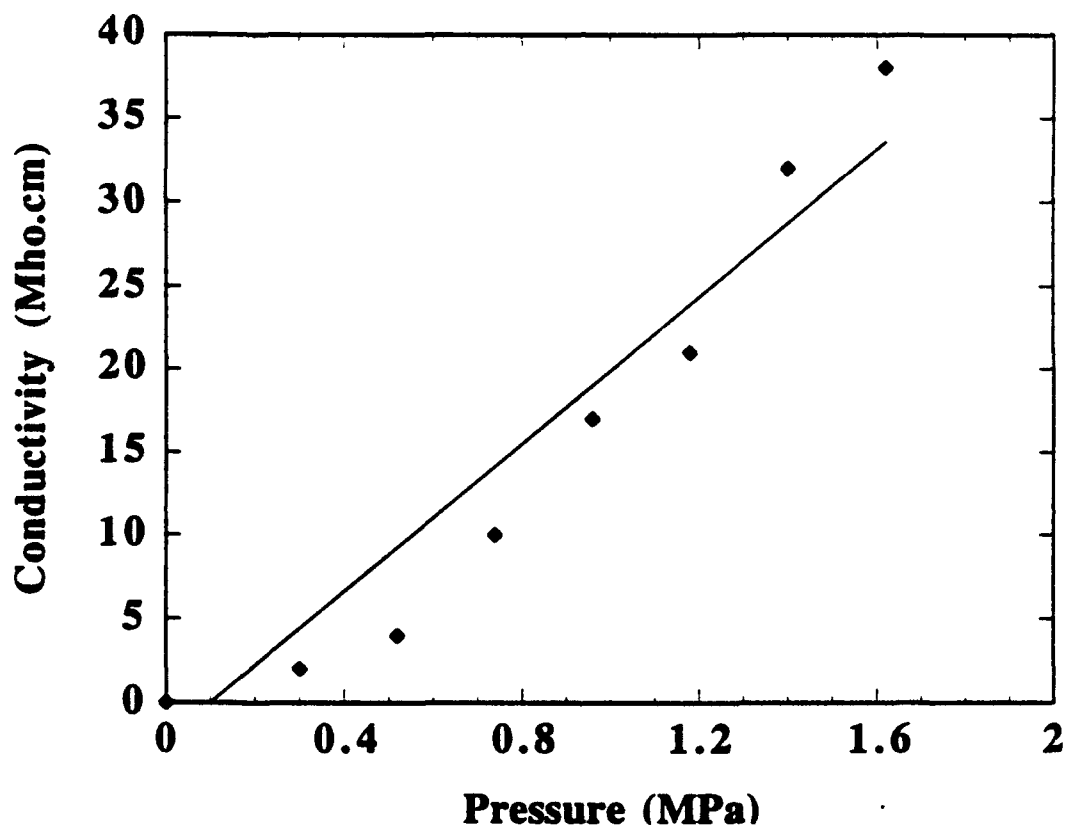are silver coated glass beads. Reproduced with permission of A. Nur.

35

Figure 17
Dependence of measured electrical conductivity on applied hydrostatic pressure for
a packing of silver coated glass beads. Reproduced with permission of A. Nur.

fraction was approximately 60% and the structure was formed under a pressure of 40 MPa. The Young's modulus of $PbTiO_3$ is 150×10^9 Nm^{-2} and its Poisson's ratio is 0.20. The relative permittivity of the pure ceramic is approximately 230. The Voigt model predicts a composite permittivity of 140 while the Reuss model predicts a permittivity of 12. A relative permittivity of 23 is predicted using Eq. (6). Although the observed permittivity (45) is significantly higher, this new model has produced a closer estimate than either the Voigt or Reuss models. Furthermore, no arbitrary "shape factor" has been employed, as is generally used in the conventional "modified cubes" model [7]. Ideally, the accuracy of the new model should be improved by attaining a better understanding of the number of contact points, and their areas, for cases where particles are not perfectly spherical and do have a finite size distribution.

An expression for determining the conductivity of a close random packing of high conductivity spheres has been developed. It takes account of all the key factors. These include particle conductivity, particle elastic properties, applied pressure, particle volume fraction and the number of points of contact per particle. The expression is valid only for a very limited range of particle volume fractions. However, this range encompasses those which are of most practical importance. Using an observed linear relationship between particle volume fraction and applied pressure, the expression correctly predicts the widely observed linear relationship between effective conductivity and applied pressure. The expression gives a limited insight into the parameters critical to the successful manufacture of piezoelectric ceramic powder composites. However, it is known that the physical mechanisms governing the permittivity in ferroelectric powders are rather complex [21]. For example, the permittivity near the surface of a ferroelectric particle is less than that in the interior. Additionally, the permittivity and piezoelectric coefficients of practical ferroelectric powders are a function of particle size. The technique employed here has assumed uniform properties independent of size. Incorporation of these phenomena, and development of effective medium models for elasticity and piezoelectricity, will require further exploitation of the principles presented here.

3.2 Observations Made Regarding Factors Crucial to 0:3 Composite Manufacture

The technical literature relating to 0:3 composite transducer design is now extensive. A short review, collecting generally observed factors relevant to successful manufacture, is presented.

37

The observation that a ceramic volume fraction in the range 60% to 70% is desirable is general [8,9,22,23]. Additionally, the best results have been obtained using particles which are rounded in shape and which possess a narrow distribution of size [10,24,25] Two techniques, which give similar net results, are available. The co-precipitation technique developed by Lee et al [10], involves mixing $Pb(NO_3)^2$, $TiCl_4$, H_2O_2 and NH_4OH into a solution. The precipitate is dried at 100° C and calcined at $800-900^o$ C to produce globular particles with a size of around $4\mu m$. The more common route to obtaining desirable particle characteristics involves quenching the ceramic immediately after calcination. The ceramic breaks down easily to virtually single domain crystallites due to the high strain ratio found in $PbTiO_3$ [25]. Composites manufactured using powder obtained by milling solid ceramic have, without exception, displayed inferior piezoelectric properties [22].

Figure 18 illustrates the particle size distribution obtained using the quenching technique [25]. Furthermore, the size of the particles may be controlled by altering the PbO content of the powder during calcination [25]. Giniewicz [24] also states that particle size may be controlled by varying firing temperature/time, or by doping the $PbTiO_3$ with Bi and Fe. NTK further improved the quality of their powder by etching it in an acid (eg HCl). This has the effect of dissolving very small particles (outside the desired size range), rounding any sharp particle corners and leaving the surfaces well prepared for wetting to the polymer [25].

There is general agreement that $PbTiO_3$ should be used as the ceramic phase. This is because of its low permittivity and high g_{33} compared to, for example, PZT. However, several different polymers have been used successfully. NTK use "Fluororubber," as described in detail in their patent [25]. Giniewicz [24], who has produced composites possessing $d_h g_h$ coefficients comparable to those of NTK, recommends the use of a soft polymer on the basis that it might better accommodate realignment of the domains during poling. Low viscosity is obviously desirable and Eccogel 1365–25 [26] has been used with success. Giniewicz recommends a thorough technique for mixing the phases [24]. The filler is passed through a sieve directly into the prepared polymer to prevent unnecessary agglomeration. The mixture is then shear blended using a broad flexible knife to maximize the degree of wetting between the ceramic and polymer.
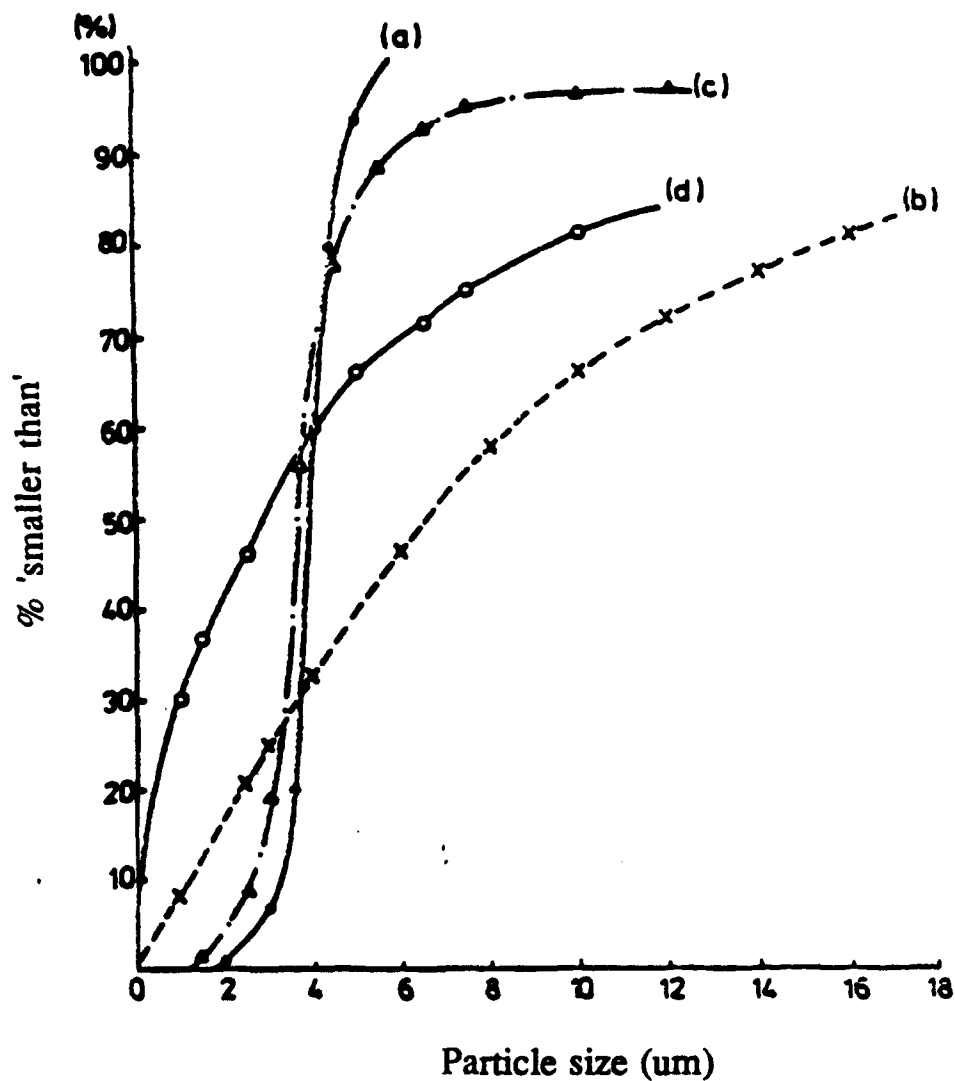
Figure 18
Particle size distribution obtained by NTK ("percentage particles smaller than")
(a) PbTiO₃ ceramic quenched directly from oven.
(b) PbTiO₃ ceramic allowed to cool, then milled.
(c) PZT ceramic quenched directly from oven.
(d) PZT ceramic allowed to cool, then milled.

39

The pressure used during formation of the composite prior to curing is also critical. Westinghouse [27] typically used low pressures of around 6 MPa. It is believed that their use of low pressure during formation, combined with the use of less than perfect ceramic particles, contributed to their major poling problems. NTK [25] claim to use a pressure of approximately 14 MPa. Amongst the numerous results obtained by Pennsylvania State University, the best dhgh results were obtained when the highest reported pressure was used. Lee et al [10] report obtaining a $d_h g_h$ coefficient of 4170×10^{-15} m^{2}N^{-1} when a pressure of 65 MPa was used to compress globular 4 μm particles obtained by the co-precipitation method.

After curing under pressure according to the temperature/time schedule recommended for the polymer, the composite is ready for electroding. The surfaces are generally lightly lapped to expose a bare ceramic surface. Generally, silver paint has been used [8,10] but NTK have successfully used a polymer loaded with carbon black, as described in detail in their patent [25]. A carbon loaded polymer (similar polymer to that within the composite) may have the advantages of greater robustness and temperature/ expansion compatibility with the composite material.

Generally, poling has been performed under the following conditions. A DC field of 75–100 kVcm^{-1} is applied for approximately 30 minutes while the sample is immersed in oil at 75°C–100°C [8,10]. The field should probably be ramped up and down over a short time interval. Since the transducer is essentially a capacitor, rapid fluctuations in voltage will result in current surges which do not help to align the domains but may result in damage in the form of electrical breakdown and/or thermal runaway. Corona poling has also been tried [28], but when directly compared with results obtained by conventional poling, the difference in d_{33} and ε_r is scarcely significant. However, in the case of corona poling, if breakdown occurs at one location, then poling of the rest of the sample may continue. In conventional poling, any breakdown will immediately short the entire high voltage electrode to ground and a destructive current surge will occur.

Various techniques have been attempted for improving poling efficiency. Sa-Gong et al [29] considered the effect of adding carbon, germanium and silicon fillers to the polymer. Since the conductivity of the ceramic phase is several orders of magnitude higher than that of the polymer phase, there is a danger that most of the applied poling field will be across the polymer phase. Typically the poling field used for a 0:3 composite is five times higher th n that which would be used across pure ceramic. Therefore, if there are

40

inconsistencies (eg agglomerations) in the composite structure, then localized fields which occur may be sufficient to cause breakdown. The addition of semiconducting fillers did ease poling but resulted in higher dielectric loss in the resulting material. However, the best results obtained were inferior to those obtained by Lee et al [10] who used no fillers. Giniewicz considered improving poling performance by doping the $PbTiO_3$ with Mn [24]. This has the effect of lowering the conductivity of the ceramic, and hence enhancing the field across the particles during poling. An improvement of 40% in $d_h g_h$ figure of merit was obtained. However, even this result is lower than that obtained by Lee et al [10]. In fact the d_{33} obtained by Lee is virtually identical to that observed in single phase $PbTiO_3$. This implies that almost ideal polarization has been achieved. It is concluded that Lee's method [10] is the best. Fortunately it is simple in that no special fillers are used and relies upon very high pressure formation using globular particles with a narrow size distribution.

Another process worthy of mention is the "fired composite" technique developed at Pennsylvania State University [28,30,31]. $PbTiO_3$ powder is prepared by the co-precipitation technique described by Lee [10]. Therefore, it can be assumed that the particles are globular and of narrow size distribution. The ceramic powder was mixed with PVA binder and pressed into pellets at extremely high pressure (140 MPa). The pellets were then placed in an oven and fired at temperatures of up to 900°C. The best results, in terms of highest d33, were obtained when the highest temperature was used [31]. In one case corona poling was employed and found to produce marginally better results than conventional poling [28]. In this case poling was performed prior to polymer impregnation. It was stated that corona poling was ineffective when performed on impregnated composites. It is hypothesized that a limited amount of breakdown occurred during corona poling due to the presence of air voids. This may have the beneficial effect of placing more of the applied field across the individual particles. Presumably, if conventional poling techniques are applied to unimpregnated composites, catastrophic breakdown will occur due to the rapid establishment of a low resistance, high current path between the high potential top electrode and the grounded electrode. Composite transducers manufactured using the "fired" technique generally have high volume fractions ranging from 65% to 70% —implying extremely compact particle-particle contact. Consequently, they could be poled at slightly lower fields (50 kVcm^{-1}). The highest dhgh figure of merit reported using the "fired" technique was 1750×10^{-15} m^{2}N^{-1}, which is less than half of that obtained by Lee [10]. However, this figure does not relate to a device formed at the highest (optimum) temperature.

The key characteristics relevant to successful manufacture have now been established. This section will conclude with a brief analysis of the importance of particle size. Relatively little quantitative comparable information is available. However, NTK PR306 and NTK PR305 have been compared by Banno [32]. PR306 is composed of particles approximately 1 μm across while PR305 is composed of 10 μm particles [33]. The large particle material (PR305) has a $d_h g_h$ figure of merit of 5084×10^{-15} m^2N^{-1} whereas the small particle material (PR306)has coefficient of 1160×10^{-15} m^2N^{-1}. The low pressure reception sensitivity of the larger particle material is 7dB higher than that of the other material. However, while the reception sensitivity of the small particle material is virtually independent of hydrostatic pressure, the g_h of the large particle material falls by approximately 25% as the pressure is increased to 10 MPa [32]. During the same pressure increase, the relative permittivity of the large particle material rises by 10% whereas the permittivity of the small particle material does not. It has been proposed that that the pressure instability of the large particle material is due to voids which collapse under high pressure [34]. Since it is generally desirable for the sensitivity of a hydrophone to be pressure independent and tolerant of multiple pressure cycling, the conclusion is drawn that smaller particles are preferable. Giniewicz [8] obtained reasonably pressure independent results using 5 μm particles. The composites were pressed at 40 MPa but allowed to cure at atmospheric pressure. An interesting observation may be made regarding the parameter pressure dependency illustrated in Fig. 19. As soon as pressure is applied a small jump in g_h sensitivity is observed. It is hypothesized that the particles are being pressed into better contact. The sensitivity declines very slightly with further pressure increase. Since d_h is constant over this range, the slight decrease in g_h must be due to increasing permittivity, which might also be related to particle contact. On release of pressure, g_h is generally lower than on the pressure increase cycle. This may be due to breaking particle-particle bonds. This data would suggest that high pressure should be used during formation and curing so that subsequent pressure cycling is negligible in comparison to that endured during manufacture.

In summary, the optimal results are obtained using $PbTiO_3$ powder formed by quenching or co-precipitation. The ceramic particles are globular in shape and have a narrow size distribution. The particles should be etched in acid to clean them, remove sharp corners and to eliminate small particles. The particles and the chosen polymer (Eccogel 1365-25 is adequate) are carefully blended and formed into tablets at high pressure (65 MPa) and cured. Conventional poling in oil at 75°C, in a field of 75-100 kVcm^{-1} for 30 minutes is sufficient to obtain characteristics competitive with the best available [10,32]
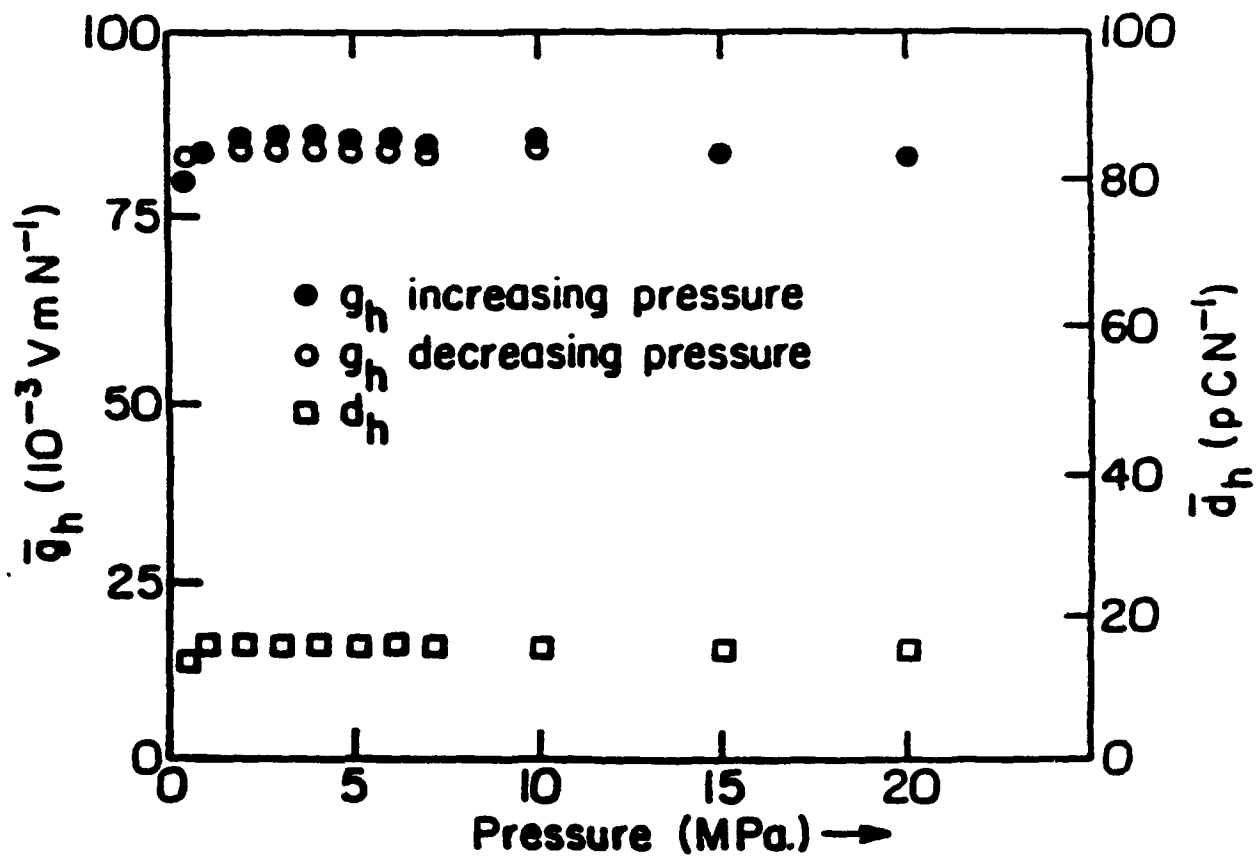
Figure 19
Hydrostatic Piezoelectric Coefficients, Observed by Giniewicz, as a
Function of Pressure

43

4. TRANSDUCERS COMPRISING MULTIPLE ACTIVE LAYERS

Nomenclature

F	Force (N)
h	Piezoelectric constant (N/C or V/m)
C_0	'Clamped' capacitance of transducer (F)
t_i	Wave transit time across layer 'i' (s)
V_S	Voltage across source (V)
V_i	Voltage across electrodes of transducer layer 'i'
Z_S	Electrical impedance of source (Ω)
Z_i	Mechanical impedance of layer 'i' (kgs^{-1} : ρvA ; A = area)
Z_F	Mechanical impedance of front load
Z_B	Mechanical impedance of back load
s	Laplace operator (Bar symbol denotes Laplace quantities).

Thickness mode, backed and matched, piezoelectric transducers perform a central role in medical ultrasound, non-destructive examination and high frequency sonar applications. However, transducer performance is frequently a factor limiting ultimate system performance. The concept of using multiple active layers provides the potential for simultaneously enhancing both bandwidth and sensitivity. It offers the prospect of optimized transducer performance, and takes advantage of recent hardware developments that have, in many ways, resulted in an imbalance between transducer and processing hardware technologies.

Conventionally, the thickness mode transducer has been composed of a single piezoelectric layer and one, or more, matching layers serving as a passive piezoelectric transformer. It has recently been proposed that the matching layer should also be piezoelectric and that voltage functions be applied to it in order to further enhance the sensitivity and bandwidth of the transducer [35,36]. The configuration of the new transducer is illustrated in Fig. 20. Of particular importance is the ability to design a transducer with a finite output at a frequency where normally a null would exist. Previous work [35,36] concentrated on the transmission characteristics of multiple layer transducers in which independent stimulation was applied to each layer. These techniques are briefly reviewed. This section concentrates on the design of multiple layer transducers as receivers. The performance of a multiple layer transducer in the reception mode is critically dependent on optimal design. However, the same

44

Layer 1   Layer 2

A1 | A2   AF

BB

B1 | B2

Backing   Load

0   1   2

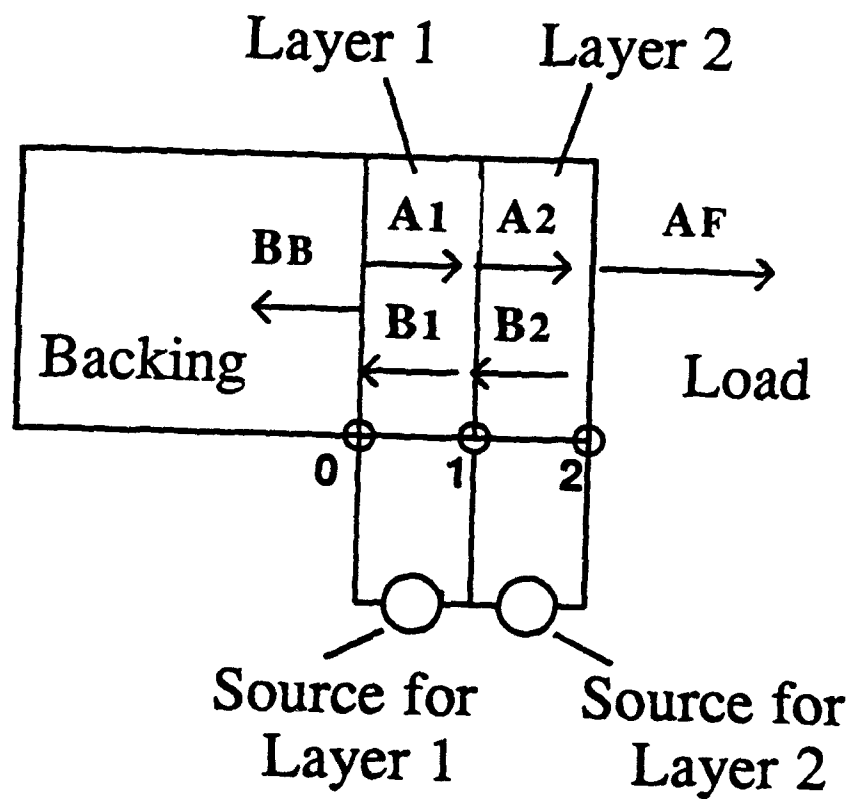Source for   Source for
Layer 1   Layer 2

Figure 20
Configuration of the new double active layer transducer. The particle displacement
functions within each layer are defined.

benefits of enhanced sensitivity and bandwidth are achievable. Hence, high performance pulse-echo operation is feasible. Additionally, the stability of the technique with respect to deviations in actual design parameters is investigated.

4.1 Transmission

Two configurations are considered. In the "active matching layer" scheme the input to the principle active layer (layer 1) is pre-defined. A Laplace domain matrix technique, based on that described by Lewis [37], has been used. For the case of a two layer system, where the excitation voltages are specified, one obtains the matrix problem illustrated in Fig. 21 [36]. Notice that the known quantities (input voltages) are on the right hand side and the known quantities (output displacements) are on the left hand side. In the "active matching layer" case, the output force and the excitation to layer 1 is defined. The voltage required across layer 2, in order to satisfy the physical constraints on the system, must be established. The matrix is altered to obtain the solution to this problem by exchanging the positions of the relevant quantities in the matrix (enclosed in boxes in Fig. 21). It should also be noted that by placing a quantity pertaining to the incident force on the right hand side, it is possible to obtain the received open circuit voltage response across each layer [36].

In the "optimized excitation" technique there is no need to pre-specify the excitation of any layer. Only the required output force is specified. Although the result is a multiple input, single output problem, with an infinite number of solutions, an optimized solution is established.

Since we are dealing with a linear system, the total force output, in the Laplace domain, may be expressed as follows

$$\bar{F} = \bar{\beta}_1 \bar{V}_1 + \bar{\beta}_2 \bar{V}_2 + \text{.......} \bar{\beta}_n \bar{V}_n \qquad (22)$$

where "n" is the number of layers, and the β_i's are the transfer functions between the applied voltages and the output force.

The quantity β_1 may be obtained by measuring F when $V_1 = 1.0$ and $V_i = 0.0$, $i = 2$ to n. β_i, $i = 2$ to n, may be evaluated in a similar manner. If one considers a circuit analogy model for the transducer system, this is simply a use of the principle of current superposition.

46

$$
\begin{bmatrix}
1 & -1 & -1 & 0 & 0 & 0 \\
s\,Z_B & s\,Z_1+G_1(R_1^{-1}-1) & -s\,Z_1+G_1(R_1-1) & 0 & 0 & 0 \\
0 & R_1^{-1} & R_1 & -1 & -1 & 0 \\
0 & -s\,Z_1+G_1(R_1^{-1}-1) & s\,Z_1+G_1(R_1-1) & s\,Z_2+G_2(R_2^{-1}-1) & -s\,Z_2+G_2(R_2-1) & 0 \\
0 & 0 & 0 & R_2^{-1} & R_2 & -1 \\
0 & 0 & 0 & -s\,Z_2+G_2(R_2^{-1}-1) & s\,Z_2+G_2(R_2-1) & s\,Z_F
\end{bmatrix}
\begin{bmatrix}
B_B \\ A_1 \\ B_1 \\ A_2 \\ B_2 \\ A_F
\end{bmatrix}
=
\begin{bmatrix}
0 \\ -h_{S1}C_{o1}V_1 \\ 0 \\ h_{S1}C_{o1}V_1 \\ -h_{S2}C_{o2}V_2 \\ 0 \\ h_{S2}C_{o2}V_2
\end{bmatrix}
$$

Where

$$G_i = h_i\, h_{Si}\, C_{oi}$$

$$R_i = \exp(st_i)$$

$$h_{Si} = \frac{h_i}{1 + s\, C_{oi}\, Z_{Si}}$$

A_1 and B_1 etc. are coefficients of particle displacement as described in Fig. 1

Figure 21
The governing matrix for the double active layer transmitter example. Known quantities (inputs) are on the right, and unknown quantities (outputs) are on the left. If required, the matrix elements may be rearranged.

47

The net current in the output loop is the sum of those due to the voltage sources considered independently.

For the sake of simplicity, let $V_i = 1.0\ \angle 0°$, $i = 1$ to n. Then, Eq. 22 reduces to

$$F = \beta_1 + \beta_2 + ... \beta_n \tag{23}$$

or

$$|F|\angle\theta = |\beta_1|\angle\theta_1 + |\beta_2|\angle\theta_2 + ... + |\beta_n|\angle\theta_n \tag{24}$$

At this point, the discussion will be limited to the two layer case. The phasor quantities, β_1 and β_2, are represented graphically in Fig. 22. Force output, $|F|\angle\theta$ is maximized if $\theta_2 = \theta_1$. In this case $\beta_1 V_1$ and $\beta_2 V_2$ are in phase and form a straight line when summed. This may be achieved by adjusting the phase angle of V_2 to compensate for the phase difference between β_1 and β_2. The desired result is obtained by setting $V_2 = V_1\ \angle(\theta_1 - \theta_2)$. Hence, for this configuration, Eq. 24 becomes

$$|F_M|\angle\theta_1 = (|\beta_1|\angle\theta_1)(|V_1|\angle 0°) + (|\beta_2|\angle\theta_2)(|V_1|\angle(\theta_1 - \theta_2)) \tag{25}$$

where F_M is the maximized value of output, F. Equation 25 represents the optimized 'transfer function' of the system.

Suppose that the desired output is $|F'|\angle\theta'$. This is obtained by multiplying Eq. 25 throughout by $\dfrac{|F'|\angle\theta'}{|F_M|\angle\theta_1}$.

Equation 25 then becomes

$$|F'|\angle\theta' = (|\beta_1|\angle\theta_1)(|V_1|\angle 0°)\underbrace{\frac{|F'|\angle\theta'}{|F_M|\angle\theta_1}}_{V'_1} + (|\beta_2|\angle\theta_2)(|V_1|\angle(\theta_1-\theta_2))\underbrace{\frac{|F'|\angle\theta'}{|F_M|\angle\theta_1}}_{V'_2} \tag{26}$$

In this way, the excitation functions, V'_1 and V'_2 are obtained. Their time domain counterparts, $V'_1(t)$ and $V'_2(t)$, are obtained using an inverse FFT.

48

Figure 22

Phasor diagram illustrating β_1 and β_2, and the effect of phasing β_2 by multiplying it by $1.0 \angle (\theta_1 - \theta_2)$ and adding to β_1.

49

In this way, the excitation functions, V'_1 and V'_2 are obtained. Their time domain counterparts, $V'_1(t)$ and $V'_2(t)$, are obtained using an inverse FFT.
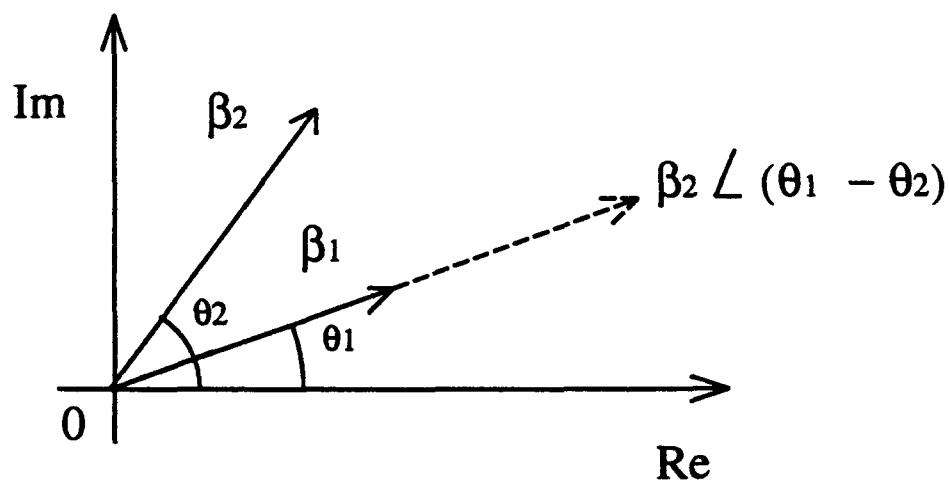
The nature of the optimized "transfer function" of a double layer transducer is a function of its design. Clearly, a wide smooth response is desirable. Figure 23 illustrates the optimized "transfer function" of Transducers A and B. (The transducer designs are described in Appendix II.) The responses obtained for the cases where the phase angle between the excitation functions of layers 1 and 2 were kept equal to zero are shown for comparison. In the case of both transducers, a significant output is achievable at the second harmonic frequency simply by using the optimized phasing technique. It is readily evident that a smoother, and more desirable, response has been obtained using Transducer B, which is more heavily acoustically dampened. If one considers that both sensitivity and bandwidth are quantities which are to be maximized, then one can use the integral of sensitivity with respect to frequency as a useful figure of merit. When the integrals of the curves illustrated in Figure 23 were calculated, it was found that by using optimum phasing, as opposed to zero phasing, the figures of merit of both Transducers A and B were increased by approximately 90%.

The transmission characteristics of Transducer A were measured experimentally. The response was measured in the far field (range = 200 mm) using a sensitive hydrophone [38] possessing a hydrophone/ pre-amplifier sensitivity of –222 dB (0 dB = 1 V/μPa). For comparison with experiment, it was necessary to include the effect of diffraction on the theoretical pressure response emanating from the transducer face. The transducer's diffraction impulse response was calculated for this geometry [39] and convolved with the pressure response at the transducer face. In this case, at this range, the diffraction effect is approximately equivalent to differentiating with respect to time. Consequently, high frequency components are emphasized. The result, for both optimal and zero phasing, illustrated in Figs. 24 and 25 indicates that the transducer is performing as predicted.

The phase angles $(\theta_1 - \theta_2)$ required to achieve the optimal "transfer functions" are illustrated in Fig. 26. In both cases, the characteristics are smooth with no discontinuities. The phase characteristic of Transducer B is less wavy and may be more closely approximated by a straight line. This is significant, since a straight line phase characteristic corresponds to a 'delay' in the time domain. A transducer possessing a perfectly straight optimum phase characteristic would be perfectly matched. This implies a lack of reverberation within the transducer structure. While it is readily possible to compensate for reverberation in
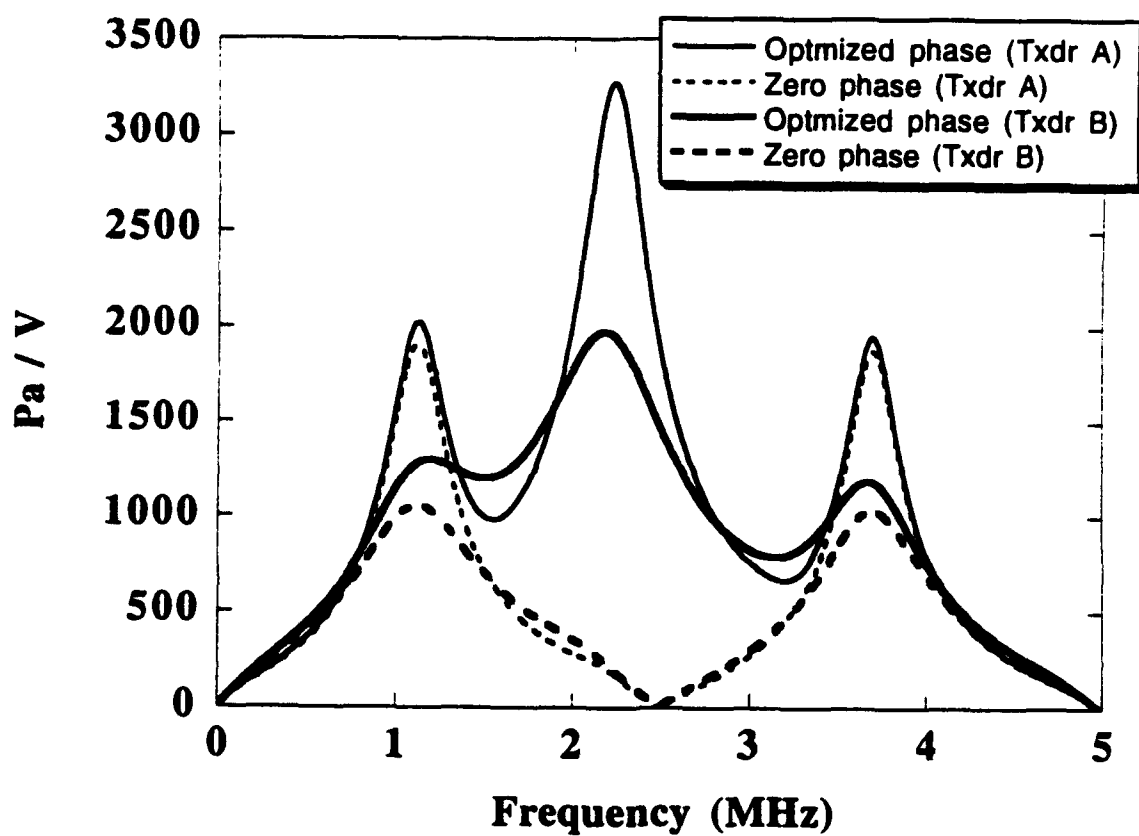
50

Figure 23
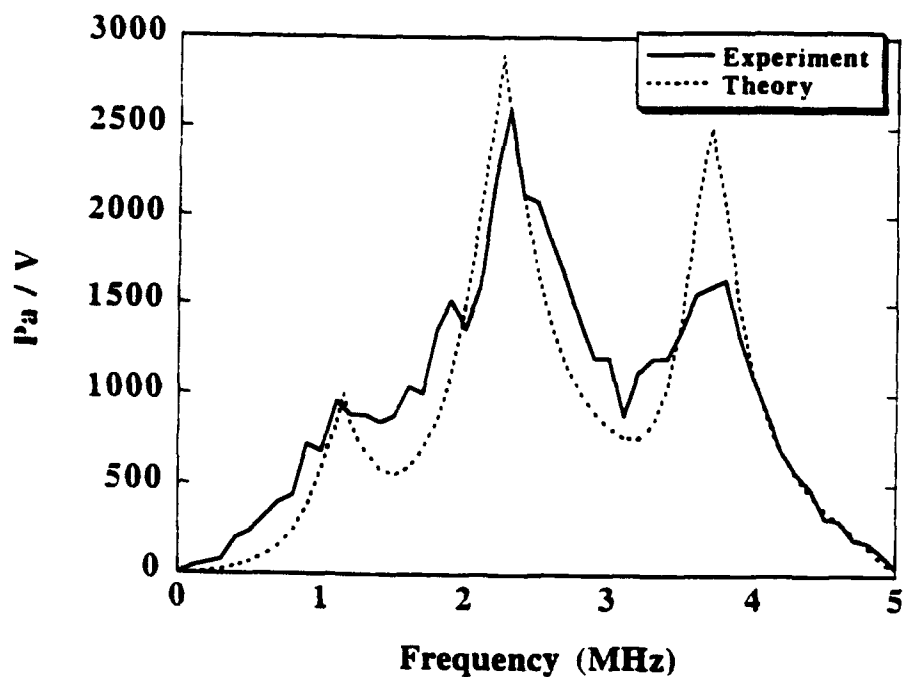Transmission "transfer functions" of Transducer A and Transducer B.

Figure 24

Transmission "transfer function" of Transducer A, using optimal phasing, taking account of diffraction effects.
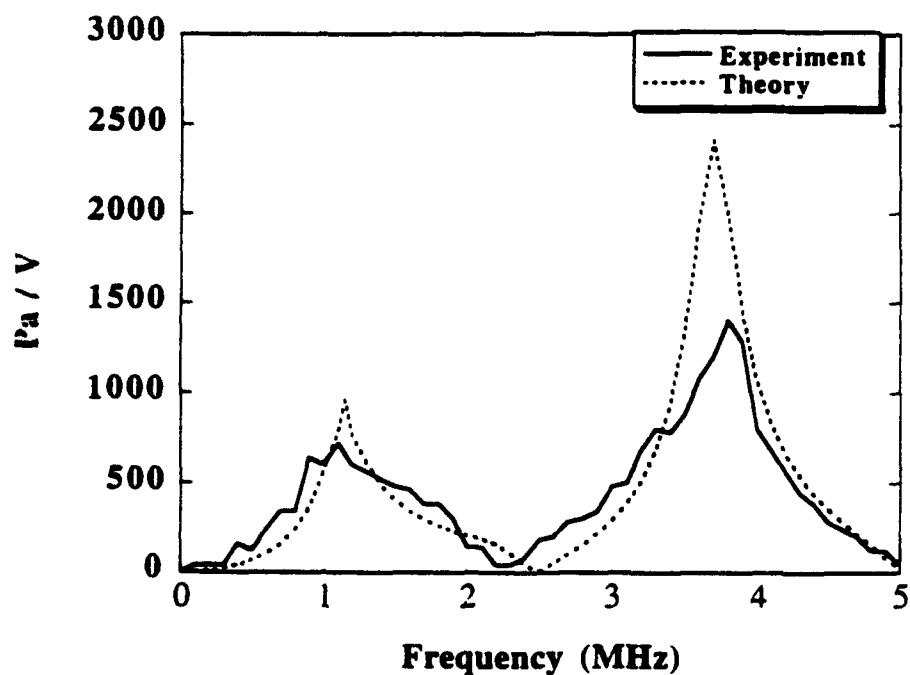

Figure 25

Transmission "transfer function" of Transducer A, using zero phasing, taking account of diffraction effects.
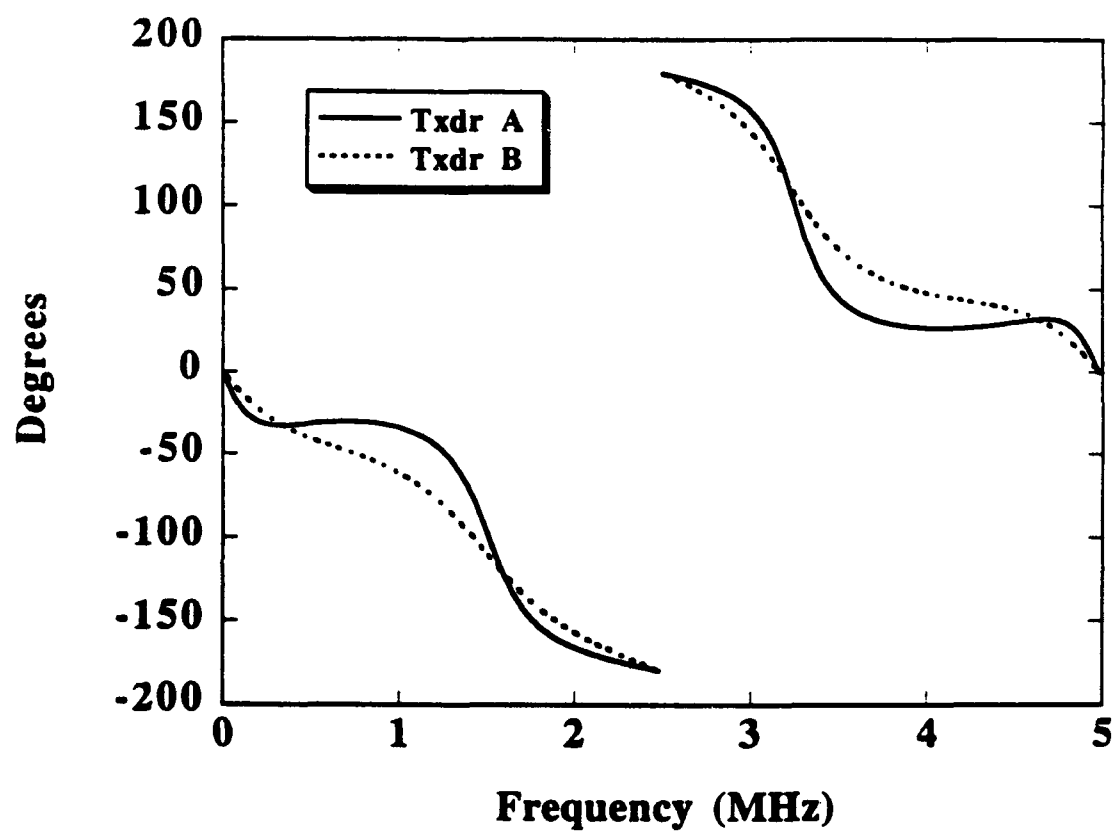
52

Figure 26

Phase characteristics, (θ_1 - θ_2), to be applied to Transducer A and Transducer B
in order to achieve the optimal "transfer function."

53

transmission, by canceling its effects using the stimulation functions, this is not possible in the reception mode. The desirability of a well matched transducer structure is evident.

The "optimum excitation" technique has been tested experimentally for non harmonic signals using Transducer C. A 1.5 MHz single cycle sinusoidal pulse, with peak amplitude 10 kPa, was desired. Using the above technique, the required excitation functions for layers 1 and 2 were determined. These are illustrated in Fig. 27. Notice that they are simple in form and are similar except that the stimulation for layer 2 is delayed by approximately 0.15 ms with respect to layer 1. The waveforms were sampled at 20 MHz and programmed into a HP 8175A Arbitrary Function Generator (AFG). The sensitivity of the hydrophone was excellent and hence the transducer could be driven directly from the AFG output. The response was measured at a range of 3 mm so that the plane wave output could be obtained. This response, illustrated in Fig. 28, indicates a good match with the desired waveform. The "tail," that may be observed at the end of the pulse, has been attributed primarily to an imperfect bond layer. It is confidently expected that transducers with substantially better bond layers can be made in the future. Alternatively, if the characteristics of the bond layer can be quantified comprehensively, compensation for them can be made when the excitation functions are being calculated.

4.2 Reception

As in the transmission case, two techniques are available. The first of these, the "active matching layer," is the corollary of the corresponding technique described for the transmission case. In principle, if there is an incoming pressure wave, a signal may be applied to layer 2 so that the signal monitored across layer 1 fits some pre-defined function. However, the technique is of limited practical importance since the precise nature, amplitude and time of the input function must be known in advance. Generally, this requirement is not fulfilled.

The "delay and sum" technique is related to the "optimal excitation" method used in transmission. This technique has also been described recently by Chofflet et al [40]. It has been found that in a perfectly matched transducer, the optimum phase characteristics, describing the excitation of layer 2 with respect to layer 1, was closely related to the transit delay of a wave propagating through layer 2. Since, in the reception case, the inputs are time domain signals, it is desirable to approximate the exact phase requirement with a simple time delay which should be applied to the response of layer 2 prior to summing with the response of layer 1. Using this technique, a finite sensitivity can be achieved continuously from below the fundamental resonant frequency to above the third harmonic. However, the "delay and sum" technique does
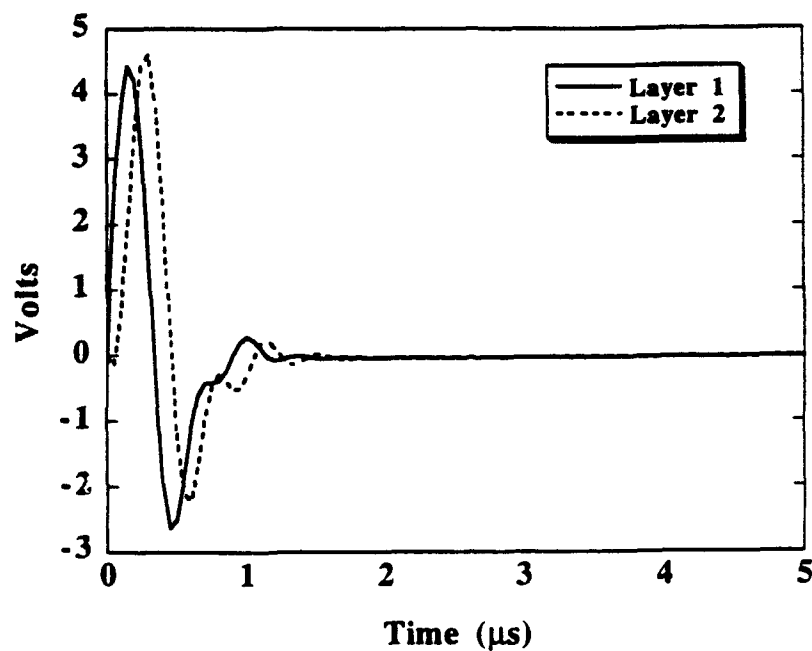
Figure 27
Excitation functions to be applied to Transducer C to achieve a 1.5 MHz, single
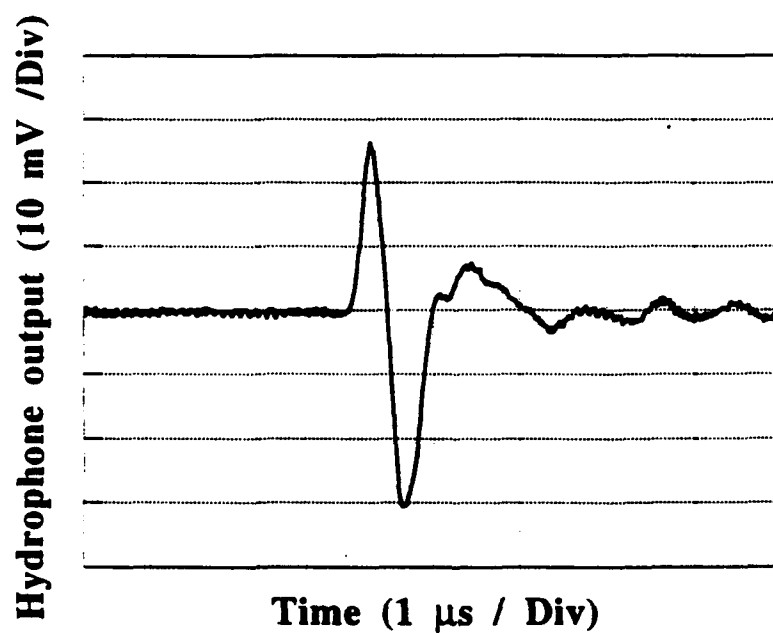cycle pressure profile with amplitude 10 kPa

Figure 28
Experimentally observed waveform when the functions illustrated in Fig. 27 were
applied to Transducer C.

not eliminate the effects of reverberation within the transducer. Reverberation is only a significant problem at higher frequencies where the wavelength is short relative to the layer dimensions. The solution to the problem of reverberation is to use a perfectly matched backing to eliminate reflection at the layer/ backing interface.

Figure 29 illustrates the receiver voltage output of Transducer D using the "delay and sum" technique. Responses are shown for a two layer system for the case where a 0.13 μs delay was applied to the response of layer 2 and for the case where no delay was applied. The substantial improvement in usable bandwidth is readily evident. Alternatively, if we consider the response of a single layer transducer, with thickness half that of the two layer system, one obtains a similar bandwidth to the "delay and sum" result, but with only half the sensitivity.

Figure 30 illustrates the response of Transducer D obtained for three Gaussian pulses with center frequencies of 1.8, 3.6 and 5.4 MHz and peak amplitudes of 10 kPa. These correspond approximately to the frequencies of the fundamental, second and third harmonics. The responses have been displayed so that they are not superimposed. Undistorted pulses have been obtained in each case. The response obtained when using Transducer C to monitor the 5.4 MHz signal is shown for comparison. In this case some distortion is evident due to reverberation in the active layers. Although it is not necessary to have matched backing in order to obtain finite output by using the "delay and sum" technique, it is necessary if the effects of reverberation on high frequency signals are to be totally eliminated. Unfortunately, practical multiple layer transducers have not been tested in the reception mode. Since the transducers operate largely according to theoretical prediction in transmission, it is reasonable to assume that their practical reception performance also matches theoretical results.

4.3 Pulse-Echo Applications

It is clearly possible to combine a transmission system using the "optimized excitation" technique with a reception system using the "delay and sum" technique. As discussed above, it is preferable to use a matched backing in order to optimize the reception performance. If piezoelectric ceramic/ epoxy composites or piezoelectric polymers are employed, this constraint is not unduly burdensome. The electronic hardware which would be required to achieve the required functions for the transmission mode would not need to be particularly elaborate. Synthetic waveforms may be stored digitally in memory. Sequential digital values may be read out and converted to analog signals prior to amplification. The "delay and sum" function
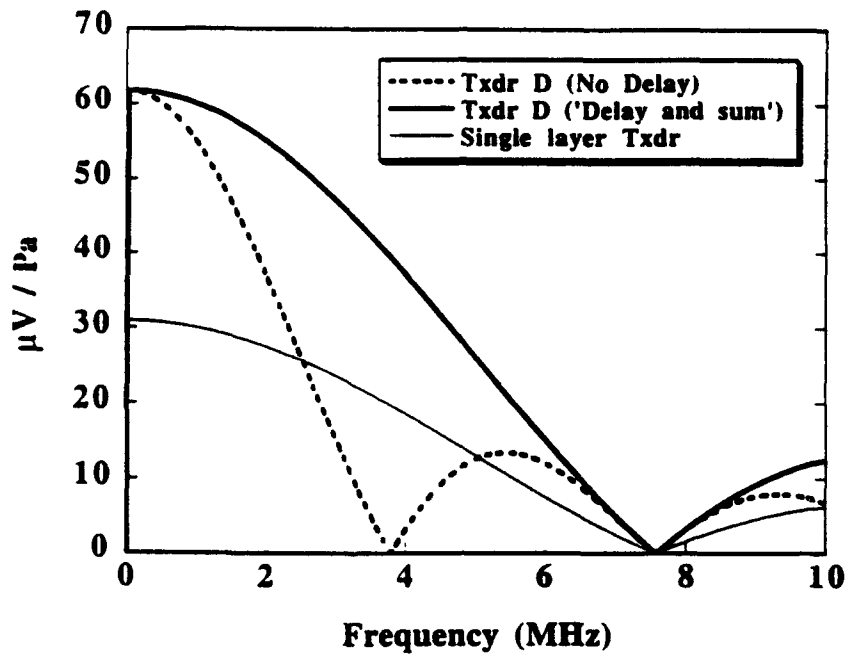
Figure 29
Theoretical reception magnitude characteristic of Transducer D.
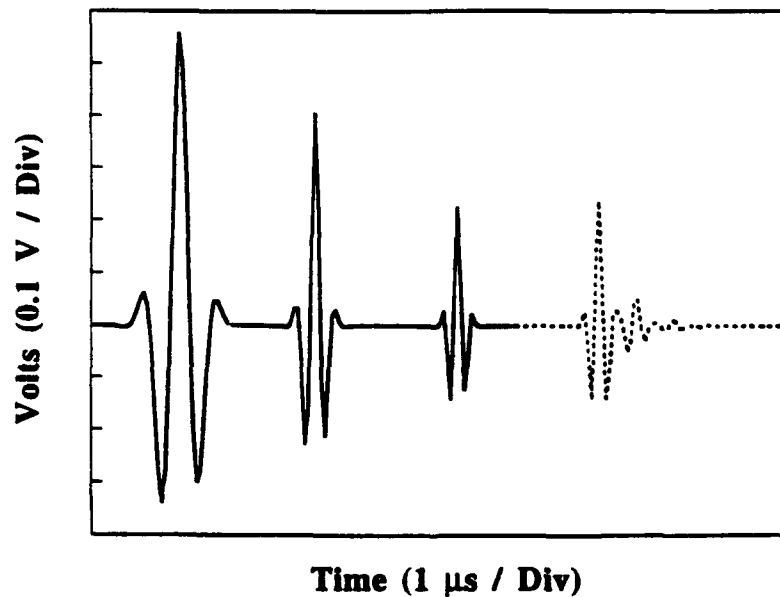

Time (1 μs / Div)

Figure 30
Theoretical reception response of Transducer D, using the "delay and sum" technique, for sequential input gaussian pressure profiles, with peak amplitudes of 10 kPa, and center frequencies of 1.8, 3.6 and 5.4 MHz, respectively. The fourth response is that obtained using Transducer C when the input is the 5.4 MHz gaussian pulse.

57

requires only the use of simple delays similar to those conventionally used in an imaging process. The "delay and sum" function may be implemented in either hardware or software.

4.4 Stability

The stability of the "optimized excitation" method for transmission is considered. Since the technique involves modifying more than one input in a manner which relies on the ability to model the practical system, it is natural to be concerned that small deviations in the input quantities, resulting from any one of a number of possible causes, will result in a relatively distorted output.

The stability of the technique with respect to deviations in the applied phase characteristics has been examined. Figure 31 illustrates the dependence of the magnitude of output pressure on frequency and phase angle, θ_1 - θ_2, for Transducer C. The complete range of phase angles has been considered. A smooth, rounded and continuous surface is evident. The absence of discontinuities indicates that small phase errors will not result in substantial errors in the output quantity. The surface can be made more even, in terms of magnitude, by improving the acoustic match between the piezoelectric layers and the backing or load media.

The influence of errors in layer dimension, layer material properties, layer stimulation level and the impact of a finite epoxy bond layer, have also been considered. It was supposed that Gaussian pulses, with peak amplitude 10 kPa, and center frequencies of 1.8 and 3.6 MHz, were to be generated using Transducer C. These frequencies correspond to the fundamental and second harmonic of the combined two layer system. Hence, the 3.6 MHz pulse required that the excitation functions to layers and 1 and 2 be approximately antiphase with respect to each other. Figure 32, illustrating the effect of reduced layer 2 stimulation applied to layer 2, indicates minimal distortion and modest attenuation of the signal. By contrast, Figure 33, illustrating the effect of reducing the thickness of layer 2 by 20%, indicates that some distortion has been introduced. As might have been anticipated, this distortion is greater at the higher frequency, where the phase characteristics of the applied signals are more diverse. Similarly, the effect of altering the material properties of layer 2, by increasing density by 20%, illustrated in Figure 34, indicates more distortion at the higher frequency. Figure 35 illustrates the consequence of the most probable practical defect. The introduction of a 5 μm epoxy bond layer between layers 1 and 2 results in minor distortion at the higher frequency.
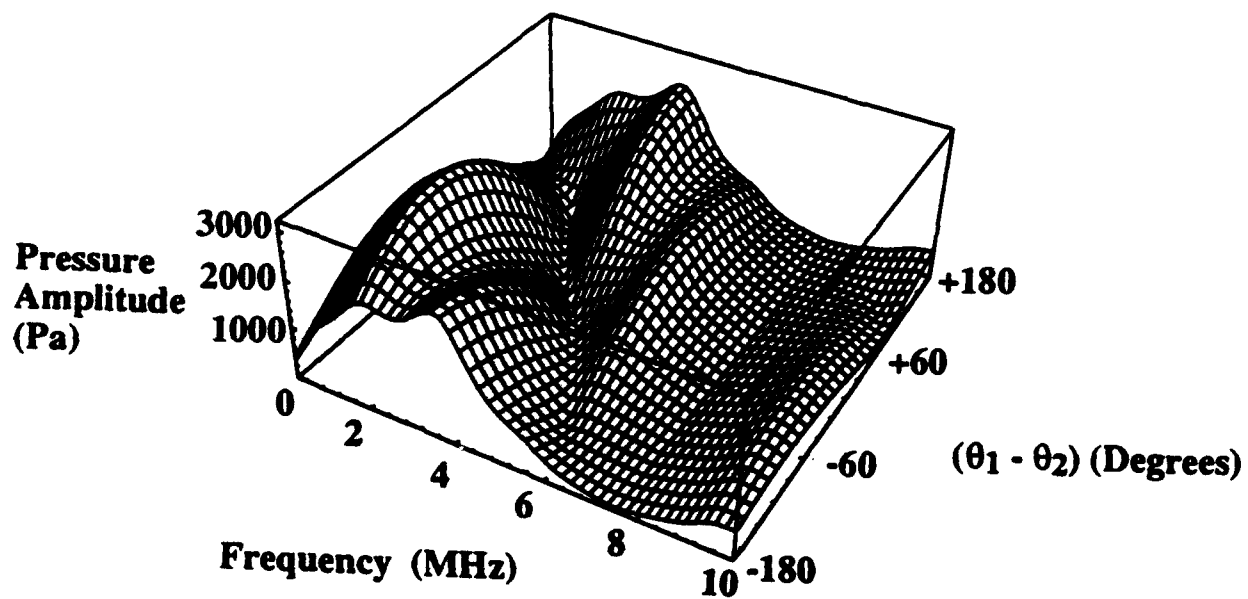
58

Figure 31
Surface profile indicating dependence of pressure output magnitude on phase angle,
$\theta_1 - \theta_2$, and frequency for Transducer C.

Figure 32

Theoretical output of Transducer C when the required functions are sequential 1.8 and 3.6 MHz pulses, respectively. The desired peak amplitude is 10 kPa. In this case, the stimulation of layer 2 was artificially reduced by 20%. The response is virtually identical to the desired response except for a reduction in amplitude of approximately 10%.
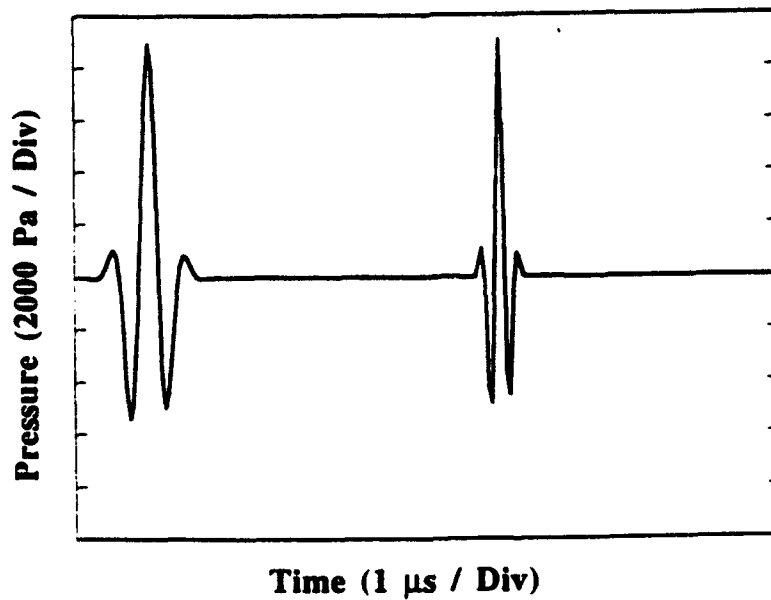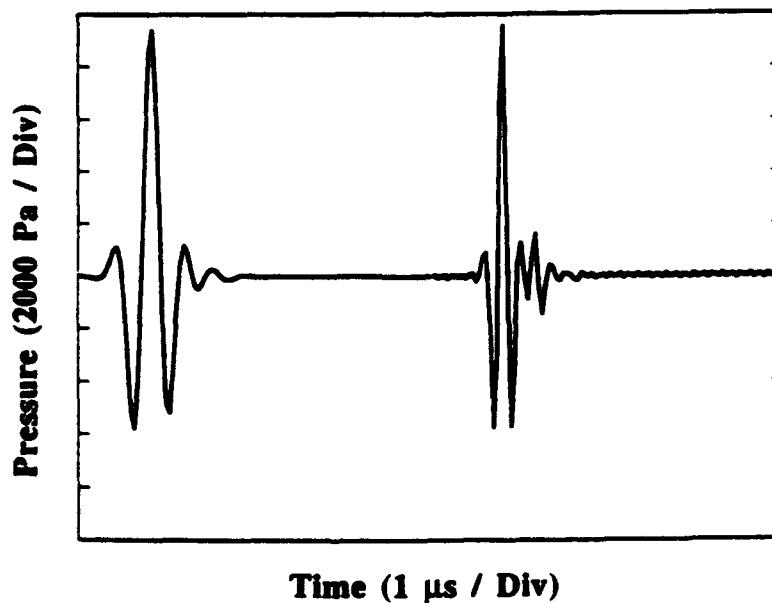

Figure 33

Theoretical output of Transducer C when the required functions are sequential 1.8 and 3.6 MHz pulses, respectively. The desired peak amplitude is 10 kPa. In this case, the thickness of layer 2 was artificially reduced by 20%.

60

Figure 34
Theoretical output of Transducer C when the required functions are sequential 1.8 and 3.6 MHz pulses, respectively. The desired peak amplitude is 10 kPa. In this case, the density of layer 2 was artificially increased by 20%.
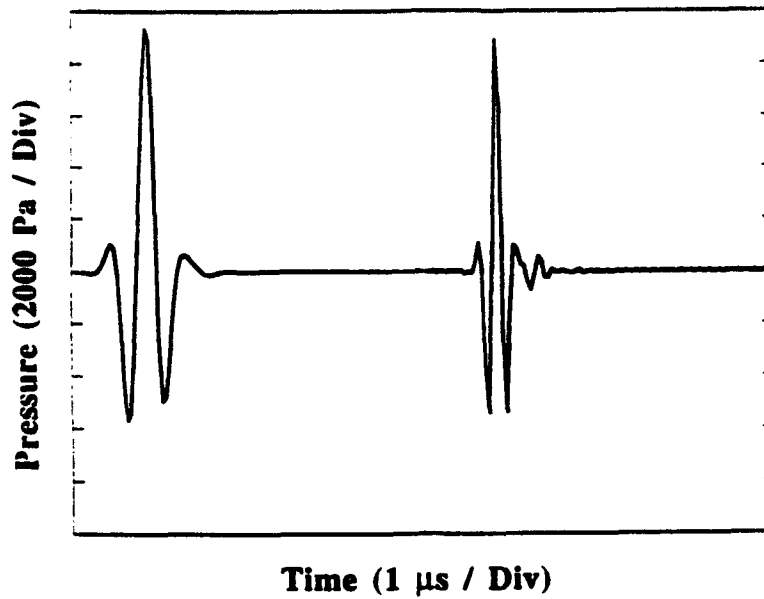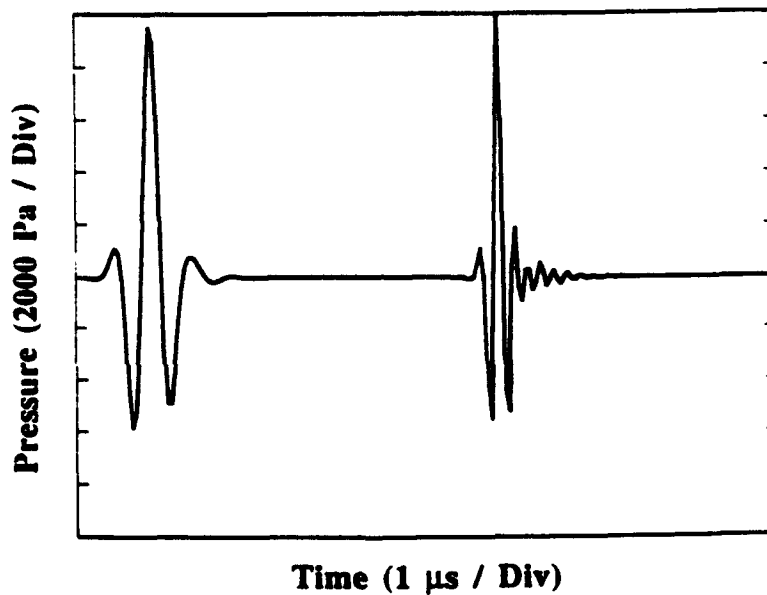

Figure 35
Theoretical output of Transducer C when the required functions are sequential 1.8 and 3.6 MHz pulses, respectively. The desired peak amplitude is 10 kPa. In this case, a 5 mm epoxy bond layer has been included in the simulation.

The deviations which have been considered here are relatively extreme and the resulting distortions have generally been minor. It can be concluded that the technique is generally stable but that the importance of quantifying the structure accurately is more significant when higher frequencies are employed.

4.4 Conclusions on Multiple Active Layer Transducers

The sensitivity and bandwidth characteristics of thickness mode transducers can be enhanced by using multiple active layers. The variety of design variables, including dimensions, material properties and electrical stimulation, offer the designer immense versatility. It is impossible to determine a design which is optimal for all applications. In transmission, any deficiencies in the physical design may be compensated for by adjusting the stimulation functions. However, for optimized reception characteristics there is a strong motivation for using a design which includes a backing that is acoustically matched to the piezoelectric layers. The mathematical technique for determining the excitation functions is straightforward and the required electronic hardware can be implemented using standard, low cost components. The technique may be extended to pulse-echo operation. The stability of the technique has been examined and been found to be generally good. Although only two layer cases have been considered here, it is possible to extend the concept by using more active layers, and consequently obtain even higher bandwidths.

5. ENHANCED 1:3 COMPOSITE TRANSDUCERS

Composite transducers, comprising aligned piezoceramic pillars embedded in a polymer matrix, have been studied extensively and have found applications in medical ultrasound, non-destructive examination and high frequency sonar. However, their efficiency is limited by the positive Poisson's ratio observed in all conventional polymers. It has recently been shown that device performance could be significantly improved if a filler possessing a negative Poisson's ratio could be used [41]. Since the use of negative Poisson's ratio materials is not readily feasible at present, a compromise, which in effect simulates a zero Poisson's ratio material, is presented here. Aligned compressible inclusions are formed in a standard polymer filler. These absorb lateral strain without associated Poisson's ratio cross-coupling into thickness strain. Typically, these inclusions are gas filled holes drilled into the polymer. The resulting structure is illustrated in Fig. 36. Notice that when standard notation [42] is used, the resulting composite is a 1:3:1 composite in contrast to the conventional 1:3 composite. The first phase (ceramic) is

Vertically aligned
ceramic pillars
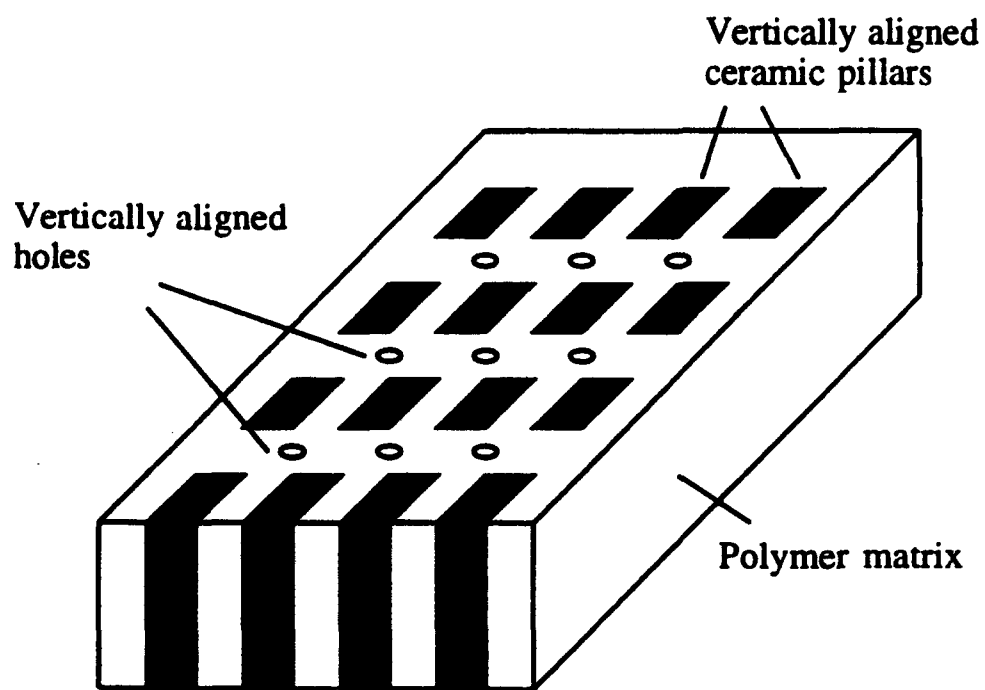
Vertically aligned
holes

Polymer matrix

Figure 36
New composite structure with aligned holes.

connected only in the thickness direction. The second phase (polymer) is connected in three dimensions and third phase (gas) is connected only in the thickness direction.

5.1 Thickness Mode Transmitters and Receivers

In a conventional 1:3 composite transducer, comprising ceramic pillars and a polymer matrix, the situation illustrated diagrammatically in Fig. 37 may arise. In transmission, the ceramic is the active displacement initiating phase. The Poisson's ratio of the ceramic is typically +0.35 for Lead Zirconate Titanate (PZT) and the polymer's Poisson's ratio varies between +0.35 for epoxy and +0.47 for polyurethane. Hence, significant antiphase cross coupled strain results in the thickness direction. Consequently, the net thickness displacement of the polymer may be antiphase with respect to that of the ceramic. A degree of cancellation of thickness displacement occurs and the net surface displacement is reduced. This has had a significant bearing on polymer selection. A compliant polymer possessing a low Poisson's ratio would be ideal. Unfortunately, compliant polymers generally have high Poisson's ratios. For this reason, less compliant epoxy is generally favored in preference to polyurethane, which is more compliant. The properties of these two polymers are presented in the Appendix I. Clearly, the extent of the problem is a complex function of geometry and material properties. Additionally the static consideration presented here is modified in the high frequency thickness resonant case. Furthermore, practical transducers are three dimensional structures. A numerical analysis, namely finite element analysis, is required to obtain a useful model of the phenomena present.

Nevertheless, if we consider the modified transducer, illustrated diagrammatically in Fig. 38, with compressible gas filled inclusions, it is immediately evident that all induced lateral strains in the polymer are absorbed by the inclusions. Immediately, a result is obtained which simultaneously leads to improved thickness displacement uniformity and has the potential for increased electromechanical coupling efficiency. The only coupled thickness motion in the polymer is due to thickness extensional coupling across the ceramic/ polymer boundary. Naturally, this thickness extensional coupling in the polymer is in phase with the ceramic. Considerable importance has been attached to ensuring that the spacing between adjacent pillars is not sufficiently great that parasitic shear standing waves can resonate in the vicinity of the thickness operating frequency [43,44]. This is a different phenomenon, occuring only in the dynamic regime. Notice that the presence of the holes

Ceramic   Polymer

Unstrained

Strained
(Contraction)
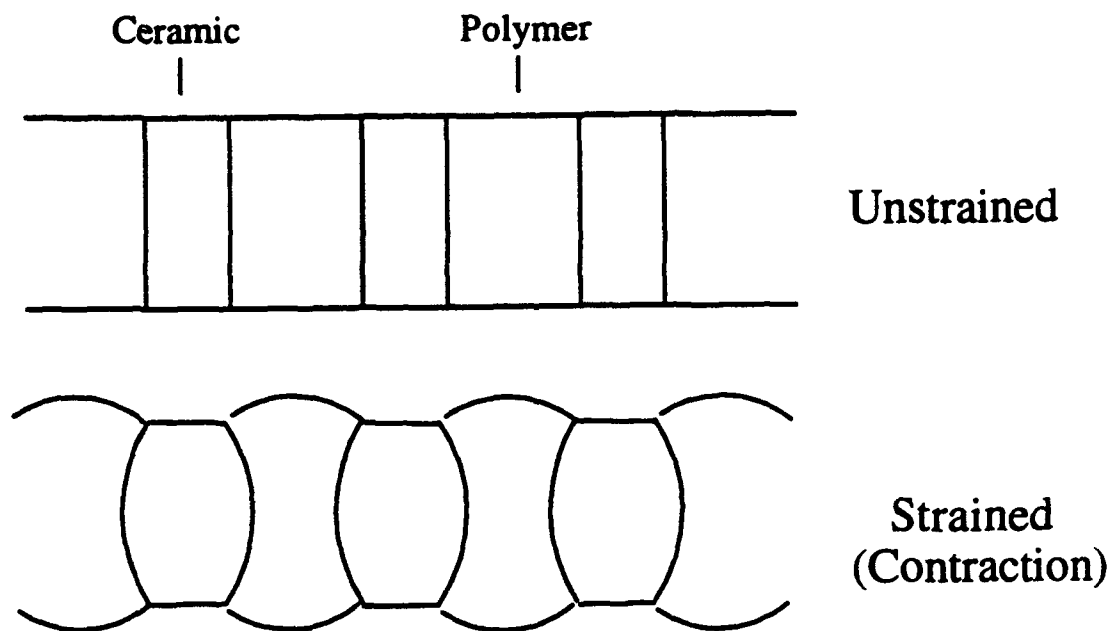
Figure 37

Exaggerated illustration of anti-phase motion resulting from positive Poisson's ratio in ceramic and polymer phases.

Ceramic   Polymer   Hole
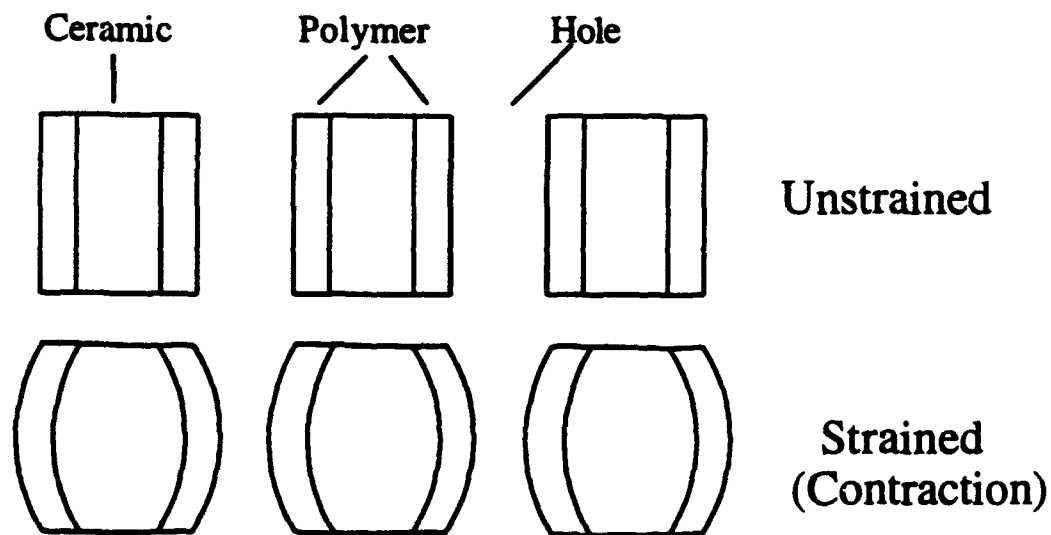
Unstrained

Strained
(Contraction)

Figure 38

Exaggerated illustration of compressible inclusions absorbing strains without cross-coupling to thickness direction.

65

will probably have a disruptive effect on the lateral standing waves normally occurring in a conventional composite transducer.

A very important associated effect is that, since the polymer resists lateral displacement of the ceramic (Fig. 37), a significant degree of lateral clamping pressure is applied to the lateral surfaces of the ceramic. This has the effect of reducing the potential electromechanical coefficient (k_{33}) of a PZT 5A [45] bar from 0.70 towards the "laterally clamped" coefficient (k_t), which is 0.49. This decrease will be reduced in the new 1:3:1 structure. A less significant associated effect is that as lateral stiffness is reduced in the composite so also is stiffness in the thickness direction. Hence a modest reduction in the thickness mode resonant frequency is obtained. This implies that the acoustic impedance of the composite is also reduced in the new structure. This is a desirable effect for the majority of applications.

In the current program of work, finite element analysis has been performed using the commercially available ANSYS code [46]. A full discussion of the development of the theory relating to the finite element analysis of piezoelectric materials may be found in the literature [47,48]. Furthermore, the application of the ANSYS finite element code to composite transducers, with experimental validation, is discussed in detail in Reference 49. In all cases, unless specifically noted otherwise, the natural resonant frequencies, and the nature of the associated modal displacements, have been evaluated using eigenvalue analysis [47]. Relative displacement, as opposed to absolute displacement, information is generated. Repeating the analysis for both short circuit and open circuit electrode conditions permits the resonant and antiresonant frequencies to be evaluated [49]. Subsequently, the electromechanical coupling coefficient associated with a particular mode may be evaluated. An additional indication of the practical significance of a particular mode is obtained by considering the relative thickness displacements of the nodes on the transducer surface. Clearly a mode in which all nodes displace by a similar extent is of more practical usefulness than a mode in which certain modes displace in one direction and others in the opposite direction.

Since the composite structures considered here have quarter symmetry in the X-Y (lateral plane) and strongly coupled modes are symmetric in the Z (thickness direction), it is only necessary to model a one eighth section of the unit cell. Naturally, care is taken to impose the appropriate boundary conditions. No perpendicular displacement of nodes lying on a symmetry plane, with respect to the plane, is permitted. The material properties of the

66

PZT 5A ceramic, a typical epoxy polymer, and polyurethane are presented in Appendix I. The performance improvement induced by the modification discussed in this paper is far more apparent when polyurethane is employed. Consequently, the new design is most applicable to devices incorporating this material. Comparisons with results obtained when epoxy is used are made, as required.

Figure 39 illustrates a one eighth section modal displacement representation of a 25% ceramic volume fraction composite transducer. Plot A, referring to a device containing a conventional polymer possessing a Poisson's ratio of +0.47, indicates uneven thickness displacement, with a degree of antiphase motion. By contrast, Plot B indicates the results for an identical device except that the Poisson's ratio of the polymer is 0.0. In accordance with the argument set out above, it is observed that in case B a more even displacement occurs. The immediate aim is to experimentally realise an approximation to this case by introducing compressible inclusions into the polymer. A practically viable method would be to drill, or otherwise form, holes in the material. Alternatively, one could saw along the X-Y directions between adjacent ceramic/ polymer cells. This would decouple each ceramic/ polymer cell from neighboring cells and virtually zero net lateral stress conditions would exist. Three hole geometries are illustrated in Fig. 40 in addition to the inter pillar sliced geometry. For convenience these geometries will subsequently be referred to as "diagonal," "parallel," "combined," and "sliced"—as defined in the figure. It is immediately evident that a virtually infinite range of ceramic/polymer/hole geometries is possible. A limited range is considered here with a view to obtaining a limited understanding of the phenomena present so that informed design decisions can be made.

A substantial simplification of the finite element mesh is afforded if it is assumed that both the ceramic pillars and the holes are rectangular in cross-section. This avoids the more complex geometry associated with fitting circular features within rectangular frames. In practice the ceramic pillars are normally square but the holes would probably be circular. The influence of the exact shape is of little significance in the examples presented here and the added complexity of a more realistic mesh is not justified. Analysis of the relative performance of circular and square section ceramic pillar composites described in Reference 49 serves to justify this approximation.

One might suppose that an alternative approach would be to use a ceramic with a low Poisson's ratio. Unfortunately, modified Lead Titanate (PT), the only ceramic with such a characteristic, has a relatively low electromechanical coupling coefficient in the bar
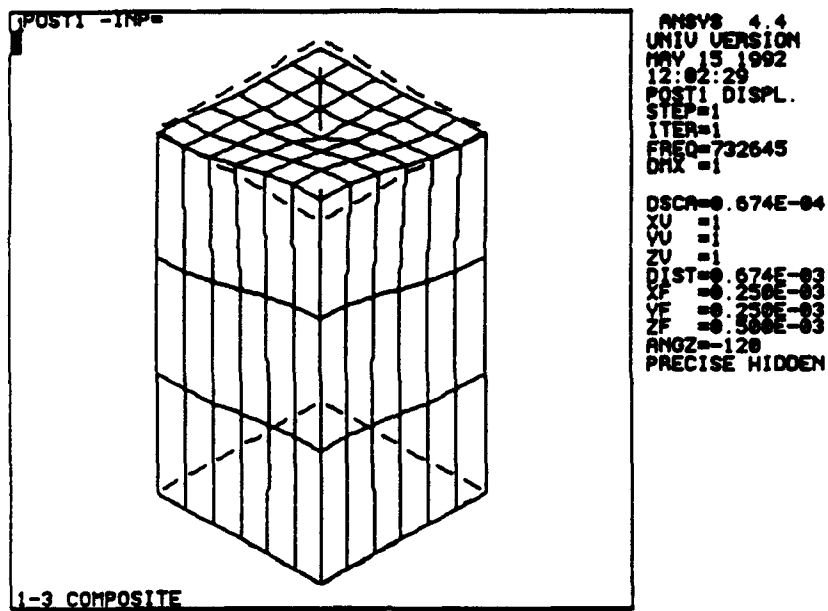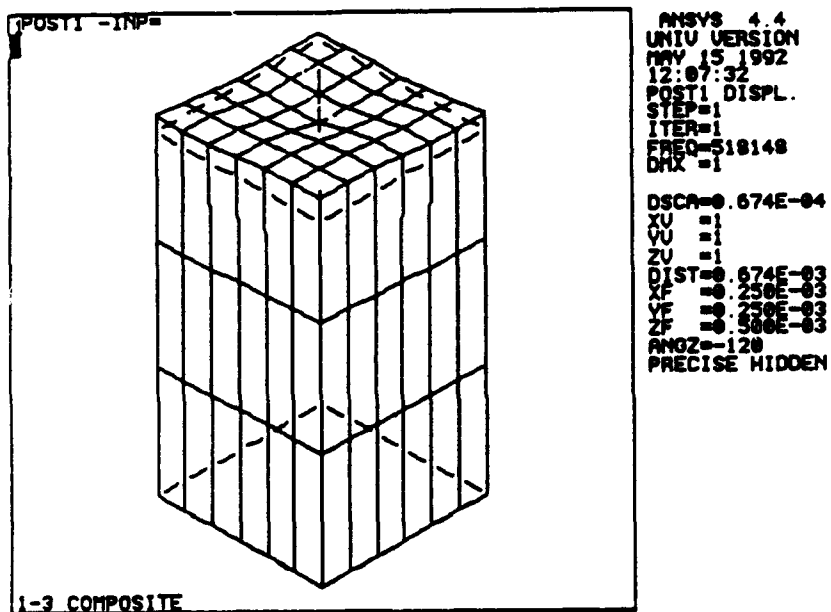
Figure 39

Modal displacement at the thickness resonant frequency in a 25% ceramic volume fraction composite containing two types of polymer. A one-eighth section is illustrated. The ceramic pillar is 0.5 mm wide and 2 mm high.

Static — — — — — — — — — —

Modal displacement shape ——————————

(a) Polyurethane polymer (Poisson's ratio = 0.47)
(b) Modified polymer (Poisson's ratio = 0.0)

68
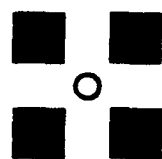
'Diagonal'

'Parallel'

'Combined'

'Sliced'

Figure 40
Cross-sections of various hole geometries.

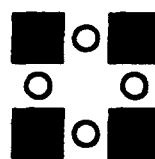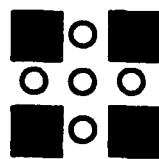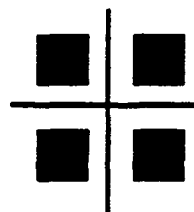mode In PT, k_{33} = 0.50, whereas, for PZT k_{33} = 0.70. Additionally, PT has a low dielectric permittivity. This problem is compounded in a composite since the net permittivity is further reduced due to the replacement of part of the ceramic with polymer in the structure.

Results obtained using finite element analysis were obtained for ceramic volume fractions of both 25% and 50%. In order to shift the effect of parasitic lateral modes to frequencies well separated from the thickness resonant frequency, a pillar width to height (aspect) ratio of 0.1 has been used.

In the first theoretical test case, the effect produced by increasing the number of holes in the structure is investigated. The same basic mesh geometry is used so that relative comparisons of nodal displacements are valid. In practice the locations of the nodes were constant but an increasing number of polymer elements were replaced by empty spaces simulating holes. In the 25% ceramic volume fraction case, each hole occupied 6.25% of the total volume, whereas, in the 50% ceramic volume fraction case, each hole occupied 2.14%. These geometries were chosen so as to provide a regularly spaced geometric mesh.

Figure 41 illustrates the influence of hole geometry on the thickness mode electromechanical coupling coefficient. For both the 25% and 50% ceramic volume fraction composites a significant improvement is achieved simply by inserting one hole diagonally between adjacent pillars. Smaller improvements are obtained with increasing numbers of holes. As would be expected, the "sliced" geometry, which is totally unconstrained in the lateral direction, provides the optimal result.

A measure of the degree of nodal displacement uniformity is presented in Fig. 42. The standard deviation of perpendicular nodal displacement on the transducer's vibrating surface has been calculated. Since modal analysis generates only relative, not absolute, displacement information, the largest displacement was normalized to 1.0 and all other displacements were scaled by a similar factor. Subsequently, the statistical standard deviation of these normalized displacements was calculated. Although there is no monotonic improvement in the uniformity of nodal displacement, it is readily apparent that a significant improvement is obtained by fabricating one or more holes. The exact nature of the nodal displacement is a complex function of geometry and consequently it is not possible to predict intuitively that the uniformity of nodal displacement will always improve with increasing numbers of holes. It is evident that the "sliced" structure, which is

70
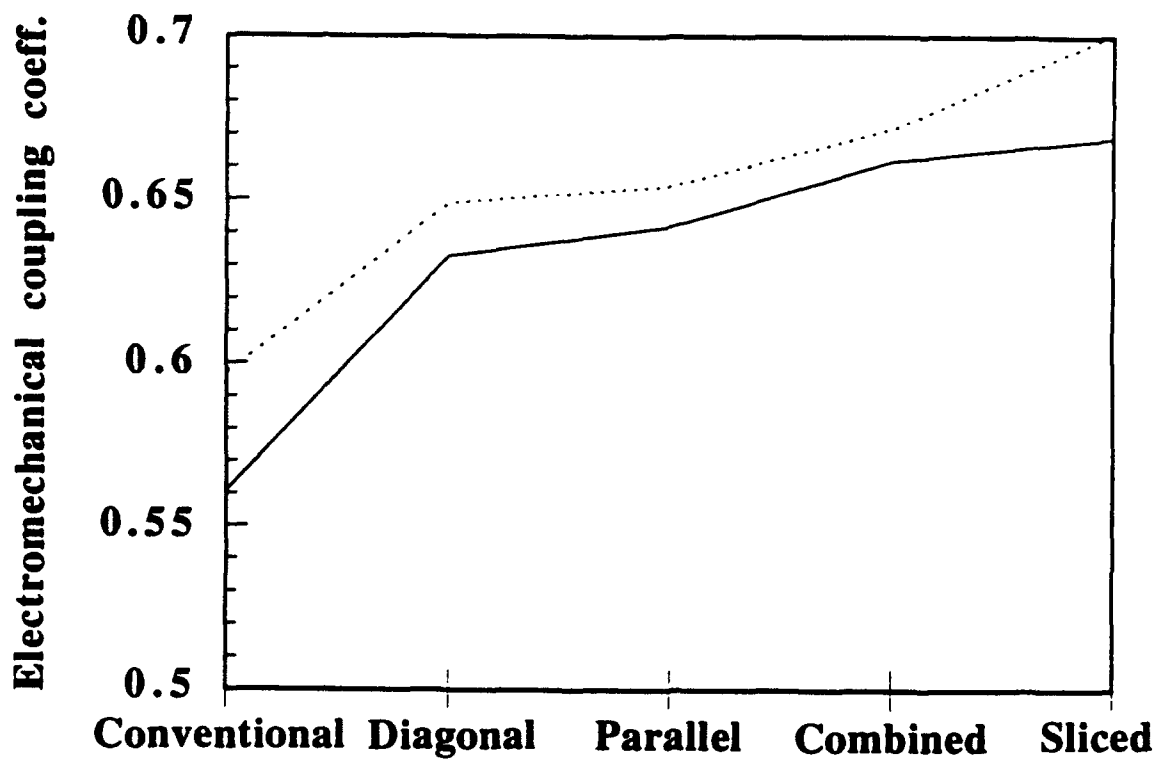
Figure 41
Theoretical dependence of thickness mode coupling coefficient on hole geometry
————————— 25% Ceramic volume fraction
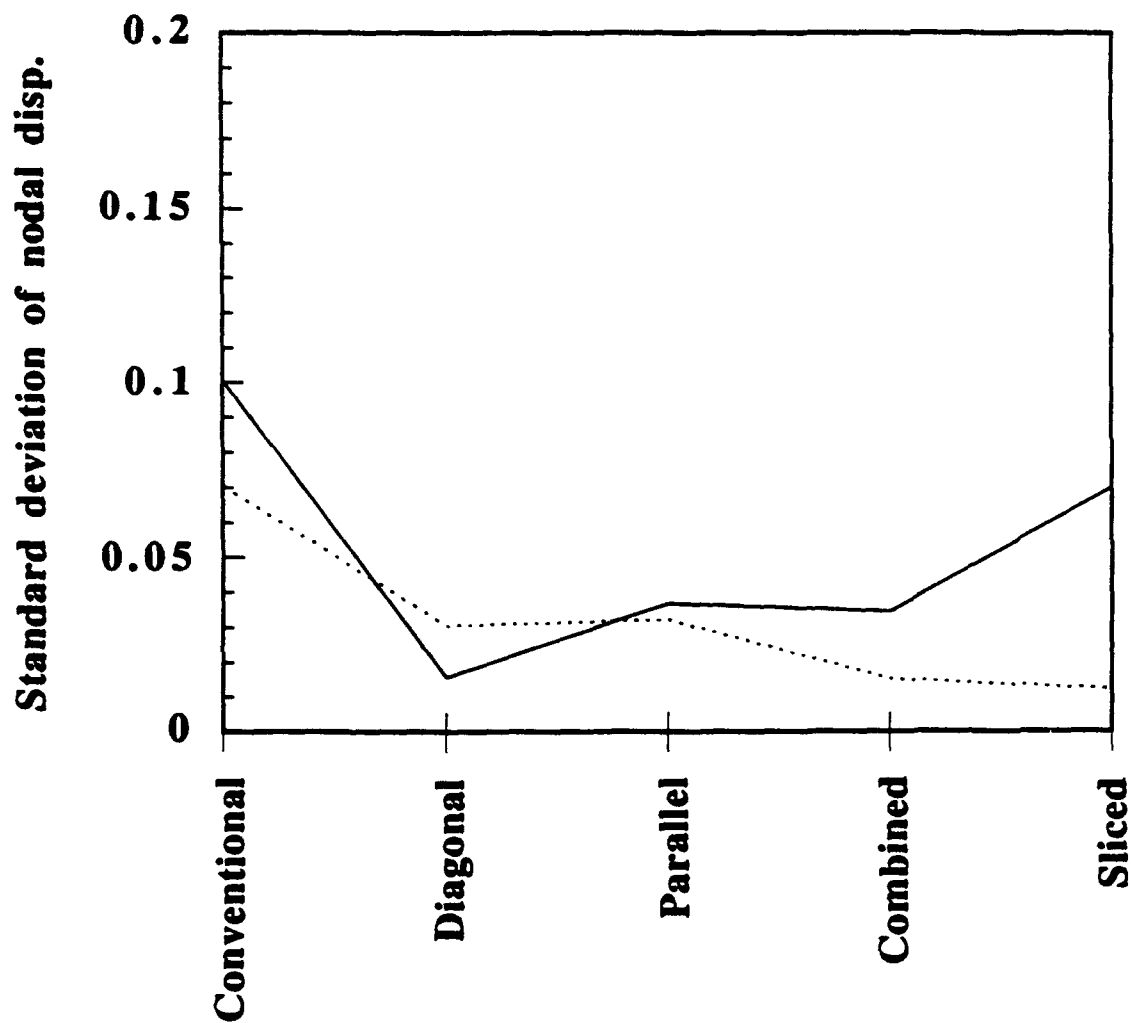· · · · · · · · · · · · · 50% Ceramic volume fraction

Figure 42

Theoretical dependence of nodal displacement uniformity (thickness direction) on hole geometry

———————— 25% Ceramic volume fraction

· · · · · · · · · · · · · 50% Ceramic volume fraction

completely unconstrained on the lateral surfaces of each pillar/polymer unit cell, does not always vibrate uniformly. However, the high electromechanical coupling coefficient associated with this structure compensates to a large extent for this potential deficiency.

Figure 43, illustrating longitudinal wave velocity in the thickness direction, as a function of hole geometry, indicates a general reduction in velocity as the number of holes is increased. This parameter was calculated from the anti-resonant frequency using the assumption that this corresponds to a $\lambda/2$ resonant condition. This characteristic is in accordance with intuitive expectation. Increasing numbers of holes result in reduced lateral 'clamping' which cross couples to the thickness direction in the form of reduced stiffness in the thickness direction, as noted previously.

Up to this point the analyses have considered one mesh for the 25% ceramic volume fraction device and another for the 50% ceramic volume fraction device. Hence, as the number of holes increases, so also does the void volume fraction. It is instructive to consider independently the effects of increasing numbers of holes, and increasing void fraction.

Figure 44 illustrates the dependence of electromechanical coupling coefficient on void volume fraction for the 25% ceramic volume fraction composite. Analysis was performed for the diagonal, parallel and combined hole geometries. The coupling coefficient associated with a conventional structure and with a sliced structure are also illustrated. It is evident that the coupling coefficient is enhanced as the void fraction increases. However, the improvement levels off at higher void fractions. It is also evident that the diagonal hole design is the most effective of the three geometries. This may be due to the fact that the hole dimension is greatest when only a single hole is employed. The results for the 50% ceramic volume fraction composite, illustrated in Fig. 45 demonstrates similar trends. It is physically impossible to achieve a large void fraction with a single square hole in a 50% ceramic volume fraction composite. Hence, some corresponding data points are missing. It is apparent that substantial improvements are achieved with smaller void fractions in the case of the 50% ceramic volume fraction composites. This is probably related to the fact that the polymer volume fraction is also less in this case.

Similar trends were observed when the analysis was performed for epoxy filled composites. The only difference was that the degree of enhancement of thickness mode coupling coefficient was approximately one third of that shown in Figs. 41, 44 and 45.
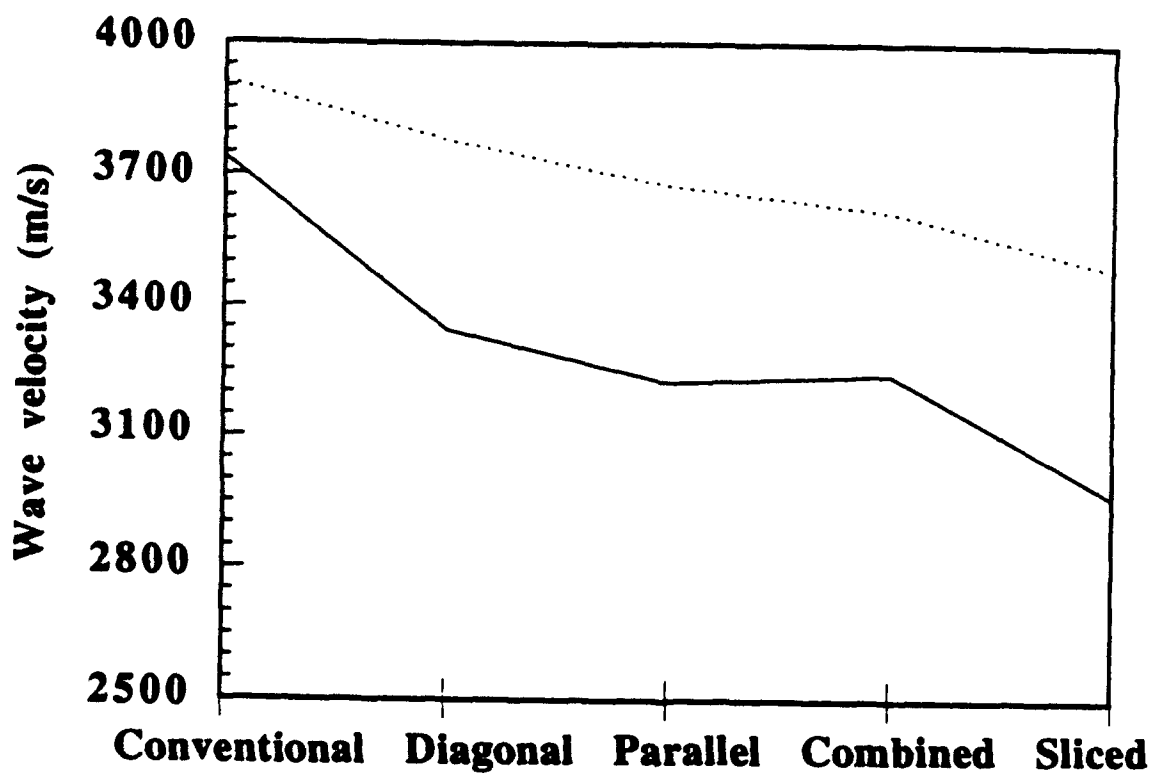
Figure 43
Theoretical dependence of longitudinal wave velocity (thickness direction) on hole geometry

——————————— 25% Ceramic volume fraction
· · · · · · · · · · · · · · 50% Ceramic volume fraction

74
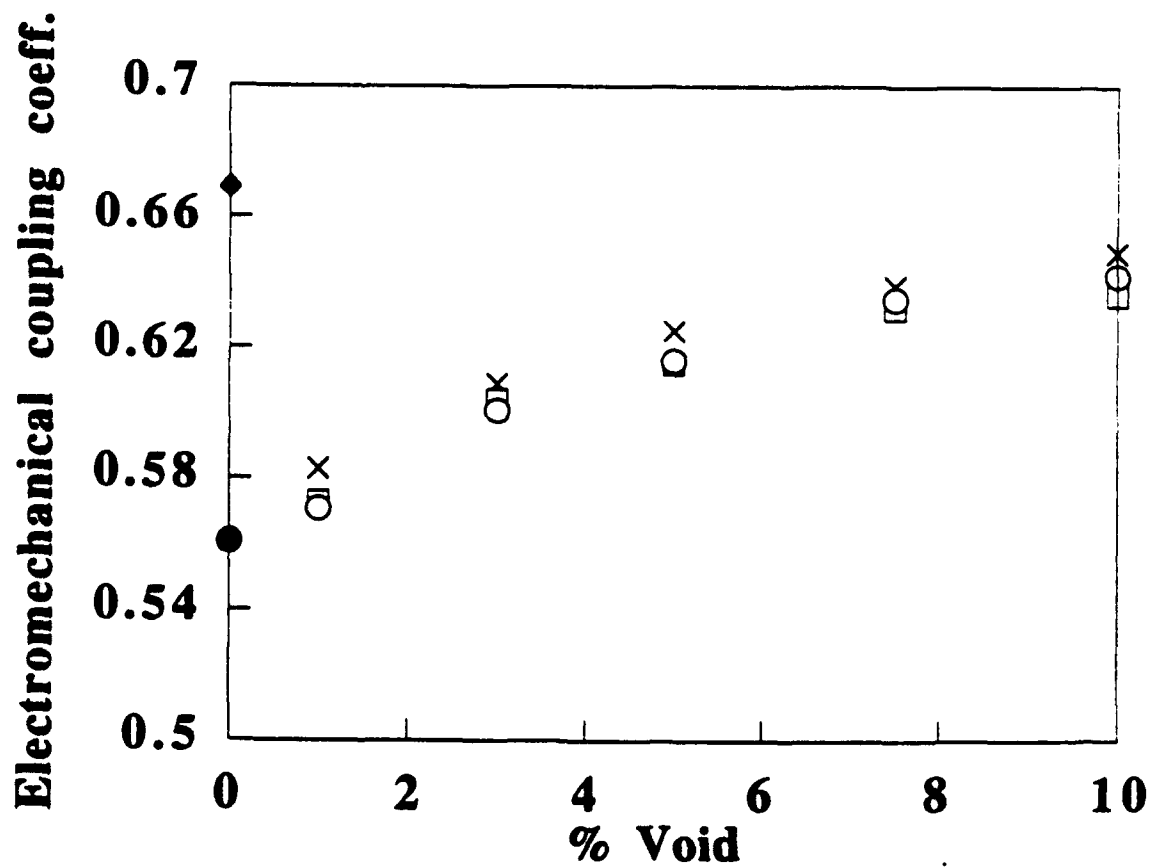
Figure 44
Theoretical dependence of thickness electromechanical coupling coefficient on void
volume fraction in a 25% ceramic volume fraction composite

- •   No void
- ♦   Sliced
- ×   Diagonal
- □   Parallel
- o   Combined

Figure 45
Theoretical dependence of thickness electromechanical coupling coefficient on void
volume fraction in a 50% ceramic volume fraction composite

- •   No void
- ◆   Sliced
- ×   Diagonal
- ☐   Parallel
- o   Combined

Two prototype enhanced composite transducers have been manufactured and tested. The geometries of these are described in Appendix III. Unfortunately, only epoxy was available as a polymer and hence any improvements d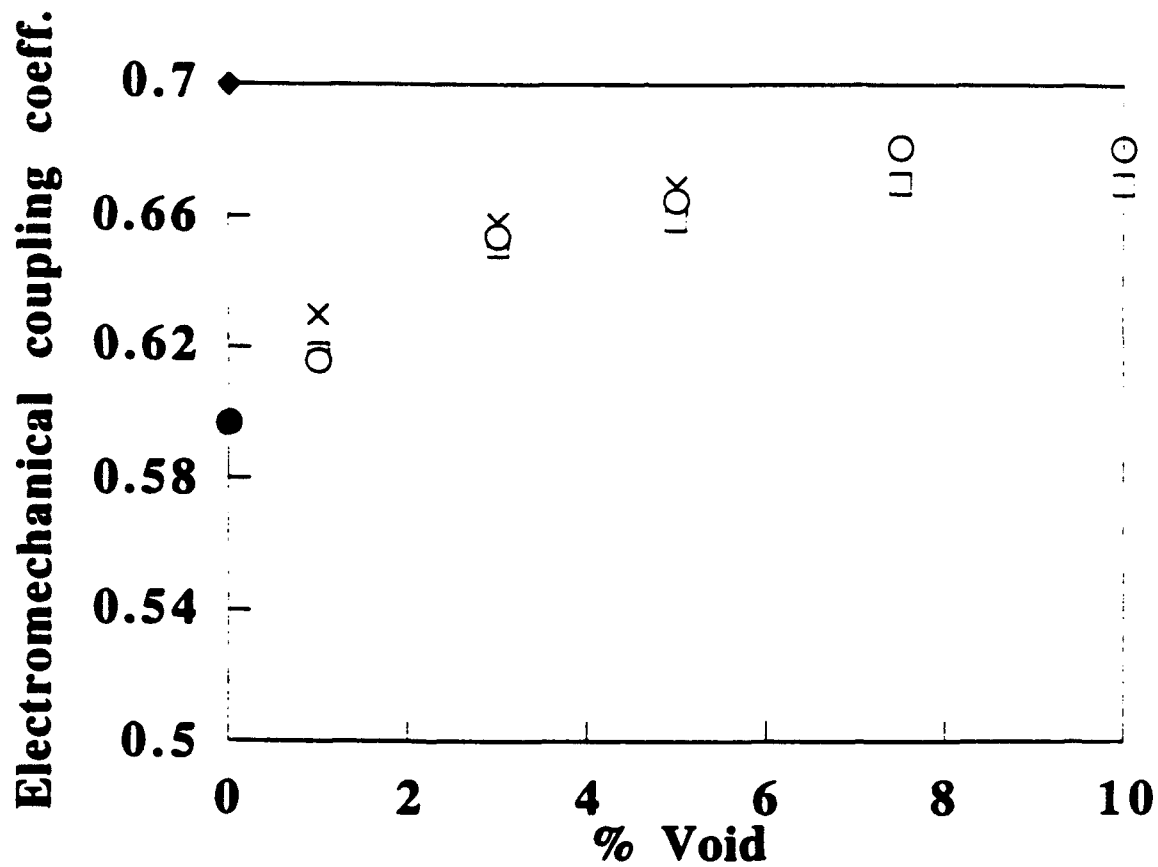emonstrated are less than might have been obtained had polyurethane been used. Also, practical limitations on the size of the holes constrained the overall geometry. Since the holes were hand-drilled, it was necessary to use relatively wide spacings between the pillars. This gave rise to the presence of additional resonant modes slightly higher than the thickness resonant frequency. This prevented accurate measurement of the electromechanical coupling coefficients. The transmission performance was measured with a hydrophone placed on axis, in the far field, in a water tank. A sinusoidal burst, at the center frequency and approximately ten cycles long, was applied to each transducer. The responses were normalized with respect to the response of the conventional composite transducer and are indicated in Table I.

TABLE I
Measured, normalized transmission and reception
performance of Transducers I and II

Hole Configuration	Conventional	Diagonal	Parallel	Combined
Transmission (Txdr A)	1.00	1.11	1.11	1.15
Transmission (Txdr B)	1.00	1.18	1.18	1.18
Reception (Txdr A)	1.00	1.25	1.31	1.25
Reception (Txdr B)	1.00	1.12	1.12	1.20

Improvements in sensitivity, in the range 10% to 20% were achieved in these cases. The reception response was measured using a wideband transmitting transducer operating in the far field, with the distance between the transmitter and the detecting transducer greater than the sum of the near field/ far field transition ranges of both transducers. A fixed amplitude, sinusoidal burst, at the center frequency, was applied to the transmitter. The response of each receiving transducer was monitored and the amplitude normalized with respect to the response of the conventional design. Improvements in the range 10% to 30% were obtained by using the new designs. The results clearly indicate that improved performance is obtainable. However, it will be desirable to develop manufacturing techniques which would permit accurate manufacture of pillar/polymer/hole geometries finer than those available at this time. It is also evident that, for the purposes of demonstrating the effectiveness of the technique, it would be desirable to use polyurethane rather than epoxy.

In conclusion, improvement in composite transducer performance, in terms of electromechanical coupling coefficient, surface displacement uniformity and reduced longitudinal wave velocity, is achievable by employing aligned compressible inclusions. It would appear that this improvement is significant when polyurethane is employed. However, the improvement observed when epoxy filled composites were considered was far less. This is explained by the observation that Polyurethane possesses a far higher Poisson's ratio. Nevertheless, there has been a long-standing interest in soft polymers for use in flexible composite structures. These soft polymers have been largely abandoned as a component in composites because of their large Poisson's ratio. The new technique provides a means for circumventing the problem of a high Poisson's ratio.

5.2. Hydrophones

The physical design of a hydrophone using the new composite is identical to that discussed above for the thickness mode transmitter/ receiver. However, the principle of operation is quite different. In the hydrostatic mode, the net charge generated by hydrostatic pressure is determined by d_h charge coefficient This parameter is related to d_{33} and d_{31} in the following manner.

$$d_h = d_{33} + 2\,d_{31} \qquad (27)$$

The hydrostatic charge coefficient is d_h (units C/N or m/V), while d_{33} is the coefficient relating thickness induced charge to applied thickness stress and d_{31} is the coefficient relating thickness induced charge to applied lateral stress. PZT materials are very efficient charge generators. However, for PZT 5A, $d_{33} = 374 \times 10^{-12}$ m/V and $d_{31} = -171 \times 10^{-12}$ m/V. Therefore, the d_h coefficient is only 32×10^{-12} m/V. It is evident that the objective in the design of hydrophones incorporating PZT should be to decouple the thickness and lateral stresses. A composite design achieves this to an extent since the polymer phase may serve to absorb lateral strains. However, if the polymer has a high Poisson's ratio, thickness strain is still strongly coupled to lateral strain. The phase relationship of this induced strain, with respect to the thickness strain, implies that the net induced charge is reduced. One technique for reducing the extent of cross coupling of strain in the polymer phase is to introduce porosity [50]. A foam type structure achieves this effect successfully but it is vulnerable to collapse when subjected to high hydrostatic pressure [50]. Another approach involves weaving glass fibers into the composite matrix. These absorb some of the lateral stress but enhance the net charge generating effect to a lesser extent than the foamed polymer technique. Another design uses a substantial air void

78

surrounding all the ceramic pillars [51]. High sensitivity is achieved but it is evident that the design is vulnerable to damage at high hydrostatic pressures.

The new hydrophone design comprises of the same aligned compressible inclusions as discussed in the previous section. Perhaps the greatest attribute of the technique is that a highly anisotropic net polymer/ void characteristic is achieved. Pressure waves impinging perpendicular to the thickness facing surface encounter a "parallel springs" structure of alternating ceramic, polymer and gas. The ceramic is the dominant "spring" and hence it preferentially absorbs the induced stress. However, in the lateral direction, an incoming wave encounters a "series spring" structure composed of ceramic, polymer and gas. Naturally, the gas dominates in the series case and absorbs virtually all induced str'n. Hence, optimal use is made of a highly anisotropic composite structure.

The effect of introducing holes in a composite has been evaluated theoretically using finite element analysis. One basic design has been tested. The ceramic volume fraction was 25% and the ceramic pillars were 4 mm long and 1 mm across. Devices containing epoxy and polyurethane have been evaluated separately. Since, in a practical system, it is necessary to have a layer over the surface to protect the electrode and to prevent water ingress into the holes, the design has also been tested with a 0.5 mm thick layer on the top and bottom surfaces. The holes, where they have been introduced, were 0.5 mm across and extended throughout the thickness of the active composite material. It is anticipated that the design will be resistant to high hydrostatic pressure since the holes need only possess a small cross-sectional area. Additionally, unlike the foamed structures considered previously, these are ordered structures and hence weak points can be avoided by judicious design. The finite element analysis was performed by applying a known static pressure in three planes. The charge induced was related to the applied force to yield the effective d_h coefficient. The technique was initially tested using a reference ceramic sample. The d_{33} coefficient calculated using this technique matched the manufacturer's tabulated value [45].

The theoretical results obtained are presented in Table II. It may be observed that very substantial increases in the d_h coefficient are obtainable Generally, the two hole design does not produce results substantially different from the one hole design. However, using the combined hole design yields better results. The "sliced" design produces by far the best results. In this case, the lateral force is entirely decoupled. This design would be substantially more vulnerable to collapse at high hydrostatic pressure. It is also evident that, as in the case of the thickness resonant transducers, a far greater enhancement is obtained

TABLE II
Dependence of theoretical d_h coefficient on composite geometry and material.
(d_h values in units 10^{-12} C/N)

| | No layer | | With layer | |
	Polyurethane	Epoxy	Polyurethane	Epoxy
No hole	1.87	8.05	4.09	9.07
Diagonal	13.27	19.12	17.40	20.76
Parallel	10.51	16.67	19.45	22.07
Combined	27.69	32.24	38.73	38.59
Sliced	272.97	248.06	288.17	259.34

by using holes when the polymer is polyurethane rather than epoxy. This is because polyurethane is largely incompressible and hence strains are strongly coupled between the lateral and thickness directions when the polymer is in bulk form. At least in the case of epoxy, the presence of a protective layer does not significantly modify the degree of improvement that one might expect from using the technique. When it is considered that the commonly used $d_h g_h$ coefficient [52] is related to d_h^2, it is clearly evident that the technique presented here is capable of producing very substantial improvements in performance.

6. PROGRAM OF COLLABORATION WITH FMI

A collaboration program with FMI, Maine, was established. This provided Stanford with a facility for obtaining samples and experimental results, and FMI with a means of improving their understanding of composite behavior with a view to establishing optimal practical designs. FMI has a manufacturing technology with greater flexibility than that of the conventional dice-and- fill technique. Specifically, elements can be inserted in a polymer substrate in a completely arbitrary two-dimensional pattern.

Various phenomena were to be investigated:

1. Reducing parasitic mode behavior using the following techniques.
   a) Specialized geometries resulting in canceling of piezoelectric coupling to specific bandedge resonances.
   b) Statistically varying inter-pillar dimensions
   c) Filler materials

2.   Performance as a function of polymer properties

3.   Performance of new "enhanced" composite with aligned, compressible, gas-filled inclusions.

The starting point of the program was the establishment of a suitable baseline design possessing well-characterized parasitic resonant modes. Sample #16822, using a square lattice, exhibited three clearly identifiable resonances. This sample has a ceramic volume fraction of 10%, and the PZT-5H pillars are 1 mm across. FMI HD-68 epoxy was employed as the filler. The sample measures 38 x 38 mm and is 6.35 mm thick. The three resonances illustrated in Fig. 46, at progressively higher frequencies, may be related to the parallel lateral mode, the thickness mode, and the diagonal lateral mode, respectively. When the structure was analyzed using finite element analysis, the corresponding modes, illustrated in Fig. 47 were obtained. The correlation between Figs. 46 and 47 was established by comparing the frequencies. Note that the illustrations in Fig. 47 are for a one-eighth section of a unit cell, with the centerline of the cell at the upper corner and the horizontal mid-plane at the bottom.

6.1 Reducing parasitic mode activity

a) Specialized Geometries

The first modified structure involves using a rectangular rather than a square lattice. This lattice is illustrated in Fig. 48. The principle is that at the lowest frequency bandedge resonance, there is $\lambda/2$ spacing along the horizontal axis and $\lambda/4$ spacing along the vertical axis. Alternate vertical columns vibrate anti-phase and hence the integrated piezoelectric coupling is zero. At the next higher resonance, with λ spacing horizontally and $\lambda/2$ spacing vertically, alternate horizontal rows vibrate anti-phase. Figure 49 illustrates the impedance plot of sample #16714, which possesses this geometry. It is clear that this technique does in fact result in reduced lateral mode activity. However, some remnant resonant activity is still present.

A second modified structure is similar to that illustrated in Fig. 48 except that pillars are placed in the centers of the rectr gular lattices. Scattering from the edges of the rectangular lattices are 180° out of phase with scattering from the center and hence the lowest Bragg order is suppressed. Figure 50 illustrates the plot characteristic of sample #16715, which possesses this structure. The diagonal resonance has been completely
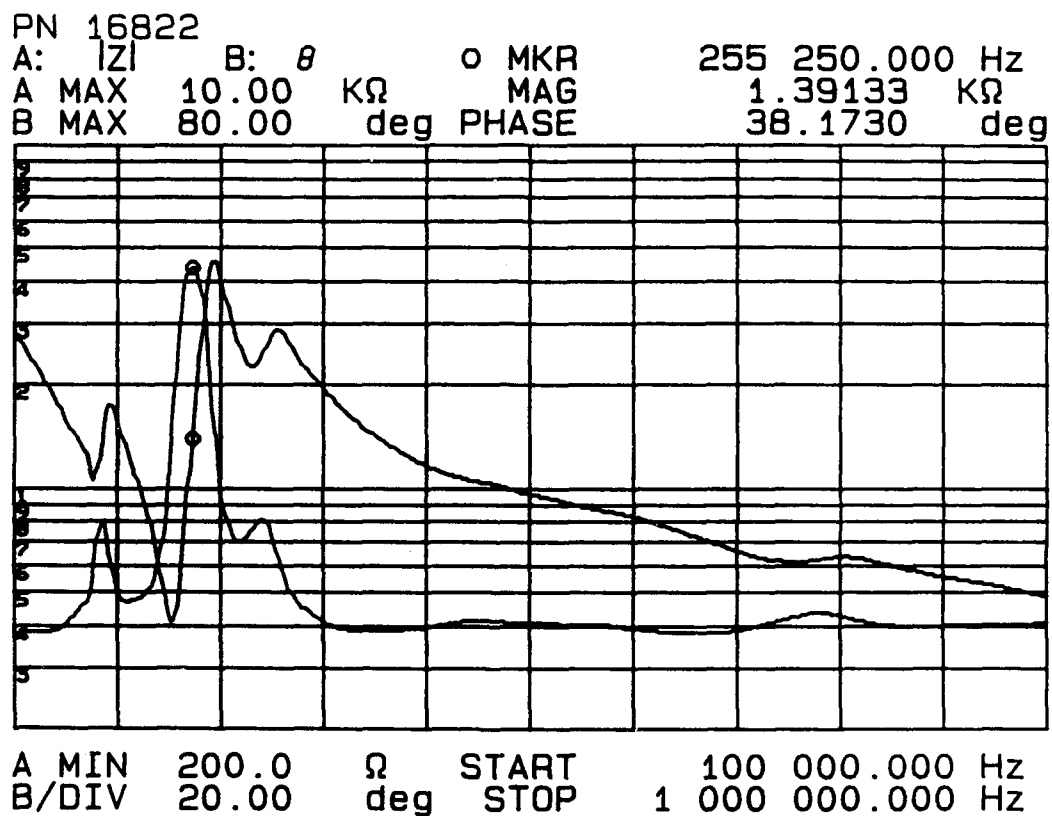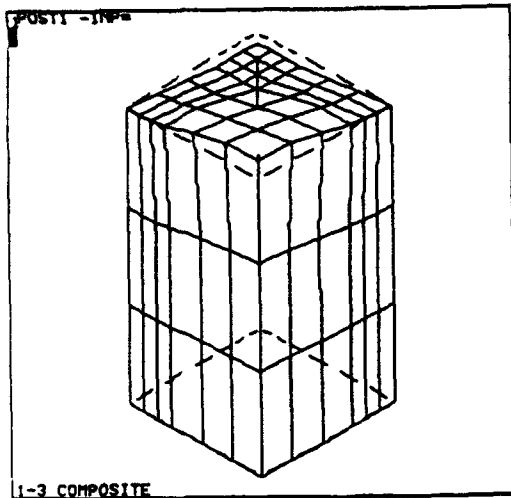
PN 16822
A: |Z| B: θ   o MKR   255 250.000 Hz
A MAX   10.00   KΩ   MAG   1.39133   KΩ
B MAX   80.00   deg PHASE   38.1730   deg

A MIN   200.0   Ω   START   100 000.000 Hz
B/DIV   20.00   deg STOP   1 000 000.000 Hz

Figure 46
Impedance characteristic of the baseline sample #16822 (Square lattice)
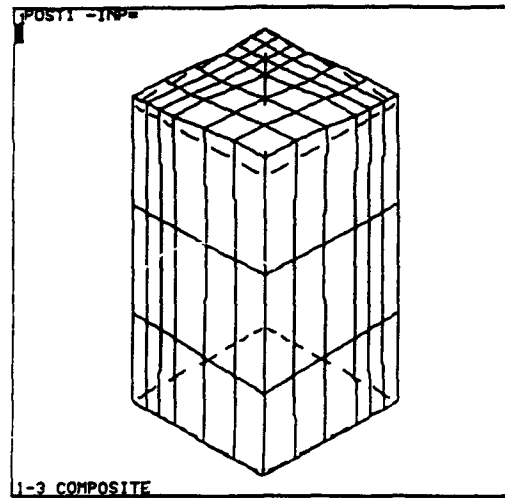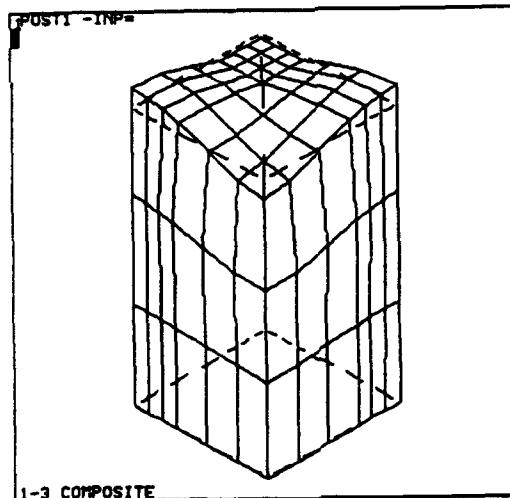
Figure 47

Finite element derived modes in the baseline sample

Modal displacement shape ————

Static shape – – – – – – – – – – – – –
       a) Parallel mode
       b) Thickness mode
       c) Diagonal mode

PZT COMPOSITE ARRAY DESIGN #1

PART SIZE: 1.5" X 1.5"

.166

.083

.040 X .040 PZT RODS
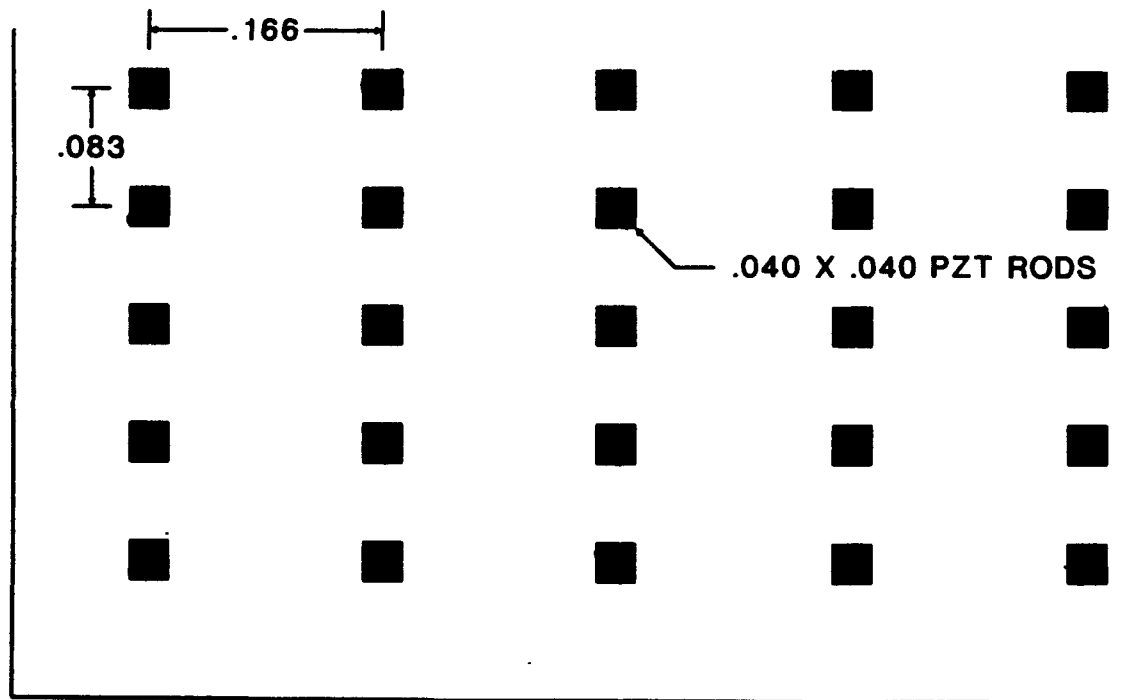
PART NUMBER 16714

Figure 48
Rectangular lattice design
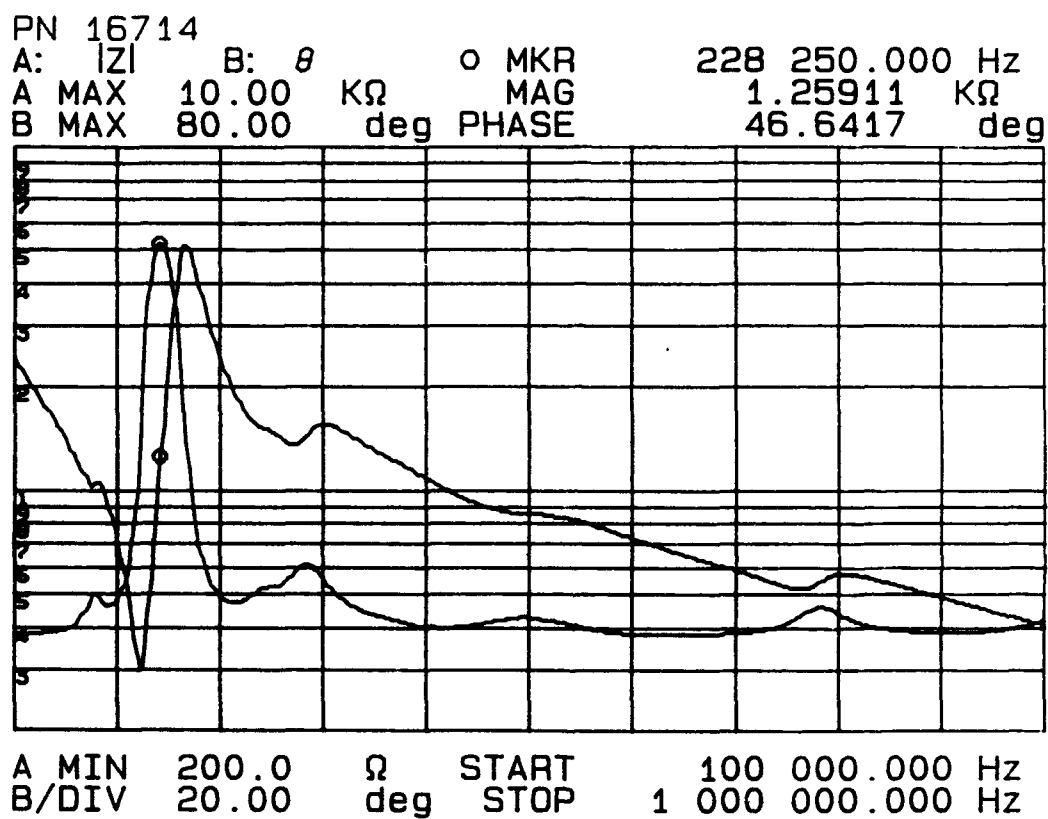
Figure 49
Impedance characteristic of sample #16714 (Rectangular lattice)

85

```
PN 16715
A:  |Z|      B:  θ        ○ MKR        298 000.000 Hz
A MAX    10.00   KΩ       MAG          1.70322   KΩ
B MAX    80.00   deg  PHASE           32.2099    deg
```

```
A MIN   200.0    Ω    START      100 000.000 Hz
B/DIV   20.00   deg   STOP     1 000 000.000 Hz
```

Figure 50
Impedance characteristic of sample #16715 (Modified lattice)

86

eliminated. The lower frequency, parallel, mode remains. The phenomena behind this result are not fully understood at present.

b) Statistically Varying Geometries

It has been established that by using a statistical distribution of inter-pillar dimensions, it is possible to eliminate strong parasitic lateral resonant activity occurring at discrete frequencies [53]. The previous work conclusively proved that the use of statistical distributions, cerated by dicing and filling with quasirandomly spread dicing cuts, is effective. The two-dimensional modeling method discussed in Section 7 suggests that quasirandom patterning of the ceramic element locations in two dimensions should be more effective in mode suppression. This kind of pattern, not realizable by the dice and fill technique, can be manufactured using FMI technology. Such composites, derived from the baseline (#16822), were manufactured by FMI with variances of 10%, 30% and 50% applied to the inter pillar spacings. The impedance spectra of these devices are illustrated in Figs. 51, 52 and 53 respectively. These results indicate that variances of 10% and 30% are ineffective in terms of reducing parasitic resonant activity. However, the sample with 50% variance does indicate a reduction in resonant activity. Previous work has conclusively proven that the use of statistical distributions is effective [53]. It is suspected that the 10% and 30% results did not appear as effective as they might otherwise have been because tolerances maintained in the manufacturing technique currently used by FMI introduce a degree of variance into the basis structure as a matter of course. The degree of variance has not been precisely quantified, since it is operator dependent. In future, the degree of variance may be more tightly controlled by the use of complete automation. Nevertheless, it would appear that a degree of variance is desirable in any case.

c) Filler Materials

A sample similar to the baseline, (#16822) except that it included glass fiber reinforcement, was manufactured and tested. Fiber reinforcement has a beneficial effect on the hydrostatic performance of composite transducers since the glass absorbs lateral stresses thus relieving the active ceramic pillars. In the hydrostatic mode it is highly desirable to decouple thickness and lateral stresses since the induced charges due to these separate stresses tend to cancel each other out. Additionally, reinforcement may lead to improved mechanical stability and result in attenuation of the lateral mode. The impedance spectrum of the reinforced device is illustrated in Fig. 54. The resonant characteristics

87

16981
A: |Z| B: θ   o MKR   257 500.000 Hz
A MAX   10.00   KΩ   MAG   1.68063   KΩ
B MAX   80.00   deg PHASE   47.5274   deg

A MIN   200.0   Ω   START   100 000.000 Hz
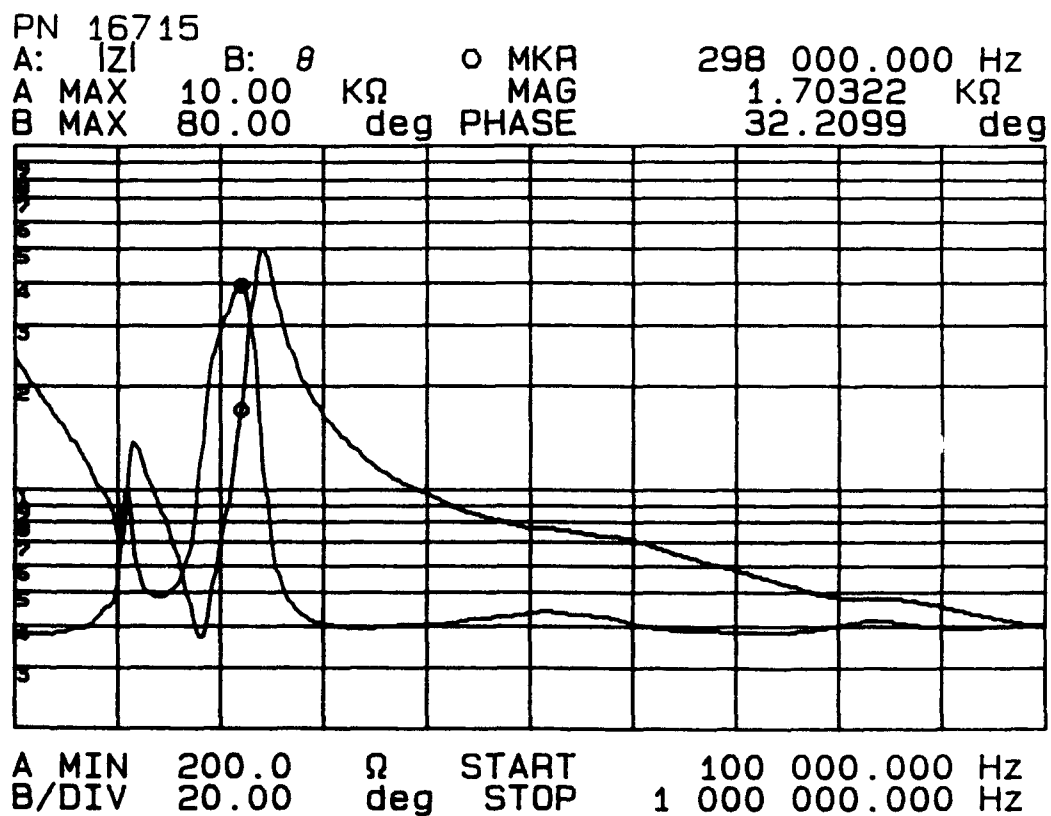B/DIV   20.00   deg STOP   1 000 000.000 Hz

Figure 51
Impedance characteristic of sample #16981 (10% variance applied to inter-pillar dimension)

Figure 52
Impedance characteristic of sample #16983 (30% variance applied to inter-pillar dimension)

89

PN 16986
A: |Z| B: θ   ○ MKR   237 250.000 Hz
A MAX   10.00   KΩ   MAG   733.470   Ω
B MAX   60.00   deg PHASE   -22.8519   deg

A MIN   500.0   Ω   START   100 000.000 Hz
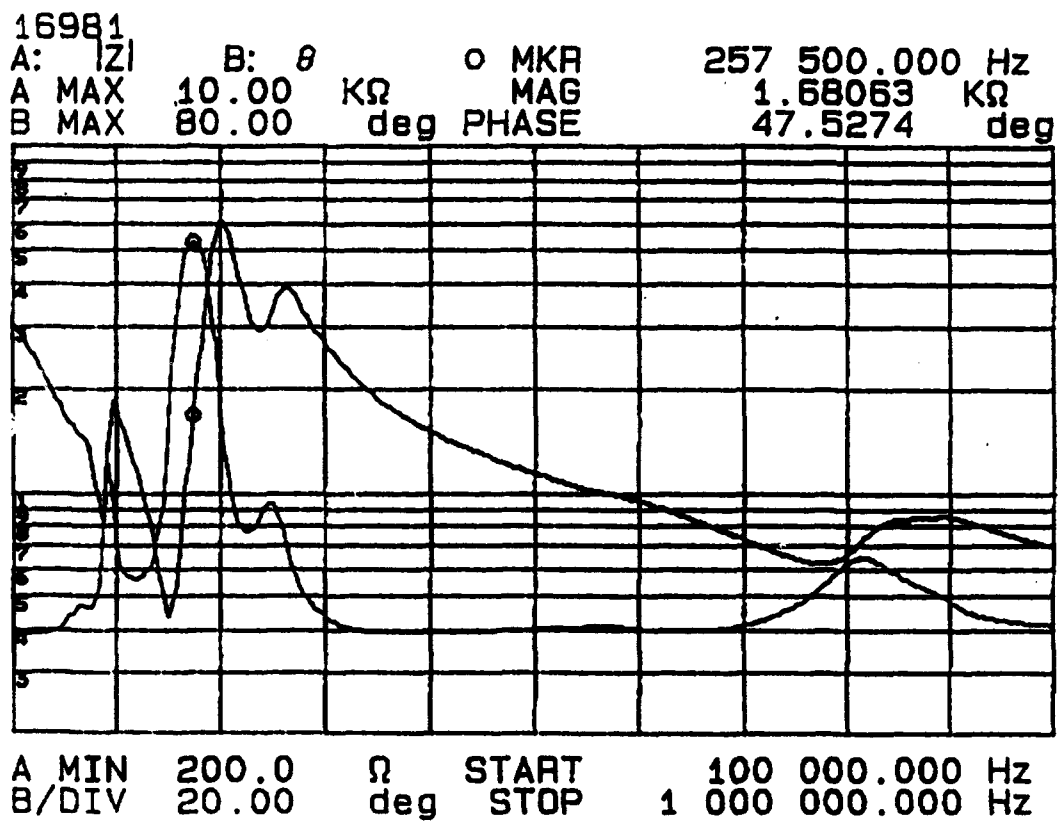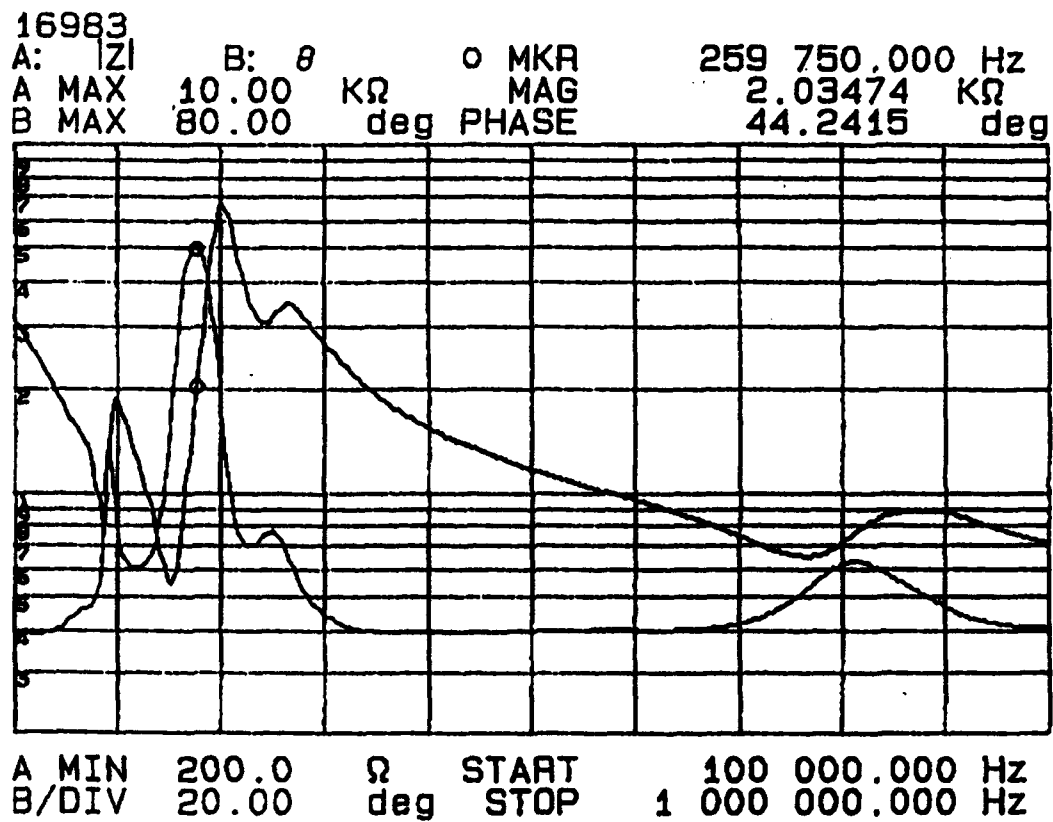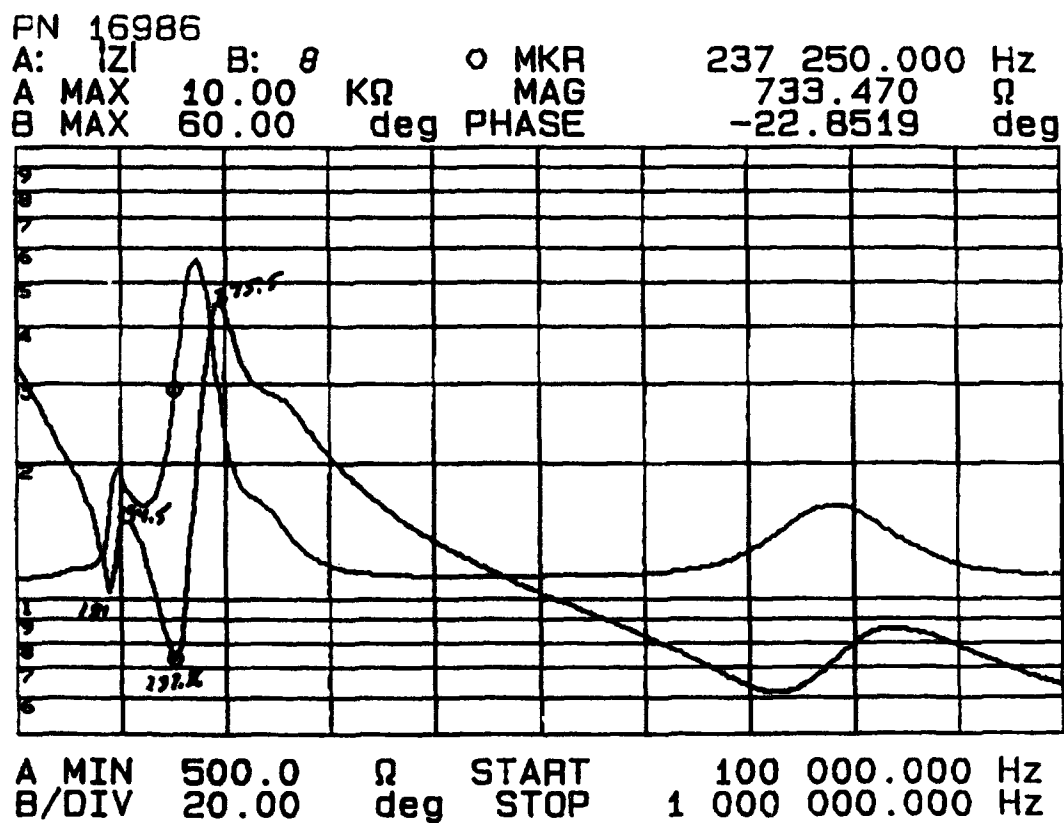B/DIV   20.00   deg STOP   1 000 000.000 Hz

Figure 53
Impedance characteristic of sample #16986 (50% variance applied to inter-pillar dimension)
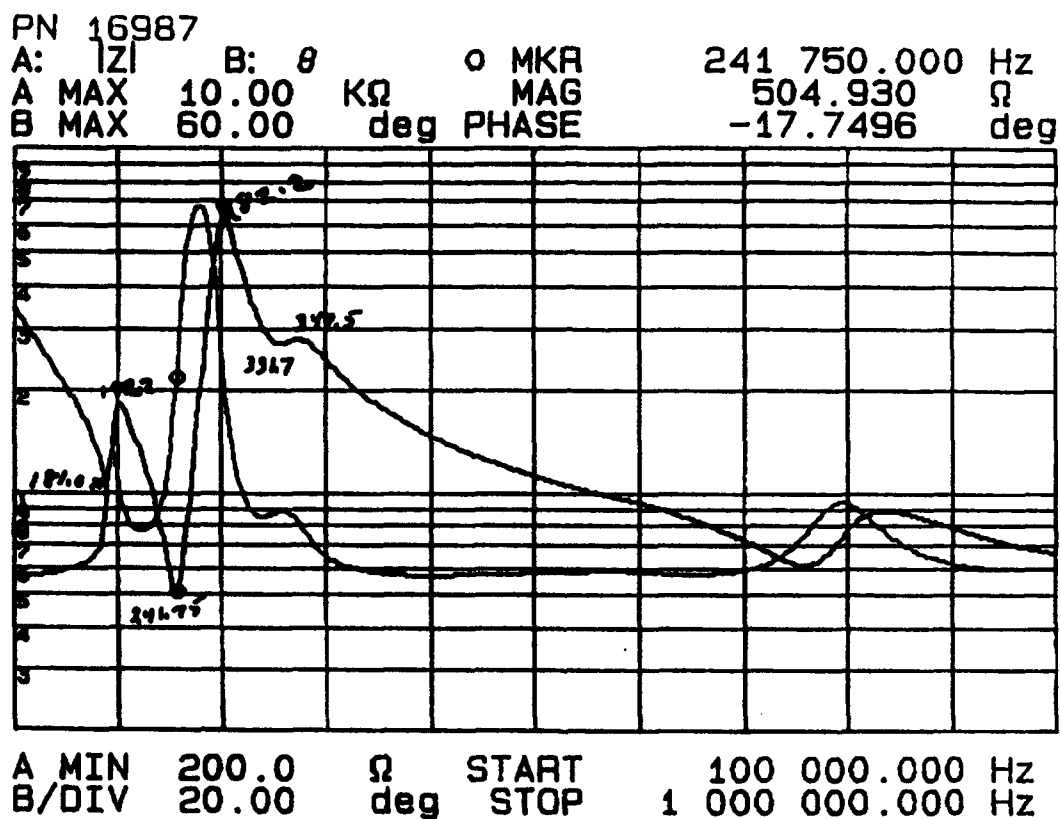
Figure 54
Impedance characteristic of sample #16987 (Glass fiber reinforced sample)

differ slightly from those of the baseline sample (Fig. 46). This may be due in part to the fact that the volume fraction of reinforcement fibers was only 5% (#16987).

A second composite possessing a reinforcement volume fraction of 10% (#17491) was also manufactured. In this case Ceramaform reinforcement was employed. The impedance characteristic for this device, illustrated in Fig. 55, also indicates strong parasitic resonant behavior. It is probable that the resonant behavior would be more significantly modified if higher reinforcement loading fractions were used. Given the vast range of possible reinforcement geometries and materials, there is clearly considerable scope for future work in this field. In any case, it appears that for less than 10% reinforcement loading, modeling of nonreinforced composites may be used to satisfactorily predict lateral mode behavior.

6.2 Performance as a Function of Polymer Elastic Properties

The dependence of parasitic mode behavior on temperature has also been investigated. As temperature is increased, the polymer passes through its "glass transition" temperature. At temperatures above this point the polymer becomes soft and highly attenuative. Generally, polymers which are relatively soft at room temperature have lower glass transition temperature. The impedance characteristics of the baseline sample (#16822) was tested from -50° to +50°C at 10° intervals. These impedance spectra are illustrated in Fig. 56. It is readily evident that the glass transition temperature of the polymer used in this sample is approximately +30°C. This is relatively low for an epoxy polymer. Many applications would require that the glass transition temperature be well outside the operating temperature range of the practical device. As the temperature increases, the frequencies of the resonances reduce as the polymer becomes more compliant. Careful examination reveals that the decrease in frequency in the resonant frequencies is greater for the lateral modes than for the thickness mode. This is probably due to the fact that the polymer's shear wave velocity decreases more rapidly than its longitudinal wave velocity. This implies that the Poisson's ratio of polymer increases as polymer softens. This is a satisfying result since it is well known that compliant polymers usually possess higher Poisson's ratios than less compliant polymers. The major feature observed as the polymer passes through the glass transition temperature is that the polymer becomes so attenuative that it can no longer support lateral resonant activity. Although this may appear to be a desirable characteristic, it is also probable that thickness energy is not being coupled efficiently between the active thickness vibrating ceramic pillars and the neighboring
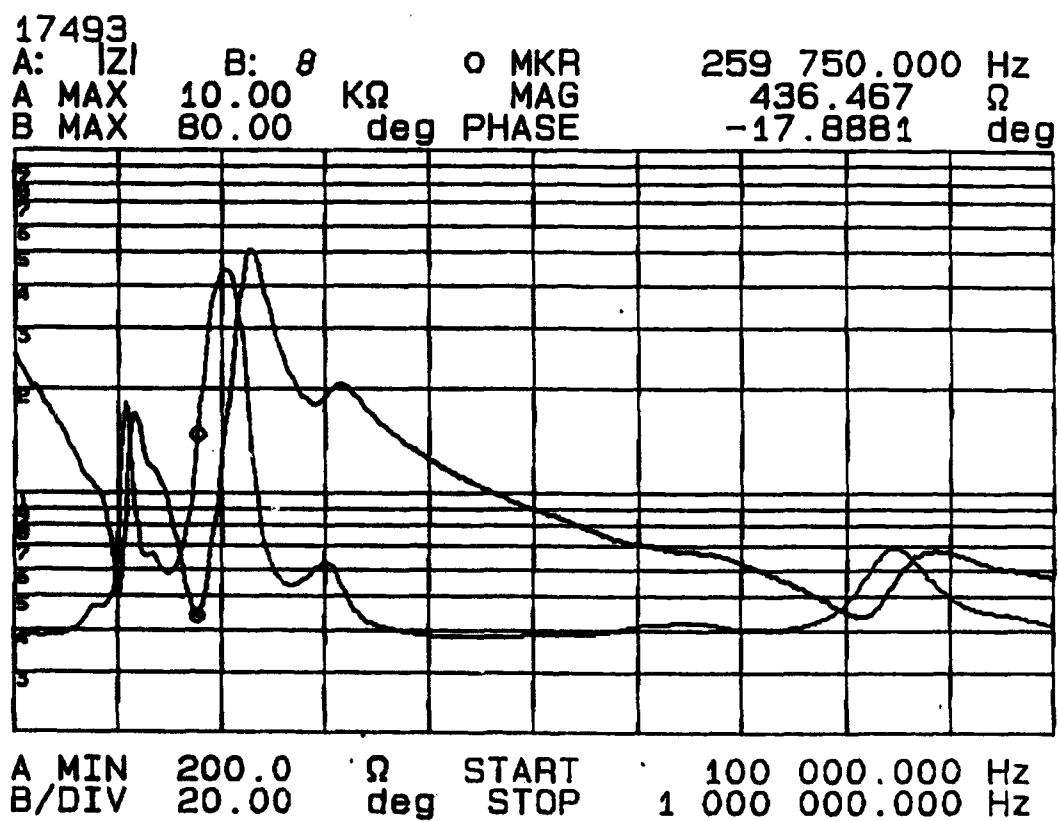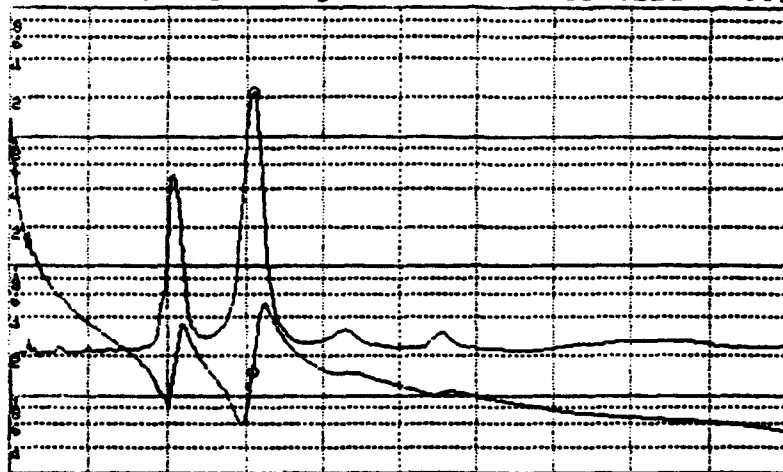
92

Figure 55
Impedance characteristic of sample #17493 (Ceramaform reinforced sample)

PN 16822B
A: IZI   B: θ   o MKR   307 569.250 Hz
A MAX 1.000 MΩ   MAG   1.53219   KΩ
B MAX 60.00 deg PHASE   23.6250   deg

A MIN 250.0   Ω   START   100.000 Hz
B/DIV 20.00   deg STOP   1 000 000.000 Hz
-50 DEG C _

PN 16822B
A: IZI   B: θ   o MKR   305 069.500 Hz
A MAX 1.000 MΩ   MAG   1.45097   KΩ
B MAX 60.00 deg PHASE   25.0283   deg
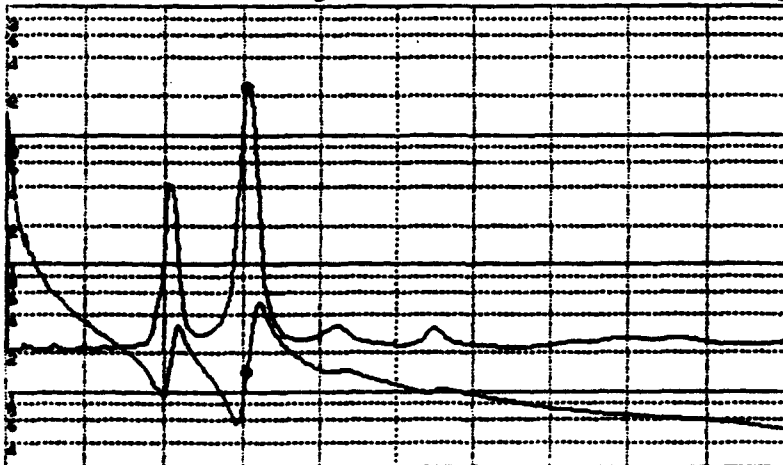
A MIN 250.0   Ω   START   100.000 Hz
B/DIV 20.00   deg STOP   1 000 000.000 Hz
-40 DEG C _

Figure 56
Impedance characteristic of sample #16822 (Baseline) measured at various
temperatures (10°C intervals)

94

PN 16822B
A: IZI   B: θ   o MKR   300 070.000 Hz
A MAX   1.000 MΩ   MAG   1.64458   KΩ
B MAX   60.00 deg PHASE   29.8430   deg
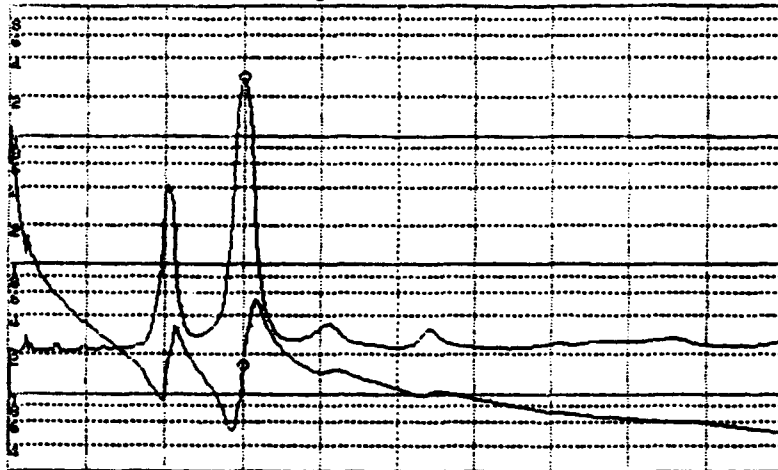
A MIN   250.0   Ω   START   100.000 Hz
B/DIV   20.00   deg STOP   1 000 000.000 Hz
-30 DEG C

PN 16822B
A: IZI   B: θ   o MKR   292 570.750 Hz
A MAX   1.000 MΩ   MAG   1.44646   KΩ
B MAX   60.00 deg PHASE   34.3040   deg

A MIN   250.0   Ω   START   100.000 Hz
B/DIV   20.00   deg STOP   1 000 000.000 Hz
-20 DEG C

Figure 56

95

```
PN 16822B
A: IZI      B: θ        o MKR      282 571.750 Hz
A MAX   1.000   MΩ        MAG          1.41460   KΩ
B MAX  60.00   deg  PHASE          38.9210   deg
```

```
A MIN   250.0    Ω   START            100.000 Hz
B/DIV  20.00    deg  STOP   1 000 000.000 Hz
-10 DEG C _
```



```
PN 16822B
A: IZI      B: θ        o MKR      280 872.000 Hz
A MAX   1.000   MΩ        MAG          1.45158   KΩ
B MAX  60.00   deg  PHASE          40.8336   deg
```

```
A MIN   250.0    Ω   START            100.000 Hz
B/DIV  20.00    deg  STOP   1 000 000.000 Hz
0 DEG C_
```
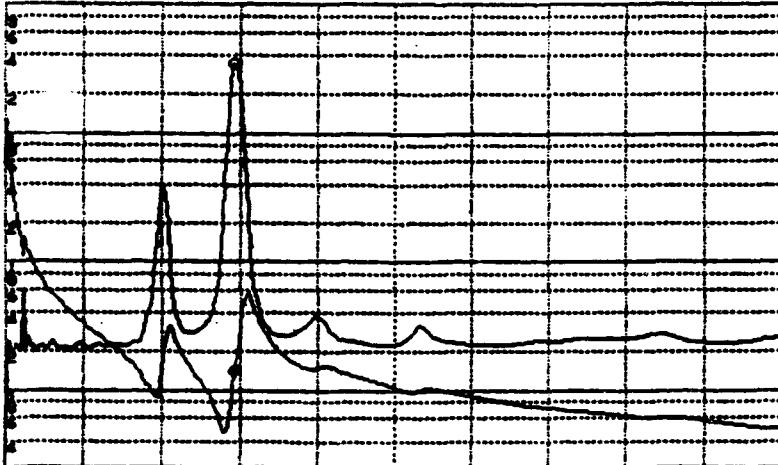
Figure 56

96

```
PN 16822B
A: IZI     B: θ        ○ MKR      272 572.750 Hz
A MAX  1.000  MΩ        MAG         1.36966  KΩ
B MAX  60.00  deg PHASE           39.7636   deg
```

```
A MIN   250.0    Ω    START           100.000 Hz
B/DIV   20.00    deg  STOP    1 000 000.000 Hz
+10 DEG C_
```



```
PN 16822B
A: IZI     B: θ        ○ MKR      262 573.750 Hz
A MAX  1.000  MΩ        MAG         1.66211  KΩ
B MAX  60.00  deg PHASE           29.1103   deg
```

```
A MIN   250.0    Ω    START           100.000 Hz
B/DIV   20.00    deg  STOP    1 000 000.000 Hz
+20 DEG C_
```

Figure 56

97

PN 16822B
A: IZI   B: θ   ○ MKR   247 575.250 Hz
A MAX   1.000   MΩ   MAG   1.27966   KΩ
B MAX   60.00   deg PHASE   24.4306   deg

A MIN   250.0   Ω   START   100.000   Hz
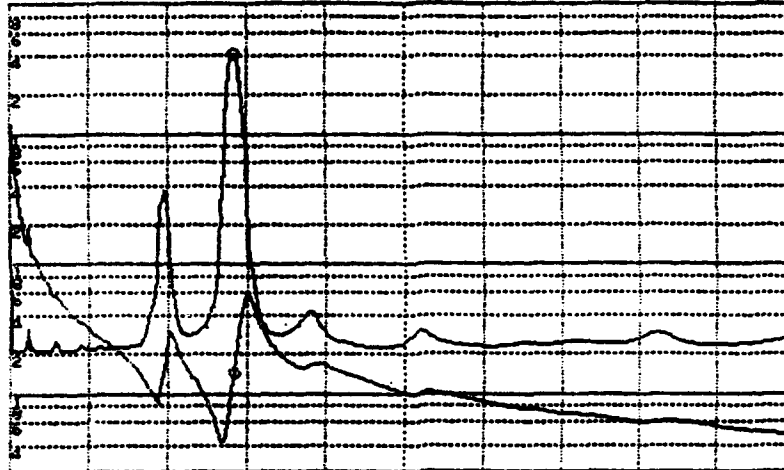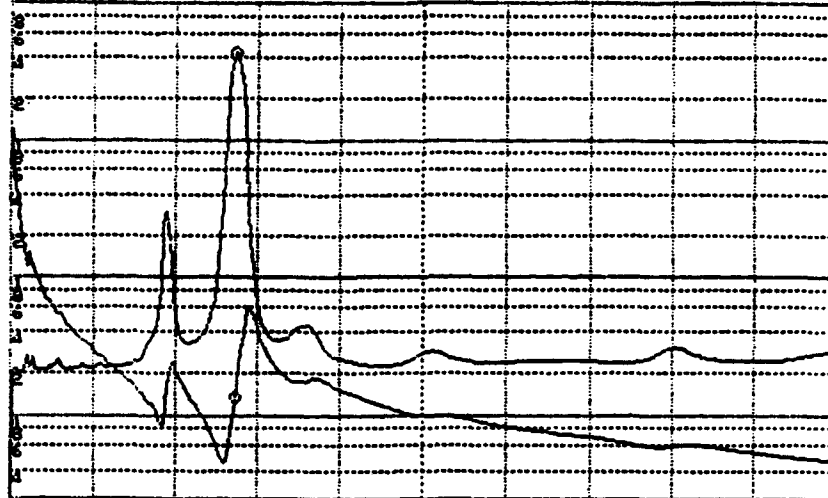B/DIV   20.00   deg STOP   1 000 000.000   Hz
+30 DEG C   _

PN 16822B
A: IZI   B: θ   ○ MKR   ˙235 076.500 Hz
A MAX   1.000   MΩ   MAG   984.156   Ω
B MAX   60.00   deg PHASE   -626.441   mdeg

A MIN   250.0   Ω   START   100.000   Hz
B/DIV   20.00   deg STOP   1 000 000.000   Hz
+40 DEG C   _

Figure 56

98

PN 16A22B
Ω: IZI   B: θ   ⊙ MKR   247 575.250 Hz
A MAX   1.000   MΩ   MAG   1.48679   KΩ
B MAX   60.00   deg PHASE   19.6273   deg

A MIN   250.0   Ω   START   100.000 Hz
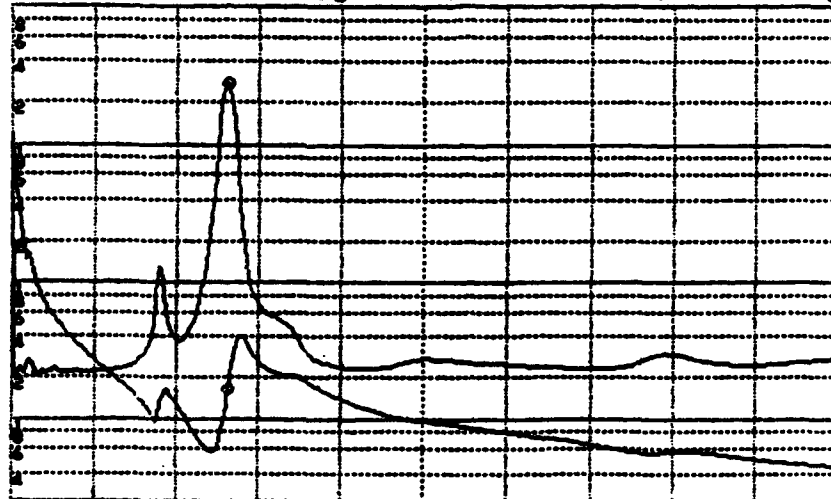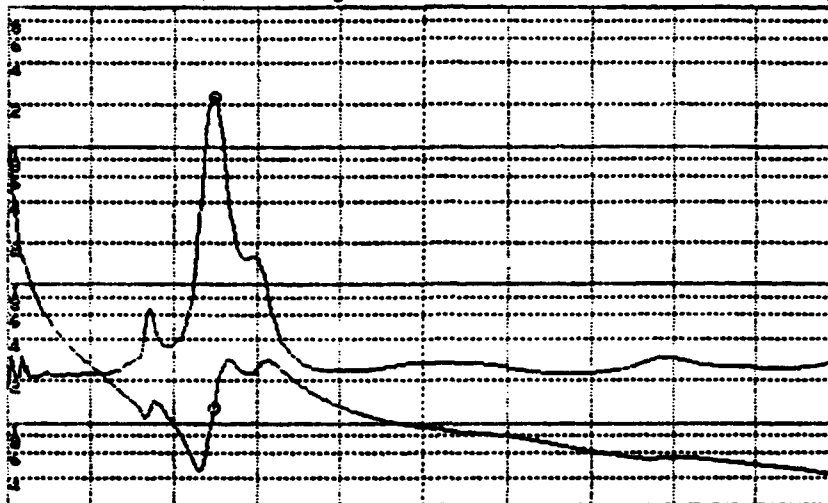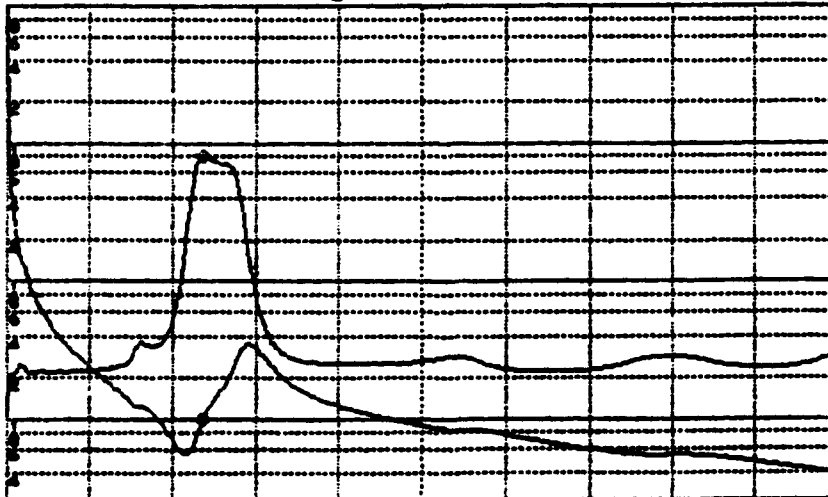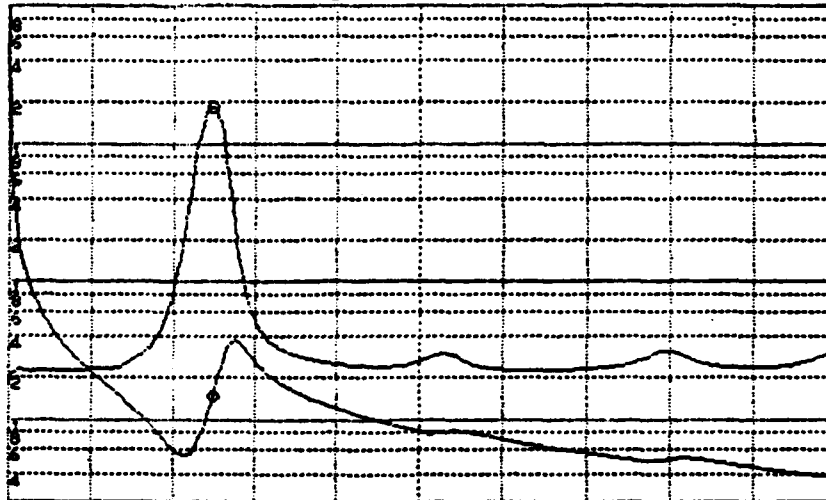B/DIV   20.00   deg STOP   1 000 000.000 Hz
+50 DEG C_

Figure 56

polymer. Efficient composite transducer operation relies upon efficient coupling of thickness polarized vibration between the pillars and the surrounding polymer matrix.

6.3 Performance of "Enhanced" Composites

The motivation for designing 1:3 composites with aligned vertical compressible inclusions has been discussed at length in Section 5. FMI manufactured three enhanced composites. Each composite was split into quadrants, each possessing a different hole geometry. These geometries are illustrated in Fig. 57. Sample #16978 (Fig. 57) is similar to the baseline design (#16822) but possesses 0.020" holes. Sample #16979 has the same pattern, but with 0.040" holes. The impedance spectra of the quadrants of these composites are illustrated in Figs. 58 and 59 respectively. It is clear that the 0.020" holes have had little impact on the resonant characteristics present in the undrilled sample. However, when the results for #16979 are considered, it is evident that the larger holes have reduced the strength of the higher frequency, diagonal, parasitic lateral mode. It was expected that the presence of holes would severely disrupt the lateral resonant characteristic. The phenomena which give rise to these results are not fully understood and further investigation would be valuable. In any case, samples #16978 and #16979 were designed for use at low frequencies where parasitic resonant behavior is immaterial. The devices were sent to NRL USRD for hydrostatic sensitivity testing. No results are available at this time.

A third enhanced composite, with a ceramic volume fraction of 30% was manufactured by FMI. This was tested at Stanford and the results obtained presented in Section 5 (Table I). A modest improvement in thickness mode transducer sensitivity in both transmission and reception was observed when the quadrants possessing compressible inclusions were used.

The work on enhanced composites is at an early stage. Initial theoretical and experimental work suggest the promise of improved efficiency. This is most evident when a low elastic modulus, high Poisson's ratio polymer is used. Additionally, greatest benefits are expected when the transducer is used in the low frequency hydrophone mode. The economics of manufacture are yet to be addressed. However, there are some techniques currently being developed which hold promise for low cost manufacture.

PZT COMPOSITE DESIGN
16978
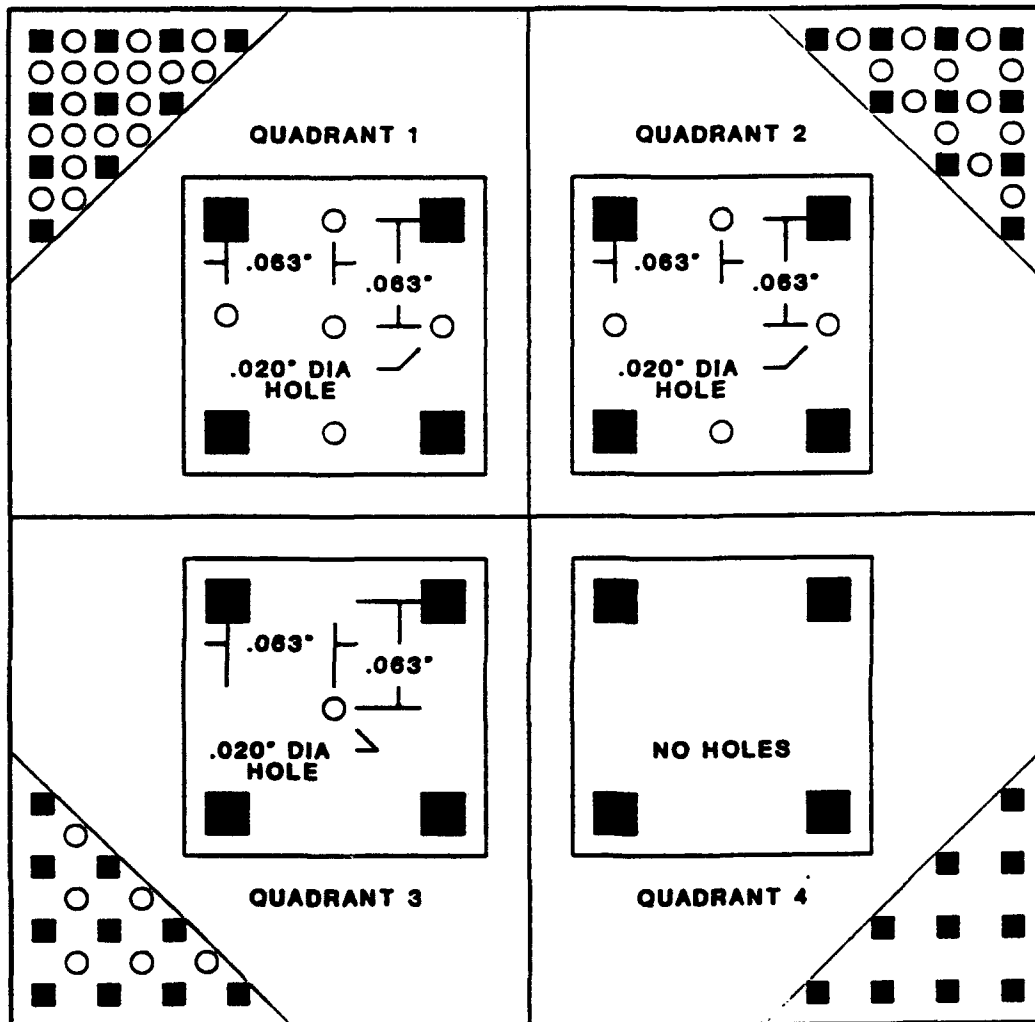
Figure 57
Configuration of holes drilled in the quadrants of sample #16978

PN 16978-1
A: |Z| B: θ   ○ MKR   262 000.000 Hz
A MAX   50.00 KΩ   MAG   5.08485   KΩ
B MAX   80.00 deg PHASE   33.1050   deg
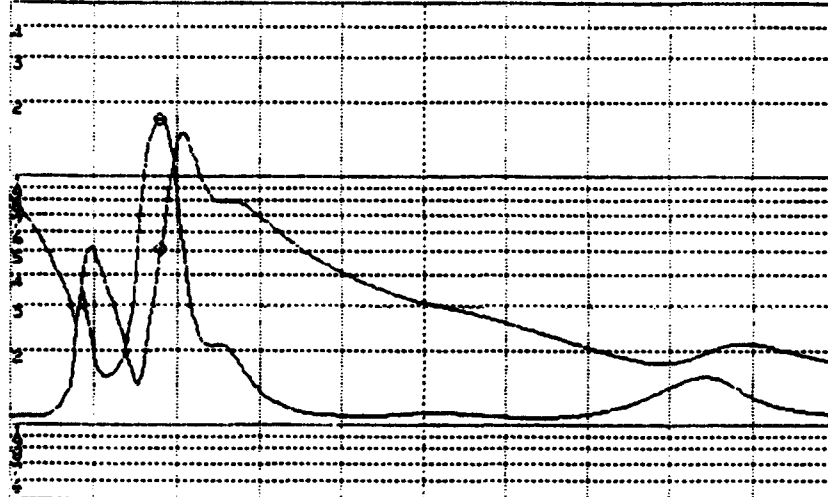
A MIN   500.0   Ω   START   100 000.000 Hz
B/DIV   20.00 deg STOP   1 000 000.000 Hz

PN 16978-2
A: |Z| B: θ   ○ MKR   257 500.000 Hz
A MAX   50.00 KΩ   MAG   4.00884   KΩ
B MAX   80.00 deg PHASE   38.1890   deg
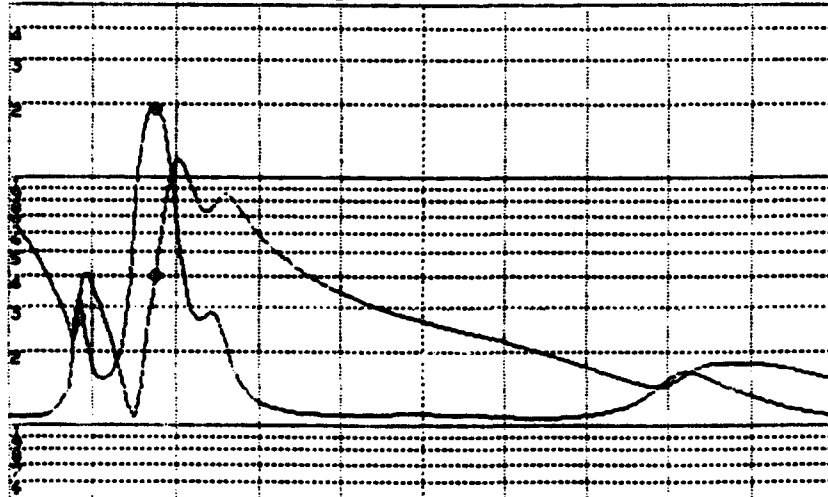
A MIN   500.0   Ω   START   100 000.000 Hz
B/DIV   20.00 deg STOP   1 000 000.000 Hz

Figure 58
Impedance characteristic of the quadrants of sample #16978 (0.020" holes)

102

PN 16978-3
A: |Z| B: θ   o MKR   262 000.000 Hz
A MAX   50.00   KΩ   MAG   4.44958   KΩ
B MAX   80.00   deg PHASE   41.3082   deg

A MIN   500.0   Ω   START   100 000.000 Hz
B/DIV   20.00   deg   STOP   1 000 000.000 Hz
-

PN 16978-4
A: |Z| B: θ   o MKR   259 750.000 Hz
A MAX   50.00   KΩ   MAG   3.92204   KΩ
B MAX   80.00   deg PHASE   44.6725   deg

A MIN   500.0   Ω   START   100 000.000 Hz
B/DIV   20.00   deg   STOP   1 000 000.000 Hz
-

Figure 58

103

PN 16979-1
A: |Z| B: θ   ◦ MKR   259 750.000 Hz
A MAX 50.00 KΩ   MAG   5.43732   KΩ
B MAX 80.00 deg PHASE   36.4047   deg

A MIN 500.0   Ω   START   100 000.000 Hz
B/DIV 20.00 deg STOP   1 000 000.000 Hz

PN 16979-2
A: |Z| B: θ   ◦ MKR   253 000.000 Hz
A MAX 50.00 KΩ   MAG   4.74197   KΩ
B MAX 80.00 deg PHASE   44.8814   deg

A MIN 500.0   Ω   START   100 000.000 Hz
B/DIV 20.00 deg STOP   1 000 000.000 Hz

Figure 59
Impedance characteristic of the quadrants of sample #16979 (0.040" holes)

104

PN 16979-3
A: IZI   B: θ   ○ MKR   280 000.000 Hz
A MAX   50.00   KΩ   MAG   6.64733   KΩ
B MAX   80.00   deg PHASE   30.7866   deg

A MIN   500.0   Ω   START   100 000.000 Hz
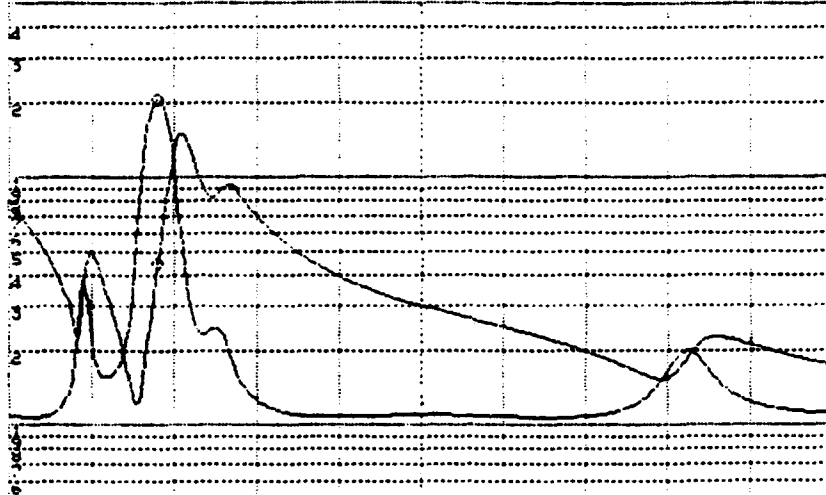B/DIV   20.00   deg STOP   1 000 000.000 Hz
-

PN 16979-4
A: IZI   B: θ   ○ MKR   262 000.000 Hz
A MAX   50.00   KΩ   MAG   4.46121   KΩ
B MAX   60.00   deg PHASE   32.7599   deg

A MIN   500.0   Ω   START   100 000.000 Hz
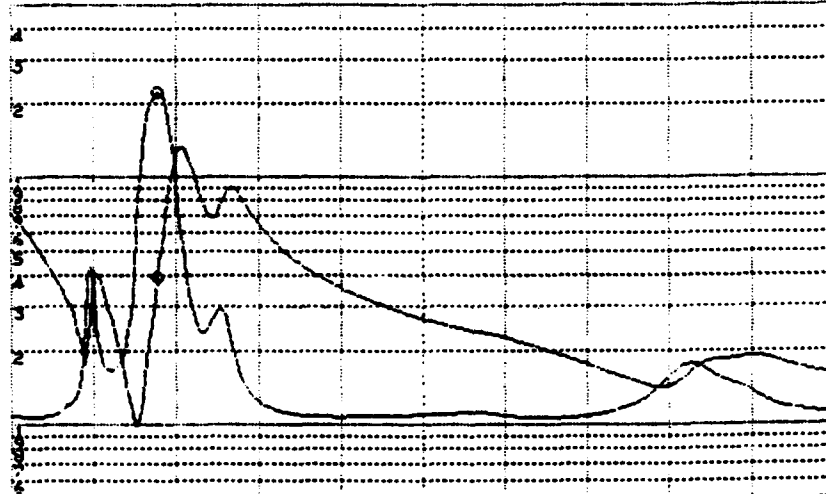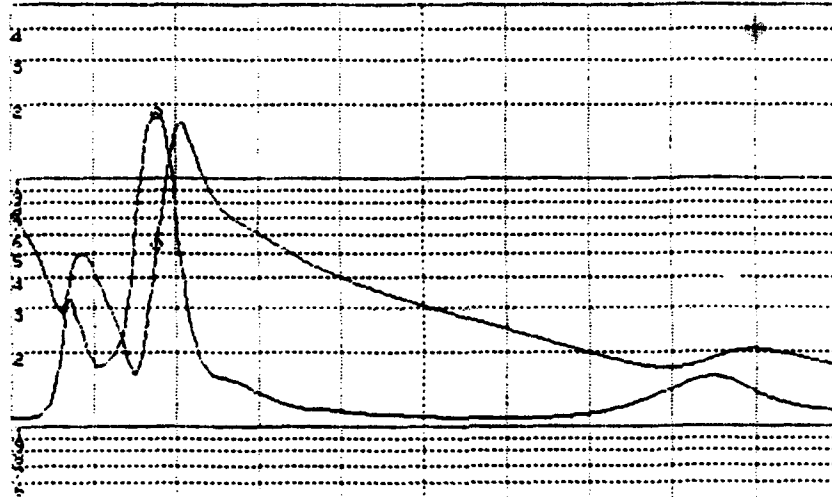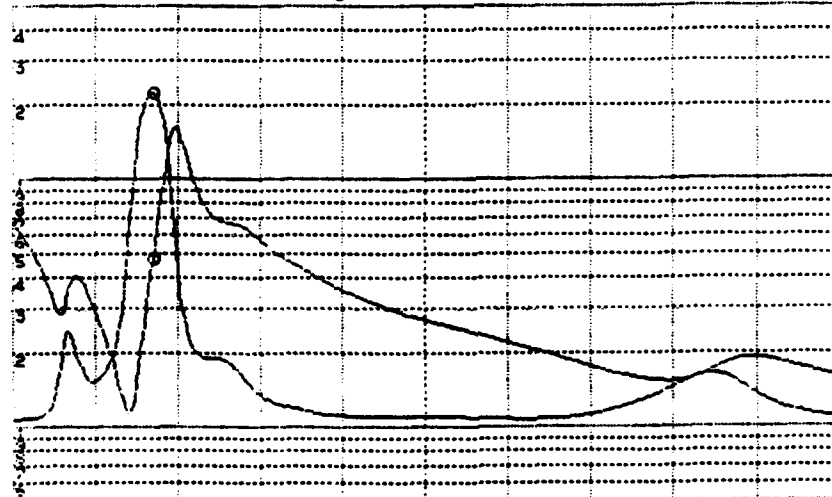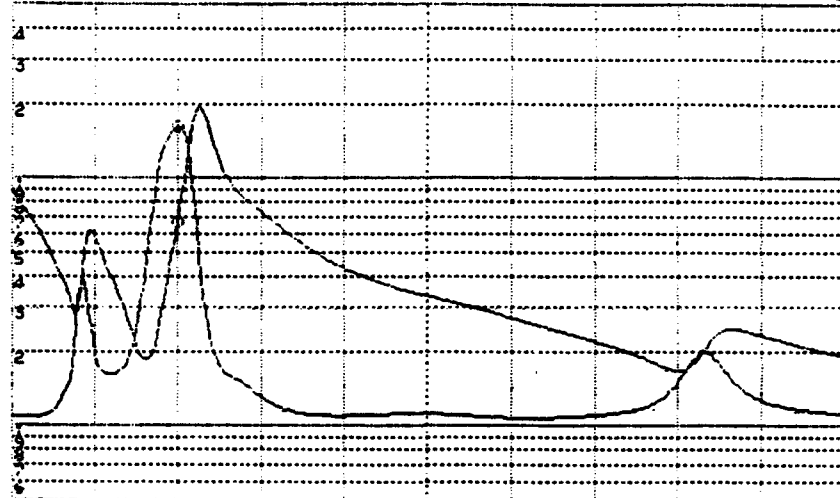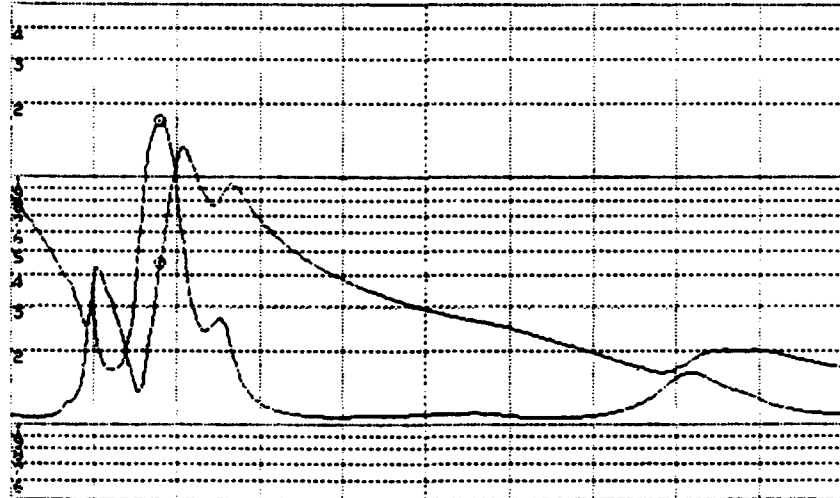B/DIV   20.00   deg STOP   1 000 000.000 Hz
-

Figure 59

105

6.4 Conclusions

During the course of this collaborative program it has become clear that the concept of using distributed period, and specialized geometry, designs is successful as a means of reducing parasitic resonant behavior. However, it would appear that it is still desirable to use the finest scale structures available within bounds set by economic and manufacturing factors. The temperature tests have yielded an improved understanding of the different modes and their dependence on polymer elastic modulus. In general it is desirable to employ a high modulus polymer with a high glass transition temperature. A limited amount of work with fiber reinforcement has proven inconclusive at this stage. It is foreseeable that the rewards of improved mechanical stability, enhanced sensitivity and reduced resonant activity suggest plentiful scope for fruitful work in future. Finally, the work on "enhanced" composites has proven very interesting and produced encouraging initial results. There is an obvious motivation for extending the currently limited understanding of the actual performance enhancement that can be achieved at an economical cost. There is also a requirement for identifying new applications for the large scale composites that have been studied. These include the non destructive examination of lossy media (concrete, wood, GRP etc.), high frequency sonar (civil and military applications) and as actuators in responsive structures, for vibration control.

7. MODELING OF TWO-DIMENSIONAL DISTRIBUTED PERIOD COMPOSITES

In a standard circular disk thickness transducer, consisting of an electroded piezoceramic disk, the main resonance is a $\lambda/2$ thickness mode excited directly by the z-directed E field due to the voltage applied to the electrodes. At the same time, lateral (radial, in this case) modes are excited through the thickness vibrational motion, by the Poisson effect at the free edge of the disk. These lateral modes are of extensional type, driven by the radial bulging in-and-out of the outer circumference of the disk. Lateral modes are not efficiently excited by the radially uniform z-directed E field driven by the electrodes, because of spatial averaging over the radial standing waves that constitute the lateral modes. In this type of transducer the lateral modes may be called dimensional modes, because they have frequencies determined by the radial dimension of the transducer.

In a 1-3 composite transducer the piezoelectric is distributed in piezoceramic elements arranged in either a strictly periodic or a distributed period lattice array that is

106

embedded in a polymer. The piezoelements may be arranged periodically in a simple square array, or in rectangular, triangular, etc., periodic arrays. Other possible configurations have additional piezoelements in each unit cell of the lattice.

The composite structures described above improve the characteristics of the thickness mode resonance. But they also alter the lateral mode spectrum. First, these structures present stopbands to the laterally propagating waves, preventing the formation of standing wave resonances at frequencies within a stopband. Second, at frequencies outside the stopbands the standing lateral waves are coupled to the electrodes only at discrete spatial positions. This means that the spatial cancellation of lateral mode coupling that occurs in a homogeneous ceramic transducer is lifted in a strictly periodic composite transducer. In particular, at the stopband edges the ceramic elements all vibrate in phase, or alternatively, in antiphase. The in-phase bandedge standing waves are strongly coupled to the electrodes, while the antiphase bandedge standing waves are totally decoupled.

To summarize, then, in a 1-3 periodic composite some of the lateral dimensional resonances are suppressed by the stopband structure of the lateral wave dispersion curves. On the other hand, certain lateral dimensional resonances at the stopband edges (the in-phase bandedge standing waves) experience greatly enhanced coupling to the electrodes. These strongly coupled lateral resonances degrade the performance of the transducer if they are located too close to the thickness resonance frequency.

The conventional approach to the problem of bandedge resonances is to reduce the period of the periodic array, shifting the resonances to frequencies much higher than the thickness resonances. Another solution is to introduce a quasirandom distribution in the spatial periodicity of the ceramic cylinder elements. A simple one-dimensional analytic model (based on transmission line theory) has shown that a large one-dimensional array having a distribution of periods exhibits a large reflective attenuation (Section 2.3), suggesting that such an array would effectively suppress all lateral resonances. Experiments on two-dimensional arrays with a Gaussian distribution of the unit cell dimensions have demonstrated that the bandedge resonances can be effectively controlled using this method—which tends to suppress the lateral resonances by virtue of the increased lateral wave attenuation. It also tends to reduce piezoelectric excitation of these modes by randomizing the phases of the coupling to the electrodes through the individual ceramic cylinders.

Up to now the design of two-dimensional distributed period 1-3 composite transducers has been almost entirely empirical. Floquet Theory is applicable only to periodic arrays; and application of the finite element method to a large two-dimensional array is impractical, as it would require computation, unless the domain of computation reduced to a single periodically repeated unit cell. For improved modeling of distributed periodic arrays there is need of an alternative approach. There appears to be no analytic method analogous to transmission line theory for one-dimensional distributed period composites. But another approach having advantages and limitations similar to those of Floquet Theory is based on a scattering analysis formulation using the Reciprocity Relation for elastic fields.

The basic idea is to use the elastodynamic reciprocity relation to calculate the reflection and transmission through a slab of composite material. In particular, this permits calculation of the transmission loss due to scattering by the ceramic elements of the composite. The transmission line model referred to above can be used to calculate transmission loss for one-dimensional composites, but not for the two-dimensional case. Using the reciprocity approach, both cases may be treated.

Scattering theory based on the reciprocity relation calculates the difference in scattering for two different geometries. In the problem at hand the two geometries are:
   (i) a uniform polymer medium (unprimed quantities)
   (ii) a composite slab embedded in polymer (primed quantities).

The change in scattering can then be expressed as

$$\Delta S = -\frac{i\omega}{4} \int_{\text{ceramic}} \left\{ (\rho' - \rho)\mathbf{v}' \cdot \mathbf{v} - \mathbf{T}' : (\mathbf{s}' - \mathbf{s}) : \mathbf{T} \right\} dV \tag{28}$$

where the primes on the density ρ and the compliance s refers to the ceramic properties. To calculate reflection, the primed velocity and stress fields are for wave incidence on the same side of the slab. For a transmission calculation the unprimed fields are for wave incidence on the left side of the slab, while the primed fields correspond to incidence on the right. Since geometry (i) has zero reflection and complete transmission, the reflection and transmission for geometry (ii) can both be evaluated from ΔS.

To illustrate, the reflection of shear waves from a slab of one-dimensional (2-2) composite can be shown, for the low volume fraction case, to be

$$R = \frac{1}{4\sqrt{\rho C_{44}}} \left[\rho' - \rho + \frac{\rho C_{44}}{C'_{44} - C_{44}} \right] \sum_{n=0}^{N-1} w_n \, e^{-j2kz_n} \qquad (29)$$

for a slab consisting of N ceramic elements at positions z_n, with thicknesses w_n. Printed material constants are for the ceramic, and unprimed for the polymer.

As stated, the formula applies to a general distributed period structure with nonuniform ceramic elements. For the strictly periodic case

$$w_n = w$$

$$z_n = nd$$

In the second case, scattering from the individual ceramic element, detailed by the summation, adds coherently to produce stopbands and bandedge resonances. For a distributed period structure this coherence is broken, eliminating the stopbands. At the same time, a broadband transmission loss results from the incoherent scattering, corresponding to the transmission coefficient

$$|T| = \sqrt{1 - |R|^2} \qquad (30)$$

The advantage of the reciprocity approach is that it can be easily extended to two-dimensional (1-3) composites. In this case the calculation is simplified by taking the two geometries in the reciprocity relation to be:

(i) a strictly periodic 1-3 composite slab
(ii) a distributed period 1-3 composite slab.

Transmission loss for case (i) can be calculated by using Floquet Theory; and from this result the transmission loss for case (ii) can be calculated using ΔS obtained from reciprocity.

109

A brief introduction to this work was given at the ONR Review of piezoelectric and electrostrictive materials for transducer materials, State College, PA, April 1, 1992. It will be elaborated in a projected review paper on 1-3 composites, theory and practice.

8. CONCLUSIONS

Theoretical work, supported by experimental results, has proven that parasitic lateral mode behavior in 1:3 composite transducers may be suppressed by using a statistical distribution of inter-pillar periods. Alternatively, a similar effect can be obtained by using double or triple periods. Factors crucial to the successful manufacture of 0:3 transducers have been identified. These include the use of clean, rounded particles, possessing a narrow size distribution compressed under high pressure. A simple model, taking account of all the relevant factors, has been developed. This represents a significant improvement over previously used models. Nevertheless, the mechanisms of ferroelectricity near the surfaces of piezoelectric ceramic particles present complex issues requiring further study. The concept of using multiple, independently excited, layer transducers has been proposed and tested. Simple, yet comprehensive, modeling techniques have been developed. It has been shown theoretically and experimentally that these transducers are capable of hitherto unheard of bandwidth performance. Recently, 1:3 transducers with compressible gas filled inclusions have been investigated. The inclusions absorb lateral strains which would otherwise couple in an undesirable manner to thickness polarized charge in the ceramic pillars. There is reason to believe that a significant improvement in hydrophone performance may be achieved using this technique.

9. ACKNOWLEDGEMENTS

110

10. PUBLICATIONS AND REPORTS

1. J. A. Hossack and B. A. Auld, "Advanced modeling and optimization of piezoelectric composites," Interim Technical Report, ONR N00014-90-J-1924, December 1990.

2. J. A. Hossack and B. A. Auld, "Advanced modeling and optimization of piezoelectric composites," Technical Performance Report, ONR N00014-90-J-1924, August 1991.

3. B. A. Auld and J. A. Hossack, "Quasirandom and double periodic structures for the suppression of spurious modes in 1-3 composites," *Electronics Letters* Vol. **25** (14) 1284-1285 (1991),

4. J. A. Hossack and B. A. Auld, "Techniques for suppressing resonant modes in 1:3 composite transducers," Proc. 1991 IEEE Ultrasonics Symposium, pp. 651-655

5. J. A. Hossack and B. A. Auld, "Multiple layer transducers for broadband applications," Proc. 1991 IEEE Ultrasonics Symposium, pp. 605-610

6. J. A. Hossack and B. A Auld, "Improving the characteristics of a transducer using multiple piezoelectric layers," Submitted to *IEEE Trans. UFFC*, February 1992.

7. J. A. Hossack and B. A. Auld, "Enhanced piezoelectric ceramic/ polymer composite transducers," Prepared; to be submitted.

8. J. A. Hossack and B. A. Auld, "Effective medium properties of a pressurized packing of spheres," Prepared; to be submitted.

11. PRESENTATIONS

1. B. A. Auld and J. A. Hossack, "Modelling and optimization of piezoelectric composites," US-Japan Workshop on Ferroelectrics, Kyoto, Japan, December 1990.

2. J. A. Hossack, "Towards an improved understanding of the piezoelectric composite transducer," NRL USRD, Orlando, FL, April 1991.

3. J. A. Hossack, "Advanced modeling of piezoceramic composites," ONR Review of piezoelectric and electrostrictive materials for transducer applications. State College, PA, April 1991.

4. B. A. Auld and J. A. Hossack. "Advanced piezoelectric composites for broadband applications: Theory and experiment," ONR Review of piezoelectric and electrostrictive materials for transducer applications, State College, PA, April 1992.

12. PATENT DISCLOSURES

1. J. A. Hossack and B. A. Auld, "Randomly diced or patterned piezoelectric composite materials," 4/18/91.

2. J. A. Hossack, "Multiple active layer piezoceramic transducers," 6/6/91.

3. J. A. Hossack, "Improved Composite Transducer," 2/4/92.

13. CONFERENCES ATTENDED AND ABSTRACTS SUBMITTED

Conferences attended:

1. Duke University Review of New Transducer Materials, Durham, NC September, 1990.

2. IEEE Ultrasonics Symposium, Hawaii, December 1990.

3. US-Japan Workshop on Ferroelectrics, Kyoto, Japan, December 1990.

4. ONR Review of piezoelectric and electrostrictive materials for transducer applications, State College, PA, April 1991.

5. IEEE Ultrasonics Symposium, Orlando, December 1991.

6. ONR Review of piezoelectric and electrostrictive materials for transducer applications, State College, PA, April 1992.

Abstracts submitted:

1. J. A. Hossack and B. A. Auld, "Enhanced piezoelectric ceramic/polymer composite transudcers," 1992 IEEE Ultrasonics Symposium, Tucson AZ. October 1992.

2. J. A. Hossack and B. A .Auld, "Improving transducer performance using multiple active layers," SPIE New Developments in Ultrasonic Transudcers and Transducer Systems, San Diego, CA. July, 1992.

3. J. A. Hossack and B. A. Auld, "Performance characteristics of piezocomposite bulk wave transducers," QNDE, La Jolla, July 1992.

4. B. A. Auld and J. A. Hossack, "Analysis of wave behavior in two-dimensional composite strutcures with multiple or distributed periods," IEEE ISAF, Greenville, SC. August 1992.

14. REFERENCES

1. J. A. Hossack and B. A. Auld, "Advanced modeling and optimization of piezoelectric composites," Interim Technical Report, ONR N00014-90-J-1924, December 1990.

2. Y. Wang, "Waves and vibrations in elastic superlattice composites," PhD Thesis, Stanford University (1986).

3. B. A. Auld and J. A. Hossack, "Quasirandom and double periodic structures for the suppression of spurious modes in 1-3 composites," Accepted for publication in *Electronics Letters*, Vol. 25 (14), pp. 1284-1285 (1991).

4. H. Banno, "Theoretical equations for dielectric, piezoelectric and elastic properties of a 0:3 composite based on modified cubes model—A general solution," *Jap J. App. Phys.* (28) Suppl 28-2, 190-192 (1989).

5. W. Voigt, "Lehrbuch der Kristallphysik," *Teubner*, Leipzig (1928).

6. A. Reuss, "Berechnung der fliessgrense von mischkristallen auf grund der plastizitatsbedingung fur einkristalle," *Zeitschrift fur Angewandte Mathematik und Mechanik* (9) 49-58 (1929)

7. Z. Hashin and S. Shtrikman, "A variational approach to the elastic behavior of multiphase materials," *J. Mech. Phys. Solid* (11) 127-140 (1963).

8. J. R. Giniewicz, K. Duscha, R. E. Newnham, and A. Safari. "$(Pb_{1-x}, Bi_x)(Ti_{1-x} (Fe_{1-y}, Mn_y)_x)O_3$–Polymer 0-3 compositesfor hydrophone applications," Proc. ISAF 1986, 323-327.

9. K. Ogura, K. Ohya and H. Banno, "Hydrostatic pressure properties of piezoelectric flexible composites," *Jap. J. App. Phys.* (28) Suppl. 28-1, 60-62 (1989).

10. Y. H. Lee, M. J. Haun, A. Safari, and R. E. Newnham, "Preparation of $PbTiO_3$ powder for a flexible 0-3 piezoelectric composite," Proc. ISAF 1986, 318-322.

11. G. K. Batchelor, "Transport properties of two phase materials with random structure," *Ann. Rev. Fluid. Mech.* (6) 227-255 (1974).

12. G. K. Batchelor and R. W. O'Brien, "Thermal or electrical conduction through a granular material," *Proc. Roy. Soc. Lond.* (355) 313-333 (1977).

13. H. Lamb, *Hydrodynamics*, Cambridge University Press (1932).

14. L. D. Landau and E. M. Lifshitz, *Theory of elasticity*, Pergamon Press (1959).

15. D. P. Marion, "Acoustical, mechanical and transport properties of sediments and granular materials," PhD Thesis, Stanford University (1990).

16. W. O. Smith, P. D. Foote, and P. F. Busang, "Packing of homogeneous spheres," *Physical Review* (34) 1271-1274 (1929).

17. G. D. Scott, "Packing of equal spheres," *Nature*, December 10, 1960 (188) 908-909.

18. J. D. Bernal and J. Mason, "Co-ordination of randomly packed spheres," *Nature* December 10, 1960 (188) 910-911.

19. D. P. Marion and A. Nur, "Percolation of electrical and elastic properties of granular materials at the transition from a suspension to a loose packing," *Physica A* (157) 575-579 (1989).

20. G. Shiers (ed.), *The telephone: an historical anthology*, Arno Press, NY (1977).

21. L. E. Cross, Private communication.

22. G. M. Garner, N. M. Shorrocks, R. W. Whatmore, M. T. Goosey, P. Seth, and F. W. Ainger, "0-3 Piezoelectric composite for large area hydrophones," *Ferroelectrics* (93) 169-176 (1989).

23. H. Banno, "Recent progress in science and technology of flexible piezoelectric composites in Japan," Proc ISAF 1986.

24. J. R. Giniewicz, "(PbBi)(TiFe)O$_3$/Polymer 0-3 composite materials for hydrophone applications," MS Thesis, Pennsylvania State University, 1985.

25. German Patent No 2922260, "Piezoelectric polymeric composite material," NGK Spark Plug Co.

26. Eccogel 1365-25, Emerson and Cumming, W. R. Grace and Co, MA.

27. Westinghouse Electric Corp., "Piezoceramic composites," Final Report, ONR N00014-bb-c-2443 (1990).

28. T. R. Gururaja, Q. C. Xu, A. R. Ramachandran, A. Halliyal, R. E. Newnham and A. Safari, "Preparation and piezoelectric properties of fired 0-3 composites," Proc. IEEE Ultrasonics Symposium 1986, 703-708.

29. G. Sa-Gong, A. Safari and, R. E. Newnham, "Poling study of PbTiO$_3$—polymer composites," Proc. ISAF 1986, 281-284.

30. A. Safari, T. R. Gururaja, C. Hakun, A. Halliyal, and R. E. Newnham, "0-3 Piezoelectric ceramic-polymer composites prepared by a new method: Fired composites," Proc. ISAF 1986, 305-308.

31. C. Madhaven, T. R. Gururaja, T. T. Srinivasar, Q. C. Xu, and R. E. Newnham, "Fired 0-3 piezoelectric composite materials for biomedical ultrasonic imaging applications," Proc. IEEE Ultrasonics Symposium 1987, 645-649.

32. H. Banno, K. Ogura, H. Sobue, and K. Ohya, "Piezoelectric and acoustic properties of piezoelectric flexible composites," *Jap. J. Appl. Phys.* (26) Suppl 26-1, 153-155 (1987).

33. K. M. Rittenmyer and F. D. Shields, "Determination of electromechanical properties of highly damped piezoelectric composite materials," US NRL USRD.

34. R. Y. Ting, "The hydroacoustic behavior of piezoelectric composite materials," *Ferroelectrics* (102) 215-224 (1990).

114

35. J. A. Hossack and B. A. Auld, "Multiple layer transducers for broadband applications," Proc. 1991 IEEE Ultrasonics Symposium.

36. J. A. Hossack and B. A. Auld, "Improving the characteristics of a transducer using multiple piezoelectric layers," Submitted to *IEEE Trans. UFFC*.

37. G. K. Lewis, "A matrix technique for analyzing the performance of multilayered front matched and backed piezoelectric ceramic transducers," *Acoust. Imaging* (8) 395-416 (1978).

38. R. L. Bedi and A. R. Selfridge, "Spot poled reflector style hydrophone for shock wave measurements," Proc. 1991 IEEE Ultrasonics Symposium.

39. P. R. Stepanishen, "Transient radiation from pistons in an infinite planar baffle,"*J. Acoust. Soc. Am..* (49) 1629-1638 (1971).

40. L. Chofflet and M. Fink, "A multi-piezoelectric structure: the stacked transducer," Proc. 1991 IEEE Ultrasonics Symposium, pp. 611-614.

41. W. A. Smith, "Optimizing electromechanical coupling in piezocomposites using polymers with negative Poisson's ratio," 1991 IEEE Ultrasonics Symposium, pp. 661-666.

42. R. E. Newnham, D. P. Skinner, and L. E. Cross, "Connectivity and piezoelectric–pyroelectric composites," *Mater. Res. Bull.* 13 (5) 525 - 536 (1978).

43. B. A. Auld, H. A. Kunkel, Y. A. Shui, and Y. Wang, "Dynamic behavior of periodic piezoelectric composites," 1983 IEEE Ultrasonics Symposium, 554-558.

44. B. A. Auld and Y. Wang, "Acoustic wave vibrations in periodic composite plates," 1984 IEEE Ultrasonics Symposium, 528 - 532.

45. Product Catalog, Morgan Matroc Inc., Bedford, OH.

46. 'ANSYS' available from Swanson Analysis Systems Inc., Houston, PA.

47. H. Allik and T. J. R. Hughes, "Finite element method for piezoelectric vibrations," *Int. J. of Num. Methods for Eng.* (2) 151–157 (1970).

48. R. Lerch, "Simulation of piezoelectric devices by two and three dimensional finite elements," *IEEE Trans. UFFC* (37) No. 2, 233–247 (1990).

49. J. A. Hossack and G. Hayward, "Finite element analysis of 1:3 composite transducers," *IEEE Trans. UFFC* (38) No. 6, 618–629 (1991).

50. M. J. Haun, P. Moses, T. R. Gururaja, W. A. Schulze, and R. E. Newnham, "Transversely reinforced 1:3 and 1:3:0 piezoelectric composites," *Ferroelectrics* (49) 259–274 (1983).

51. M. J. Haun and R. E. Newnham, "An experimental and theoretical study of 1:3 and 1:3:0 piezoelectric PZT-polymer composites for hydrophone applications," *Ferroelectrics* (68) 123–139 (1986).

115

52. A. S. Bhalla and R. Y. Ting, "Hydrophone figure of merit," *Sensors and Materials* (14) 181–185 (1988).

53. B. A. Auld and J. A. Hossack, "Quasirandom and double periodic structures for the suppression of spurious modes in 1:3 composites," *Electronics Letters*, Vol 25 (14) 1284–1285 (1991).

15. APPENDICES

Appendix I: Properties of PZT 5A, Epoxy and Polyurethane

	PZT 5A	Epoxy	Polyurethane
c_{11}^E (10^9 Nm^{-2})	121	9.63	9.01
c_{12}^E (10^9 Nm^{-2})	75.4	5.2	7.99
c_{33}^E (10^9 Nm^{-2})	111	9.63	9.01
c_{44}^E (10^9 Nm^{-2})	21.1	2.22	0.51
ρ (kgm^{-3})	7750	1140	1300
e_{31} (Cm^{-2})	-5.4	0	0
e_{33} (Cm^{-2})	12.3	0	0
e_{15} (Cm^{-2})	12.3	0	0
$\varepsilon_{11}^T/\varepsilon_0$	1730	4	4
$\varepsilon_{33}^T/\varepsilon_0$	1700	4	4

Appendix II: Design parameters of the double layer transducers

TRANSDUCER	A	B	C	D
Diameter (mm)	12	12	18	18
Layer thickness (mm)	1.0	1.0	0.5	0.5
Active material	Lead Titanate	Lead Titanate	Composite	Composite
Backing (MRayl)	10.0	20.0	10.0	16.4

NOTE: The composite material was 50% PZT-5H type ceramic. Transducers A and C were fabricated. The backings were composed of tungsten loaded epoxy. The layers were bonded via a fine epoxy layer. No matching layer, other than a thin, protective coat of paint, was used.

Appendix III: Design parameters of enhanced composite Transducers A and B

Parameter	Transducer I	Transducer II
Ceramic volume fraction (%)	20	30
Thickness (mm)	2.5	3.8
Pillar width (mm)	0.75	1.00
Hole diameter (mm)	0.5	0.5
Protective layer thickness (mm)	0.3	1.0
Center frequency (MHz)	0.5	0.35

Notes: The ceramic is PZT-5H. Transducer A employed Hysol RE2039-HD3561 epoxy. Transducer B was manufactured by FMI, Maine, and used a proprietary epoxy.